Studies in recombination and dissociation reactions for collisional energy transfer and electron transfer of nanocrystals and dye molecules

Thesis by

Zhaoyan Zhu

In Partial Fulfillment of the Requirements

for the Degree of

Doctor of Philosophy

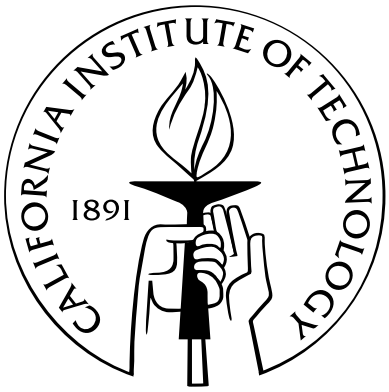

California Institute of Technology

Pasadena, California

2012

(Defended April 02, 2012)

Acknowledgements

It is almost mission impossible to express my gratitude to all the wonderful people I have had the pleasure of meeting and knowing during my time at Caltech.

To my advisor Prof. Marcus, I have been so fortunate to have Rudy as my research advisor who has provided enormous encourgement, guidance, help, patience and support. Whenever I have a question whether in research or life I know I can turn to Rudy for help and Rudy always has an answer.

And I appreciate the support from my committee, Prof. Gray, Prof. Lewis, Prof. McKoy and Prof. Kuppermann (passed away in 2011) and help from former and current group members, Evans, Jau, Meher, Nathan, Nima, Ruifeng, Sandor, Yousung and Yun- Hua. Wei- Chen has been a perfect officemate from whom I have learned so much in research, sports, history and travelling.

I would like to thank (I can not name all here), An, Guanglei, Kana, Na, Qi, Wei, Xi, Xin and a lot more friends- laughter and tear shared together and my dear family, with all you people's love I made it here.

Finally I would like to thank my husband, Tian who has tolerated a lot of bad mood from a PhD candidate for his patience, support and love.

Abstract

This dissertation consists of three parts. In the first part, the effect of the large impact parameter near-elastic peak of collisional energy transfer for unimolecular dissociation/bimolecular recombination reactions and deviation from equilibrium case is studied. To this end the conventional single exponential model, a bi-exponential model that fits the literature classical trajectory data better, a model with a singularity at zero energy transfer, and the most realistic model, a model with a near-singularity, are fitted to the trajectory data in the literature. A theory is developed for the population distribution as a function of the energy E of a dissociating model, and used to calculate the three-body low pressure recombination rate constant. In the second part, the electron transfer process in the single quantum dot fluorescence blinking phenomenon is studied. The DCET (diffusion controlled electron transfer) model has been modified to explain the exponential cutoff of the power law time distribution of the bright state and the quadratic dependence of the exponential tail on the excitation intensity. Based on ensemble measurements it is proposed that an exponential tail for the dark state time distribution for long time experiments exists for single trajectory experiments. In the last part, we develop a general MLE (maximum likelihood estimation) method to analyze experimental data with a potential distribution of power law form which can be extended to a power law with an exponential tail and more generally, many other distribution forms.

Contents

List of Figures

List of Tables

Chapter 1

Collisional energy transfer in recombination and dissociation reactions, a Wiener-Hopf problem and the effect of a near elastic peak

[This chapter appeared in the Journal of Chemical Physics **129**, 214106 (2008).]

1.1 Introduction

In the treatment of gas phase dissociation, unimolecular isomerization, and bimolecular recombination reactions, it has been recognized for many years that "weak collisions" rather than "strong collisions" play a major role in the activation and deactivation of the vibrationally hot intermediate complexes in these reactions [2–6]. Our interest in the subject was prompted by studies of ozone whose formation and isotopic effects have been of much recent interest [7–23]. In general, the formation of a molecule AB is described by

$$A + B \rightarrow AB^*, \tag{1.1}$$

$$AB^* + M \rightarrow AB + M, \tag{1.2}$$

where M is a collision partner and AB^* is a vibrationally excited intermediate. In a weak collision assumption, unlike in a strong collision one, many collisions with M are required to activate and deactivate a reactant molecule. When the collision is "weak", the AB^* may still have enough energy after the collision in reaction 2.2 to redissociate into $A + B$, instead of always being "deactivated", and so a set of such equations with different energy is considered, leading to a master equation or to a steady-state equation. The latter is then solved for the probability distribution function for the vibrational energy in the energetic intermediate AB^*.

Information on the collisional energy transfer in reactions such as in Eq. (2.2) is usually obtained from the pressure dependence of the reaction rate of the overall reaction (2.1) - (2.2), using the solution of the collisional master or steady-state equation to fit these experimental reaction rate versus pressure data [4, 6]. To this end, a functional form for the collision energy transfer probability, denoted here by $Z(E^{'}; E)$, is typically assumed and its parameters are calculated from the fit. The functional forms used for this purpose are usually the exponential model introduced by Rabinovitch, used in Subsec. (1.2.1), or a step-ladder in which the reactant molecule gains or loses energy in collisions in discrete amounts, "steps" [2,3,24,25].

Luther and coworkers also introduced a stretched exponential model [26]. A bi-exponential model was used by Brown and Miller [27] and modified by Hu and Hase [28]. Complementing these studies have been ab initio or semi-empirical calculations of the collisional energy transfer, frequently using classical mechanical trajectories for the collisions [27–37]. Analytical treatments of vibrational energy transfer have been given for particular cases [6, 35–39]. In particular, a detailed discussion of the original master equation and of its steady-state approximation is given by Penner and Forst [39], who expressed the solution in terms of hypergeometric functions.

The $Z(E^{'};E)$ is defined as the number of collisions per unit time with energy transfer for the vibrationally excited intermediate, $E \rightarrow (E^{'}, E^{'} + \mathrm{d}E^{'})$, per unit $\mathrm{d}E^{'}$. Then the number of collisions per unit time is $\int_{-\infty}^{\infty} Z(E^{'};E)\mathrm{d}E^{'}$, which will be denoted by $Z(E)$. $Z(E^{'};E)$ has units of sec^{-1} energy^{-1} when it is chosen to be the product of the concentration of colliders and the bimolecular collision rate constant for the transition $E \rightarrow E^{'}$, per unit $\mathrm{d}E^{'}$. Its theoretical calculation involves an integration over impact parameters b, using $2\pi b\mathrm{d}b$ as a weighting factor. Collisions with large b contribute mainly to the energy transfer near $E - E^{'} \approx 0$. When plotted versus $E - E^{'}$ they yield an elastic-collision peak in the classical limit at $E = E^{'}$ corresponding to $b = \infty$. The larger the average value of the energy transfer per collision in any reaction, the further the important energy transfer region is from the elastic $E - E^{'} = 0$ peak. Examples of the tendency towards a singular behavior at $E = E^{'}$ are seen in Refs. [1,27,40–42]. Ivanov and Schinke's data [1] shown in Fig. 1.1(Fig.2 in Ref. [1]) are used later as an example. From a quantum mechanical view the inelastic collisions have a lower bound for the energy transfer $|E - E^{'}|$, namely a quantum of rotational or vibrational energy, depending upon the collision. So in quantum mechanical calculations there is no such singularity, but instead there is a near-elastic literature to avoid this peak [27–36].Then a single exponential, step-ladder or bi-exponential model was usually adopted to fit the trajectory data. For example, Brown and Miller [27] neglected the bin in which $E^{'} - E \approx 0$ with a bin size of around 30 cm^{-1} in a bi-exponential fit to the trajectory data. Hu and

Hase [28] suggested that b_{max} should be identified as the value of b at which the average energy transfer equals the inverse of the state density. In such a choice the resulting collision cross section was considerably larger than the usually assumed value, but within 5% of the experimental value [28].

The paper is organized as follows: the theory is described in Sec. 1.2 for the different models. It is applied to a particular system in Sec. 1.3, the results discussed in Sec. 1.4, with concluding remarks in Sec. 1.5.

1.2 Theory

1.2.1 General aspects

In using trajectories to calculate the transition rate $Z(E^{'};E)$ a random sampling of trajectories is performed over the vibrational and rotational coordinates and their conjugate momenta of the vibrationally excited intermediate and over a Boltzmann-weighted distribution of relative velocities of the collision partners [32–37]. The calculations of energy transfer are typically made as a function of the internal energy E of the energetic intermediate, its total angular momentum J [43], and occasionally K, the projection of J along a specified principal axis of rotation, typically that with the smallest moment of inertia. For notational simplicity we suppress the symbol J in the following.

To obtain insight into the effect of the near-elastic peak at $|E^{'} - E| = 0$ in the comparison between experimental data and trajectories, it is convenient to consider the collisional steady-state/reaction equations, and obtain approximate analytical solutions. Examples of other treatments are also available [39, 44–57].

We focus on the limiting low pressure rate constant k_0. It is of particular interest, partly because it describes the maximum effect of the collisions, and partly because it is simpler to treat than the rate constant at higher pressures, where a solution of the complete master equation would have been necessary. While simple theoretical expressions for the distribution function of different (E, J) states of the reactants

and for the energy transfer can also be obtained for the high-pressure limit of k, k_∞, they do not provide insight into the effect of energy transfer on k itself, since k_∞ is independent of $Z(E^{'};E)$. The effect of the near-elastic peak should be largest at low pressures, since the average energy of the reacting vibrationally excited intermediate in a unimolecular reaction or a bimolecular recombination is well-known to decrease when the pressure is decreased [58]. Accordingly the vibrational energy of the typical molecule is closer to the energy dividing line between stable and unstable intermediates, and so is closer to the near-elastic peak when the pressure is decreased.

To treat the kinetics for the recombination of two species, $A + B \rightarrow AB$, one can either proceed from the reactants ($A + B$) or from the product (AB). If a tagged A is followed in time in its progress to form AB, and if a tagged A in AB is followed in time in its progress to form $A + B$, beginning with an equilibrium concentrations of AB for the given A and B concentration, the sum of the tagged distribution functions at any energy E is equal to the equilibrium distribution at that E. Thus, to solve the problem one can either begin with a tagged A or a tagged AB. To simplify the comparison with earlier work [45–49], we begin with AB and use the result to calculate also the rate of recombination $A + B \rightarrow AB$.

We consider the reaction in the low pressure regime

$$M + AB(E) \rightarrow M + AB^*(E^{'}), \tag{1.3}$$

$$AB^*(E^{'}) \rightarrow A + B \text{ (if } E^{'} \geqslant 0), \tag{1.4}$$

where $E^{'} \geqslant 0$ denotes the internal energies of any reacion intermediate AB^* that can dissociate into the separated reactants without a further collision. Energies $E^{'}$ in the reactants that are negative are insufficient for dissociation.

The scheme (2.8) - (2.9) is appropriate only for the low pressure limit of the dissociation rate. At higher pressures an $AB^*(E^{'})$ on a second collision can also yield an AB^* with a different $E^{'}$, where both $E^{'}$s are greater than zero. At sufficiently low pressures each $AB^*(E^{'})$ formed in reaction (2.8) with ultimately dissociates into

$A + B$ before any further collision. For this case, the problem simplifies and a large set of equations (the master equation) for $AB^*(E')$ is not needed for $E' > 0$.

We denote the probability energy distribution function for AB by $g(E)$ and write

$$k_0 = \int_{E'=0}^{\infty} \int_{E=-\infty}^{0} g(E) Z(E', E) \mathrm{d}E \, \mathrm{d}E'. \tag{1.5}$$

The equilibrium probability that AB has an energy in the range E,E+dE is $g_{eq}\mathrm{d}E$, where

$$g_{eq}(E) = \rho(E) \mathrm{e}^{-E/kT} / Q \tag{1.6}$$

and $\rho(E)$ denotes the density of quantum states of the molecule, Q is the partition function of AB in the center-of-mass system of coordinates. When the energy is measured relative to $E = 0$, the dissociation limit Q is also calculated relative to that energy, and so contains a factor $e^{D/kT}$, where D is the dissociation energy of AB measured from the bottom of its potential well to the dissociation level. When E becomes very negative in the steady-state problem, *i.e.*, when $E \to -D$ and $g(E) \to g_{eq}(E)$. This condition on $g(E)$ serves as a boundary condition,

$$g(E) \to g_{eq}(E) \; E \to -D. \tag{1.7}$$

After a short initial period $g(E)$ relaxes towards a steady-state [6]. We use a steady-state approximation here. The steady-state equation for $g(E)$ is

$$0 = \int_{-\infty}^{0} Z(E, E') g(E') \mathrm{d}E' - g(E) \int_{-\infty}^{\infty} Z(E', E) \mathrm{d}E' \quad (E \leqslant 0). \tag{1.8}$$

The latter can be rewritten as

$$g(E) = \int_{-\infty}^{0} Z(E, E') g(E') \mathrm{d}E' \Big/ \int_{-\infty}^{\infty} Z(E', E) \mathrm{d}E' \qquad (E \leqslant 0). \tag{1.9}$$

An analytical solution of this integral equation for a single exponential model for the energy transfer was first given by Troe [6], who obtained it using a trial solution

method. For the present article, we note instead that Eq. (1.9) is a homogeneous Wiener-Hopf equation of the second kind and use the Wiener-Hopf method [59] to obtain a solution.

We first study the single exponential and bi-exponential models with this method. For the single exponential model, in terms of a deactivation constant γ and of an activation constant $\gamma^{'}$, we have

$$Z(E^{'},E) = Z_0 e^{(E-E^{'})/\gamma},\ E^{'} \leqslant E, \tag{1.10}$$

$$Z(E^{'},E) = Z_0 e^{(E^{'}-E)/\gamma^{'}},\ E^{'} \geqslant E, \tag{1.11}$$

and for the bi-exponential model,

$$Z(E^{'},E) = Z_0[e^{(E-E^{'})/\gamma} + c e^{(E-E^{'})/d}],\ E^{'} \leqslant E, \tag{1.12}$$

$$Z(E^{'},E) = Z_0[e^{(E^{'}-E)/\gamma^{'}} + c e^{(E^{'}-E)/d^{'}}],\ E^{'} \geqslant E, \tag{1.13}$$

where Z_0 is a constant and γ,$\gamma^{'}$ and d,$d^{'}$ are related by microscopic reversibility (detailed balance).

The quantities $Z(E^{'},E)$ and $Z(E,E^{'})$ satisfy microscopic reversibility

$$\rho(E)Z(E',E) = \rho(E^{'})Z(E,E^{'})e^{-(E^{'}-E)/kT}. \tag{1.14}$$

For practical purpose, we can typically treat the lower limit on E as $E \to -\infty$, a minor approximation when $D \gg kT$. Neglecting the effect of the change in $\rho(E)$ between E and $E^{'}$ in the vicinity of $E = 0$, Eqs. (2.13) and (2.14) yield

$$\frac{1}{\gamma^{'}} = \frac{1}{\gamma} + \frac{1}{kT}. \tag{1.15}$$

$$\frac{1}{d'} = \frac{1}{d} + \frac{1}{kT}. \tag{1.16}$$

The constants c and d are obtained later from fitting classical trajectory calculations

data for vibrational energy transfer.

We have also examined a model with singularity at $|E^{'} - E = 0$ using another method,

$$Z(E^{'}, E) = Z_0[1 + C(E - E^{'})^{-\alpha}]e^{(E-E^{'})/\gamma}, \; E^{'} \leqslant E, \tag{1.17}$$

$$Z(E^{'}, E) = Z_0[1 + C(E^{'} - E)^{-\alpha}]e^{(E^{'}-E)/\gamma^{'}}, \; E^{'} \geqslant E, \tag{1.18}$$

γ and $\gamma^{'}$ are the same as those of the single exponential model. C and α and are obtained later from classical trajectory data.

1.2.2 Single exponential model

To compare with the earlier and insightful result in the literature by Troe [6], we use the single exponential expression for the collisional energy transfer rate, namely, Eqs. (2.13) and (2.14). The average "up"-energy transfer, defined as the average energy increase of the molecule for collisions that lead to an increase in energy, is

$$< \Delta E >_{up} = \int_E^{\infty} (E^{'} - E)Z(E, E^{'})\mathrm{d}E^{'} / \int_E^{\infty} Z(E^{'}, E)\mathrm{d}E^{'} = \gamma^{'}, \tag{1.19}$$

Similarly the average "down"-energy transfer is

$$< \Delta E >_{down} = \int_{-\infty}^{E} (E^{'} - E)Z(E, E^{'})\mathrm{d}E^{'} / \int_{-\infty}^{E} Z(E^{'}, E)\mathrm{d}E^{'} = -\gamma. \tag{1.20}$$

These quantities, $< \Delta E >_{up}$ and $< \Delta E >_{down}$ are not observables in the usual reaction rate experiments, and so can not be directly compared with experiment. In computation the quantity $< \Delta E^2 >$ is a more convenient parameter than $< \Delta E >$ [60,61]. Here in our discussion the average over impact parameter b and the other initial variables is included in the definition of $Z(E^{'}, E)$ at the given E. The rate constant k on the other hand, as a function of pressure and its limiting value at low pressure k_0, are the observables in these experiments. Nevertheless, since the values of the moments are often calculated in the literature from classical trajectories or from

approximate fits to those data, the values of these moments are often cited, and are calculated here, bearing in mind that they are not directly observable and are model-dependent.

To solve Eq. (1.9), we use a Wiener-Hopf procedure61 and, as in the standard procedure, first extend the domain in Eqs. (2.17) and (1.9) from $E \leqslant 0$ to $E > 0$ by introducing the functions $g_-(E)$ and $g_+(E)$, $g(E) = g_-(E) + g_+(E)$, with the properties

$$\begin{aligned} g_-(E) &= g(E), \quad E \leqslant 0 \\ &= 0, \qquad E > 0, \end{aligned} \tag{1.21}$$

$$\begin{aligned} g_+(E) &= 0, \qquad E \leqslant 0 \\ &= g(E), \quad E > 0. \end{aligned} \tag{1.22}$$

Here, $g(E)$ is the unknown function. From Eqs. (1.9), (1.21) and (1.22) we then obtain for the entire E -range, $-\infty < E < \infty$,

$$g_-(E) + g_+(E) = \int_{-\infty}^{\infty} Z(E, E')g_-(E')\mathrm{d}E' \Big/ \int_{-\infty}^{\infty} Z(E', E)\mathrm{d}E' \qquad (-\infty < E < \infty). \tag{1.23}$$

For $E \leqslant 0$ this equation becomes

$$g_-(E) = \int_{-\infty}^{0} Z(E, E')g_-(E')\mathrm{d}E' \Big/ \int_{-\infty}^{\infty} Z(E', E)\mathrm{d}E' \qquad (-\infty < E \leqslant 0). \tag{1.24}$$

which coincides with Eq. (1.9) for $E \leqslant 0$. For $E > 0$ we have

$$g_+(E) = \int_{-\infty}^{0} Z(E, E')g_-(E')\mathrm{d}E' \Big/ \int_{-\infty}^{\infty} Z(E', E)\mathrm{d}E' \qquad (-\infty < E \leqslant 0). \tag{1.25}$$

The idea behind the Wiener-Hopf method is to solve this pair of equations for $g_-(E)$ and $g_+(E)$ and hence, from Eq. (1.21), for $g(E)$. Because $Z(E, E')$ has one form in Eqs. (2.13) and (2.14) when $E' \geqslant E$ and has a different form when $E' \leqslant E$, there are two terms for $Z(E, E')$. On taking the Fourier transform $\tilde{f}(z) = \int_{-\infty}^{\infty} \mathrm{e}^{2\pi i z E} f(E)\mathrm{d}E$,

$z = u + iv$, where u and v are real, and using the convolution theorem we have from Eqs. (2.13), (2.14) and (1.23),

$$\tilde{g}_-(z) + \tilde{g}_+(z) = \frac{\tilde{g}_-(z)}{\gamma + \gamma'}\left(\frac{1}{1/\gamma + 2\pi iz} + \frac{1}{1/\gamma' - 2\pi iz}\right). \tag{1.26}$$

which can be rewritten as

$$\frac{2\pi iz(2\pi iz - 1/kT)\tilde{g}_-(z)}{1/\gamma + 2\pi iz} = (1/\gamma' - 2\pi iz)\tilde{g}_+(z). \tag{1.27}$$

The solution for the $\tilde{g}_-(z)$ in Eq. (1.27), obtained in Appendix A, is

$$\tilde{g}_-(z) = G_s\frac{1/\gamma + 2\pi iz}{2\pi iz(2\pi iz - 1/kT)}, \tag{1.28}$$

where G_s is a constant. The solution for $\tilde{g}_+(z)$ is not needed but is given for completeness in Appendix A. The inverse transformation of Eq. (1.28) for $\tilde{g}_-(z)$ yields

$$g_-(E) = \int_{-\infty+iv}^{\infty+iv} \tilde{g}_-(z)\mathrm{e}^{-2\pi izE}\mathrm{d}z = G_s'\left(\frac{kT}{\gamma'}\mathrm{e}^{-E/kT} - \frac{kT}{\gamma}\right), \tag{1.29}$$

where G_s' is a constant to be determined. We have from Eq. (1.21) that $g_-(E) = g(E)$ for $E \leqslant 0$ and when $E \to -\infty$, we have $g(E) \to g_{eq}(E)$. Writing $g_{eq}(E)$ as $g_{eq}(0)\mathrm{e}^{-E/kT}$, a value is obtained for the constant G_s', $g_{eq}(0)\gamma'/kT$, and hence

$$g(E) = g_{eq}(0)\left(\mathrm{e}^{-E/kT} - \frac{\gamma'}{\gamma}\right), \tag{1.30}$$

which is the trial solution given by Troe [6]. Using it the analytical solution for the low pressure "three-body" recombination rate constant k_0 can be obtained. From Eqs. (2.10) and (1.30)

$$k_0 = Z_0 g_{eq}(0)\gamma\gamma'\left(1 - \frac{\gamma'^2}{\gamma^2}\right) = Z_0(\gamma + \gamma')\frac{\gamma'^2\rho(0)}{kT}, \tag{1.31}$$

where Q contains the factor $\exp(D/kT)$. In this model the number of collisions per

unit time $Z(E) = Z_0(\gamma + \gamma')$. So that

$$k_0 = Z(0)\frac{\gamma'^2\rho(0)}{QkT}, \tag{1.32}$$

which agrees with Troe's result when we set $F_E = 1$ in his Eq. (3.9a), so neglecting the dependence of $\rho(0)$ on E in his Eq. (3.14) [6].

1.2.3 Bi-exponential model

In this model the average "up"-energy transfer is given by

$$< \Delta E >_{up} = \int_E^\infty (E' - E)Z(E, E')\mathrm{d}E' / \int_E^\infty Z(E', E)\mathrm{d}E' = (\gamma'^2 + cd'^2)(\gamma' + cd'), \tag{1.33}$$

Similarly

$$< \Delta E >_{down} = \int_{-\infty}^E (E' - E)Z(E, E')\mathrm{d}E' / \int_{-\infty}^E Z(E', E)\mathrm{d}E' = -(\gamma^2 + cd^2)(\gamma + cd). \tag{1.34}$$

For the bi-exponential model, following a procedure similar to that in Subsec. 1.2.2 for the single exponential model, we obtain

$$\frac{2\pi iz(2\pi iz - 1/kT)(2\pi iz - r_4)\tilde{g}_-(z)}{(1/\gamma + 2\pi iz)(1/d + 2\pi iz)} = \frac{(1/\gamma' - 2\pi iz)(1/d' - 2\pi iz)\tilde{g}_+(z)}{(2\pi iz - r_3)}, \tag{1.35}$$

where $r_{3,4} = 1/2kT \pm \sqrt{(1/2kT)^2 + [(\gamma + \gamma')/dd' + (cd + cd')/\gamma\gamma']/(\gamma + \gamma' + cd + cd')}$, r_3 is the positive square root one and r_4 the negative one.

The solution for $\tilde{g}_-(z)$ in Eq. (1.35), obtained in Appendix B, is

$$\tilde{g}_-(z) = G_{bi}\frac{(1/\gamma + 2\pi iz)(1/d + 2\pi iz)}{2\pi iz(2\pi iz - 1/kT)(2\pi iz - r_4)}. \tag{1.36}$$

Inversion yields (Appendix B)

$$g(E) = g_{eq}(0)(\mathrm{e}^{-E/kT} + \frac{d'(1/d + r_4) - \gamma'(1/\gamma + r_4)}{r_4(\gamma - d)} + \frac{(1/d + r_4)(1/\gamma + r_4)(\gamma' d - \gamma d')}{r_4(\gamma - d)}\mathrm{e}^{-r_4 E}, \tag{1.37}$$

after evaluating the G_{bi} by noting that $g(E)$ approaches $g_{eq}(0)\mathrm{e}^{-E/kT}$ as $E \to -\infty$. Using the relation in Eqs. (2.16) and (1.16), Eq. (1.37) can be simplified into

$$g(E) = g_{eq}(0)(\mathrm{e}^{-E/kT} - \frac{(1-\gamma' r_3)(1-d' r_3)}{r_4 kT}(1-\mathrm{e}^{-r_4 E}). \tag{1.38}$$

When $d = \gamma$, $r_3 = \frac{1}{\gamma'}$ and $r_4 = \frac{1}{\gamma}$ and so Eqs. (1.37) and (1.38) reduce to Eq. (1.30) when $d = \gamma$. From these results k_0 is given by

$$k_0 = Z_0 g_{eq}(0)[\gamma\gamma' + cdd' - (\gamma'^2 + cd'^2 + \frac{\gamma'}{1/\gamma + r_3} + \frac{cd'}{1/d + r_3})\frac{(1-\gamma' r_3)(1-d' r_3)}{r_4 kT}]. \tag{1.39}$$

This equation reduces to Eq. (1.31) when $d = \gamma$.

From calculation using parameters from Sec. 1.3 it is seen that values of given in Eq. (1.39) are about the same as those obtained by using given in Eq. (1.31).

1.2.4 Singularity model

The average "up"-energy transfer and "down"-energy transfer are given by

$$\begin{aligned} < \Delta E >_{up} &= \int_E^\infty (E' - E) Z(E, E') \mathrm{d}E' \Big/ \int_E^\infty Z(E', E) \mathrm{d}E' \\ &= \gamma'[1 + C\gamma'^{\alpha}(1-\alpha)\Gamma(1-\alpha)]/[1 + C\gamma'^{\alpha}\Gamma(1-\alpha)], \end{aligned} \tag{1.40}$$

$$\begin{aligned} < \Delta E >_{down} &= \int_{-\infty}^E (E' - E) Z(E, E') \mathrm{d}E' \Big/ \int_{-\infty}^E Z(E', E) \mathrm{d}E' \\ &= -\gamma[1 + C\gamma^{\alpha}(1-\alpha)\Gamma(1-\alpha)]/[1 + C\gamma^{\alpha}\Gamma(1-\alpha)]. \end{aligned} \tag{1.41}$$

To use a perturbation method for this case, although a suitable branch-point analysis might also be used, the $g(E)$ given by Eq. (1.30) and $Z(E', E)$ given by Eq. (1.18) are introduced into the right hand side of Eq. (1.9). A new $g(E)$ is obtained and this step is then iterated. After several iterations we find that $g(E)$ for $E < -\gamma/100$ ceases to be affected further. For $-\gamma/100 < E \leqslant 0$, $g(E)$ becomes negligible because of continuity with $g(E) = 0$ for $E > 0$. Using this $g(E) = 0$ to

calculate k_0 we obtain a value close to the one obtained using $g(E)$ from Eq. (1.30), for $g(E)$ can be used here. The expression for the rate constant k_0 thus given by Eq. (2.10) is then

$$\begin{aligned} k_0 &= Z_0 \int_{E'=0}^{\infty}\int_{E=-\infty}^{0} g_{eq}(0)(\mathrm{e}^{-E/kT} - \frac{\gamma'}{\gamma})[1 + C(E' - E)^{-\alpha}]\mathrm{e}^{-(E'-E)/\gamma}\mathrm{d}E\,\mathrm{d}E' \\ &= Z_0 g_{eq}(0)\gamma\gamma'(1 - \frac{\gamma'^2}{\gamma^2}) \\ &+ CZ_0 g_{eq}(0)\int_{E'=0}^{\infty}\int_{E=-\infty}^{0}(\mathrm{e}^{-E/kT} - \frac{\gamma'}{\gamma})\mathrm{e}^{-(E'-E)/\gamma}(E' - E)^{-\alpha}\mathrm{d}E\,\mathrm{d}E'. \end{aligned} \tag{1.42}$$

1.2.5 Near-singularity model

For this model the same functions are adopted for $Z(E', E)$ as in the singularity model. Because of the quantum limit we set a lower bound ε to the energy transfer in the integral when calculating the energy transfer and rate constant. Eqs. (1.40) and (1.41) then becomes

$$\begin{aligned} < \Delta E >_{up} &= \int_{E+\varepsilon}^{\infty}(E' - E)Z(E, E')\mathrm{d}E' \Big/ \int_{E+\varepsilon}^{\infty} Z(E', E)\mathrm{d}E' \\ &= \frac{\int_{E+\varepsilon}^{\infty}(E' - E)[1 + C(E - E')^{-\alpha}]\mathrm{e}^{(E-E')/\gamma}\mathrm{d}E'}{\int_{E+\varepsilon}^{\infty}[1 + C(E - E')^{-\alpha}]\mathrm{e}^{(E-E')/\gamma}\mathrm{d}E'}, \end{aligned} \tag{1.43}$$

$$\begin{aligned} < \Delta E >_{down} &= \int_{-\infty}^{E-\varepsilon}(E' - E)Z(E, E')\mathrm{d}E' \Big/ \int_{-\infty}^{E-\varepsilon} Z(E', E)\mathrm{d}E' \\ &= \frac{\int_{-\infty}^{E-\varepsilon}(E' - E)[1 + C(E' - E)^{-\alpha}]\mathrm{e}^{(E'-E)/\gamma'}\mathrm{d}E'}{\int_{-\infty}^{E-\varepsilon}[1 + C(E' - E)^{-\alpha}]\mathrm{e}^{(E'-E)/\gamma'}\mathrm{d}E'}. \end{aligned} \tag{1.44}$$

and we also have

$$
\begin{aligned}
k_0 &= Z_0\Big(\int_{E'=\varepsilon}^{\infty}\int_{E=-\infty}^{0} + \int_{E'=0}^{\varepsilon}\int_{E=-\infty}^{E'-\varepsilon}\Big) g_{eq}(0)\Big(e^{-E/kT} - \frac{\gamma'}{\gamma}\Big)[1 + C(E' - E)^{-\alpha}]e^{-(E'-E)/\gamma}\,dE\,dE' \\
&= Z_0 g_{eq}(0)[\gamma\gamma'(1 - \frac{\gamma'^2}{\gamma^2})e^{-\varepsilon/\gamma'} - \gamma\gamma'(kT + \frac{\varepsilon\gamma'}{\gamma^2})e^{-\varepsilon/\gamma'} + \gamma kT e^{-\varepsilon/\gamma}] + \\
C\quad & Z_0 g_{eq}(0)\Big(\int_{E'=\varepsilon}^{\infty}\int_{E=-\infty}^{0} + \int_{E'=0}^{\varepsilon}\int_{E=-\infty}^{E'-\varepsilon}\Big)\Big(e^{-E/kT} - \frac{\gamma'}{\gamma}\Big)e^{-(E'-E)/\gamma}(E' - E)^{-\alpha}\,dE\,dE'. \quad (1.45)
\end{aligned}
$$

1.3 Application to Ar + O_3

For the collisions of O_3 with Ar we obtain from the trajectory data [1] the parameters for different temperatures and calculate ΔEs and k_0s for the single exponential model, the bi-exponential model and the singularity model.

1.3.1 Comparison of single exponential and bi-exponential models

We determine γ, c and d from classical trajectory data, [1] and γ' and d' are obtained from Eqs. (2.16) and (1.16). The results for the s and s for both models are given in Table 1.1.

1.3.2 Comparison of single exponential and singularity models

We determine C and α from the classical trajectory data [1]. The average energy transfer and rate constants calculated from it are given in Table 1.2.

1.3.3 Comparison of single exponential and near-singularity models

According to Ref. [1], collisional changes in K provide a major route for the vibrational energy transfer. On that basis, a lower bound for the energy transfer is the quantum cut-off for the rotational energy, $(A-B) < 2K+1 >_J$, where A and B are

the rotational constants and where K is the projection of the angular momentum along the principal axis of rotation, as noted in Sec. 1.3.1. An average over J is used since we averaged over J in the calculation of energy transfer. In Ref. [1], $A \sim 3.5\,\mathrm{cm}^{-1}$ and $B \sim 0.4\,\mathrm{cm}^{-1}$. From these values the estimated lower bounds are given in Table 1.3, namely 15 to $30\,\mathrm{cm}^{-1}$, depending on the temperature. The resulting average energy transfer and rate constants are calculated and shown in Table 1.3.

The cases $T = 700\,\mathrm{K}$ and $T = 1000\,\mathrm{K}$ are purely hypothetical since no experimental data are available for those conditions, only trajectory results [1] are available for these temperatures.

1.4 Discussion

For Ar + O_3, the $|\Delta E|$ for the bi-exponential model is seen in Table 1.1 to be a little smaller than that from the single exponential model by about 10%-20%. The k_0 for this bi-exponential model is about the same as that for the single exponential model (Table 1.1). The $|\Delta E|$ for the singularity model is seen in Table 1.2 to be smaller than that from the single exponential model by 20%-40%. When we set a lower bound in ΔE for the singularity model, *i.e.*, the near-singularity model, and calculate the average "up" and "down"-energy transfer, the results shown in Table 1.3 agree well with those from Ref. [1], as they should if this truncated singularity model is a good description of the trajectory data. The k_0 for the singularity and near-singularity models is larger than that for the single exponential model by a large factor, 25, at room temperature, as seen in Tables 1.2 and 1.3.

These results for k_0 can be interpreted in terms of the extra contribution from large b collisions for the bi-exponential, singularity and near-singularity models, compared with the single exponential model. The single exponential model is fitted to the low b data. For the comparison of singularity and near-singularity models and the single exponential model the difference for $\Delta E_{up/down}$ is less than that for the k_0. This result can also be understood. k_0 is seen from Eq. (2.10)

to have a larger contribution from small $|\Delta E|$ values to the integral than for the single exponential model. In the case of $|\Delta E|$, the numerator in Eqs. (1.33), (1.34), (1.40), (1.41), (1.43) and (1.44) is again enhanced by this enhanced $Z(E, E^{'})$ but the denominator is enhanced even more, since the former is weighted by the small ΔE.

In Refs. [12–14] the average "down"-energy refers to the total internal energy transfer instead of only vibrational energy transfer treated here. So that value should be much larger than that if only vibrational energy transfer were considered. If we compare the total internal "down"-energy transfer $\Delta E_{int} \downarrow$ in Ivanov & Schinke's trajectory work [1] with the values in Gao & Marcus's work [12–14] used to fit experimental data, there is only a small difference in $\Delta E_{int} \downarrow$.

The authors of Ref. [1] gave a different reason for choosing a cutoff of $3\,\mathrm{cm}^{-1}$ or $10\,\mathrm{cm}^{-1}$ for $\Delta E_{int} \downarrow$, namely that the energy transfer averages gradually decrease as the value for $\Delta E_{int} \downarrow$ cutoff decreases and decrease particularly rapidly for the cutoff below the ones they chose. It was suggested that b_{max} may be found by weighting the average nenrgy transfer versus impact parameter by the differential cross section [61].

Another result seen in Table 1.1 is that both γ and d ($\gamma^{'}$ and $d^{'}$) for the trajectory data are proportional to kT, though are much smaller, and the ratios d/γ and $d^{'}/\gamma^{'}$ remain almost the same. The increase of d and $d^{'}$ with temperature means that small energy transfer behavior becomes less important at higher temperatures, as expected. The typical system is further removed from the singularity or $E^{'} - E = 0$.

1.5 Concluding Remarks

Analytical solutions for the low pressure rate constant are given, using several different approximations to the trajectory data, the single exponential, a bi-exponential, a singularity and a near-singularity models. The near-singularity model is the most realistic. The differences should be maximal in the low pressure regime. Expressions are obtained for the limiting low pressure rate constant k_0, ΔE_{up} and ΔE_{down}. The values of k_0 from the bi-exponential are similar to those from the

single exponential model. Those from the singularity and near-singularity models are an order of magnitude larger than those from the single exponential model. The origin of the difference is the large additional contribution of collisions with large cross sections in the singularity and near-singularity models that is absent in the single exponential model. The values from single exponential model for the ΔEs are somewhat larger than those from the bi-exponential model, by about 10%-20%, and larger than those from the singularity model by 20% - 40% but similar to those from the near-singularity model. The physical origin of these differences lies in the smaller contribution from the smaller cross-sections with large energy transfer in the bi-exponential and singularity models, compared with that in the single exponential model: While the numerator in Eqs. (1.33), (1.34), (1.40), (1.41), (1.43) and (1.44) is enhanced by this enhanced $Z(E, E^{'})$, the denominator is enhanced even more, since the former is weighted by the small ΔE. For the near-singularity model a big part of small energy transfer collision is removed. This cancels out the former effect.

Table 1.1: Example of correction of k_0, ΔE_{up} and ΔE_{down}: single exponential model(s) and bi-exponential model(bi).

Parameters[a]	$\frac{k_{0bi}}{k_{0s}}$ [b]	$\frac{\Delta E_{upbi}}{\Delta E_{ups}}$ [c]	$\frac{\Delta E_{downbi}}{\Delta E_{downs}}$ [c]
γ=43 cm^{-1},c=1.70,d=3.70 cm^{-1},T=298K	1.04	0.86	0.88
γ=119 cm^{-1},c=3.27,d=7.16 cm^{-1},T=700K	1.00	0.82	0.84
γ=163 cm^{-1},c=3.49,d=8.57 cm^{-1},T=1000K	1.00	0.82	0.84

[a]Values of parameters were obtained using the trajectory results of O^3/Ar collisions from Ref. [1]. [b]k_{0s} refers to the rate constant of the single exponential model and k_{0bi} refers to the one of the bi-exponential model. [c]A notation similar to that in footnote [b] is used for ΔE_{up} and ΔE_{down}.

Table 1.2: Example of correction of k_0, ΔE_{up} and ΔE_{down}: single exponential model(s) and the singularity model.

Parameters[a]	$\frac{k_{0singu}}{k_{0s}}$ [b]	$\frac{\Delta E_{upsingu}}{\Delta E_{ups}}$ [c]	$\frac{\Delta E_{downsingu}}{\Delta E_{downs}}$ [c]
α=0.20[a],γ=43 cm^{-1}[a],C=50[a],T=298K	25.1	0.81	0.81
α=0.35[a],γ=119 cm^{-1}[a],C=50[a],T=700K	10.8	0.67	0.67
α=0.41[a],γ=163 cm^{-1}[a],C=50[a],T=1000K	7.6	0.63	0.63

[a]Values of parameters were obtained using the trajectory results of O^3/Ar collisions from Ref. [1]. [b]k_{0s} refers to the rate constant of the single exponential model and k_{0singu} refers to the one of the singularity model . [c]A notation similar to that in footnote [b] is used for ΔE_{up} and ΔE_{down}.

Table 1.3: Example of cutoff effect for the near-singularity model.

Parameters[a]	$\frac{k_{0n-singu}}{k_{0s}}$ [b]	$\frac{\Delta E_{upn-singu}}{\Delta E_{ups}}$ [c]	$\frac{\Delta E_{downn-singu}}{\Delta E_{downs}}$ [c]
α=0.20[a],γ=43 cm^{-1}[a],C=50[a],T=298K	24.9	1.06	1.06
α=0.35[a],γ=119 cm^{-1}[a],C=50[a],T=700K	10.8	0.86	0.98
α=0.41[a],γ=163 cm^{-1}[a],C=50[a],T=1000K	7.6	1.04	1.04

[a]Values of parameters were obtained using the trajectory results of O^3/Ar collisions from Ref. [1]. [b]k_{0s} refers to the rate constant of the single exponential model and $k_{0n-singu}$ refers to the rate constant of the near- singularity model with a lower bound. This lower bound is 15 cm^{-1} for T=298K, 25 cm^{-1} for T=700K and 30 cm^{-1} for T=1000K. [c]A notation similar to that in footnote [b] is used for ΔE_{up} and ΔE_{down}.

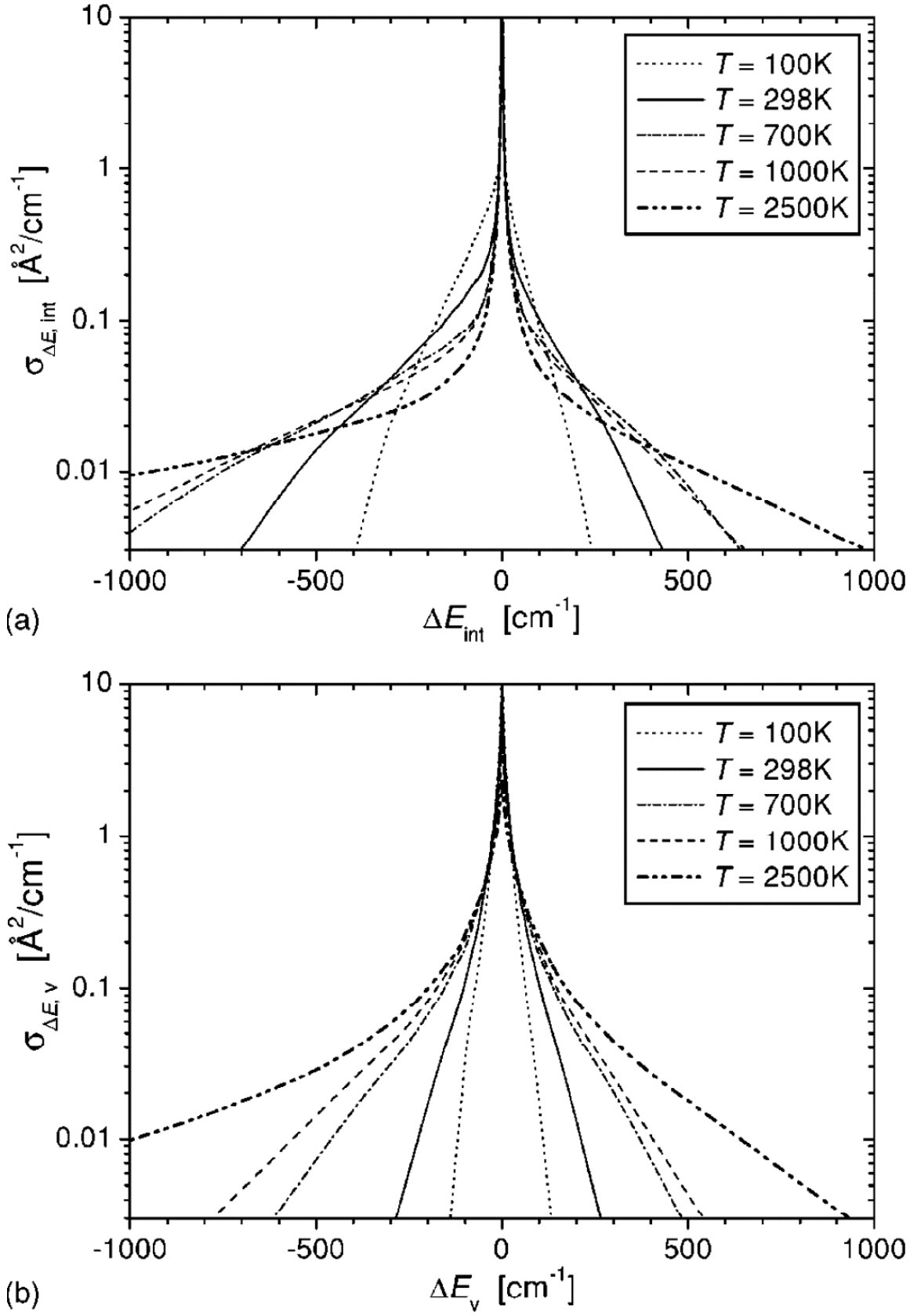

Figure 1.1: Cross sections for internal (a) and vibrational (b) energy transfers as functions of ΔE_{int} and ΔE_v for different temperatures [1].

Chapter 2

Collisional energy transfer in recombination and dissociation reactions:deviation from equilibrium

2.1 Introduction

It has been recognized for many years that ”weak” collisions instead of ”strong” collisions play a major role in the activation and deactivation of the vibrationally hot intermediate complexes in gas phase dissociation, unimolecular isomerizaion, and bimolecular recombination reactions [2–6]. The study of ozone formation and isotopic effects prompted our interest in this subject [7–15, 17–23].

2.2 Theory

2.2.1 General aspects

In general, the formation of a molecule AB is described by

$$A + B \rightarrow AB^*, \tag{2.1}$$

$$AB^* + M \rightarrow AB + M, \tag{2.2}$$

where M is a collision partner and AB^* is a vibrationally excited intermediate. In a ”weak” collision assumption, unlike in a ”strong” collision one, many collisions with an M are required to activate and deactivate a reactant molecule. When the collision is ”weak”, the AB^* may still have enough energy after the collision in reaction (2.2) to redissociate into $A + B$, instead of always being ”deactivated”, and so a set of such equations with different energy is considered, leading to a master equation or to a steady-state equation. The latter is then solved for the probability distribution function for the vibrational energy in the energetic intermediate AB^* [62].

Information on the collisional energy transfer in reactions such as in Eq. (2.2) is usually obtained from the pressure dependence of the reation rate of the overall reactions (2.1) and (2.2), using the solution of the collisional master or steady-state equation to fit these experimental reaction rateversus pressure data. To this

end, a functional form for the collision energy transfer probability, denoted here by $Z(E';E)$, is typically assumed, and its parameters are calculated form the fit. The functional forms used for this purpose are usually the exponential model introduced by Rabinovitch or a step ladder in which the reactant molecule gains or loses energy in collisions in discrete amounts called "steps" [2,3,24,25]. Hold *et al*. also introduced a stretched exponential model [26]. A biexponential model was used by Brown and Miller [27] and modified by Hu and Hase [28]. Complementing these studies have bveen *ab initio* or semiempirical calculations of the collisional energy transfer, frequently using classical mechanical trajectories for the collisions [27–37]. Analytical treatments of vibrational energy transfer have been given for particular cases [6, 35–37, 39]. In particular, a detailed discussion of the original master equation and of its steady-state approximation is given by Penner and Forst, [39] who expressed the solution in terms of hypergeometric functions. Here we adopted the widely used exponential model.

In Chapter 1, we have focused on the limiting low pressure rate constant k_0. It is of particular interest partly because it describes the maximum effect of the collisions and partly because it is simpler to treat than the rate constant at highter pressures, where a solution of the complete master equation would have been necessary. While simple theoretical expressions for the distribution function of different (E, J) states of the reatants and for the energy transfer can also be obtained for the high pressure limit of k, k_∞, they do not provide insight into the effect of energy transfer on k itself, since k_∞ is independent of $Z(E', E)$.

To treat the kinetics for the recombination of two species $A + B \rightarrow AB$, one can either proceed from the reactants $(A+B)$ or the product (AB) [45,62]. Previously we have considered the two cases equivalent, i.e., if a tagged A is followed in time in its progress to form AB, and if a tagged A in AB is followed in time in its progress to form $A + B$, beginning with an equilibrium concentrations of AB for the given A and B concentration, the sum of the tagged distribution functions at any energy E is equal to the equilibrium distribution at that E [62]. Here we try to find out whether we can justify the assumption.

2.2.2 Reaction scheme

Hereafter we denote by $g_{eq}(E)$ the equilibrium probability energy distribution function for AB, $g_r(E)$ the recombination and $g_d(E)$ the dissociation.

Consider $g_d(E)$ first,

$$\frac{\mathrm{d}g_d(E)}{\mathrm{d}t} = -k_d(E)g_d(E)h(E) - \int_{-\infty}^{\infty} g_d(E)Z(E',E)\mathrm{d}E' + \int_{-\infty}^{\infty} g_d(E')Z(E,E')\mathrm{d}E', \qquad (2.3)$$

where $h(E)$ is a unit step function,

$$h(E) = \begin{array}{ll} 0 & , \ E \leqslant 0 \\ 1 & , \ E > 0. \end{array} \qquad (2.4)$$

And then $g_r(E)$,

$$\frac{\mathrm{d}g_r(E)}{\mathrm{d}t} = k_r(E)h(E) - k_d(E)g_(r)(E)h(E) - \int_{-\infty}^{\infty} g_r(E)Z(E',E)\mathrm{d}E' + \int_{-\infty}^{\infty} g_r(E')Z(E,E')\mathrm{d}E', \qquad (2.5)$$

where $k_r(E)$ is actually the recombination rate of the two species A and B, $k_r(E) = k(E)[A][B]$.

Now consider the equilibrium situation,

$$\frac{\mathrm{d}g_{eq}(E)}{\mathrm{d}t} = k_r(E)h(E) - k_d(E)g_{eq}(E)h(E) - \int_{-\infty}^{\infty} g_{eq}(E)Z(E',E)\mathrm{d}E' + \int_{-\infty}^{\infty} g_{eq}(E')Z(E,E')\mathrm{d}E'. \qquad (2.6)$$

Comparing Eqs. (2.3-2.22) we can say that

$$g_{eq}(E) = g_d(E) + g_r(E), \qquad (2.7)$$

since the two sides satisfy the same equations.

2.3 Low pressure limit

2.3.1 Dissociation

We consider the dissociation reaction in the low pressure regime

$$AB + M \rightarrow AB^*(E) + M, \tag{2.8}$$

$$AB^* \rightarrow A + B \qquad (\text{if } E \geqslant 0), \tag{2.9}$$

where $E \geqslant 0$ denotes the internal energies of any reacion intermediate AB^* that can dissociate into the separated reactants without a further collision. Energies E in the reactants that are negative are insufficient for dissociation.

The scheme [Eqs. (2.8) and (2.9)] is appropriate only for the low pressure limit of the dissociation rate. At higher pressures, an $AB^*(E')$ on a second collision can also yield an AB^* with a different E', where both E's are greater than zero. At sufficiently low pressure, each $AB^*(E')$ formed in reaction (2.8) with $E \geqslant 0$ ultimately dissociates into $A + B$ before any further collision. For this case, the problem simplifies and a large set of equations (the master equation) for $AB^*(E')$ is not needed for $E \geqslant 0$.

The low pressure dissociation rate constant k_0 is,

$$k_0 = \int_{E'=0}^{\infty} \int_{E=-\infty}^{0} g_r(E) Z(E', E) \mathrm{d}E \, \mathrm{d}E'. \tag{2.10}$$

The equilibrium probability distribution for an AB that has an energy in the range E,E+dE is $g_{eq}\mathrm{d}E$, where

$$g_{eq}(E) = \rho(E) \mathrm{e}^{-E/kT} / Q \tag{2.11}$$

and $\rho(E)$ denotes the density of quantum states of the molecule AB, Q is the partition function of AB in the center-of-mass system of coordinates. When the energy is measured relative to $E = 0$, the dissociation limit Q is also calculated relative to that energy, and so contains a factor $\mathrm{e}^{D/kT}$, where D is the dissociation energy

of AB measured from the bottom of its potential well to the dissociation level. When E becomes very negative in the steady-state problem, *i.e.*, when $E \to -D$ and $g(E) \to g_{eq}(E)$. This condition on $g(E)$ serves as a boundary condition,

$$g(E) \to g_{eq}(E) \qquad E \to -D. \tag{2.12}$$

For the exponential model, in terms of a deactivation constant γ and of an activation constant γ', we have

$$Z(E', E) = Z_0 e^{(E-E')/\gamma}, \; E' \leqslant E, \tag{2.13}$$

$$Z(E', E) = Z_0 e^{(E'-E)/\gamma'}, \; E' \geqslant E, \tag{2.14}$$

where Z_0 is a constant and γ,γ' are related by microscopic reversibility (detailed balance).

The quantities $Z(E', E)$ and $Z(E, E')$ satisfy microscopic reversibility

$$\rho(E)Z(E', E) = \rho(E')Z(E, E')e^{-(E'-E)/kT}. \tag{2.15}$$

For practical purpose, we can typically treat the lower limit on E as $E \to -\infty$, a minor approximation when $D \gg kT$. Neglecting the effect of the change in $\rho(E)$ between E and E' in the vicinity of $E = 0$, Eqs. (2.13) and (2.14) yield

$$\frac{1}{\gamma'} = \frac{1}{\gamma} + \frac{1}{kT}. \tag{2.16}$$

For the dissociation scheme, the master equation for $E \geqslant 0$ is

$$\frac{dg_d(E)}{dt} = -k_d(E)g_d(E) - \int_{-\infty}^{0} g_d(E)Z(E', E)dE' + \int_{-\infty}^{0} g_d(E')Z(E, E')dE'. \tag{2.17}$$

After a short initial period, $g(E)$ relaxes toward a steady state. With the steady-state

approximation and result for $g_d(E \leqslant 0)$ in our last paper,

$$g_d(E) = \frac{(\gamma + \gamma^{'})\gamma^{'}/kTZ_0 g_{eq}(0)\mathrm{e}^{-E/\gamma^{'}}}{k_d(E) + Z_0\gamma\mathrm{e}^{-E/\gamma}}. \tag{2.18}$$

2.3.2 Recombination

For the recombination case, the master equation for $E \geqslant 0$ is

$$\frac{\mathrm{d}g_r(E)}{\mathrm{d}t} = k_r(E) - k_d(E)g_(r)(E) - \int_{-\infty}^{0} g_r(E)Z(E^{'},E)\mathrm{d}E^{'} + \int_{-\infty}^{0} g_r(E^{'})Z(E,E^{'})\mathrm{d}E^{'}. \tag{2.19}$$

For equilibrium, the master equation for $E \geqslant 0$ is

$$\frac{\mathrm{d}g_{eq}(E)}{\mathrm{d}t} = k_r(E) - k_d(E)g_{eq}(E) - \int_{-\infty}^{\infty} g_{eq}(E)Z(E^{'},E)\mathrm{d}E^{'} + \int_{-\infty}^{\infty} g_{eq}(E^{'})Z(E,E^{'})\mathrm{d}E^{'}. \tag{2.20}$$

Eq.(2.20)-Eq.(2.19),

$$\frac{\mathrm{d}G(E)}{\mathrm{d}t} = -k_d(E)G(E) - \int_{-\infty}^{0} G(E)Z(E^{'},E)\mathrm{d}E^{'} + \int_{-\infty}^{0} G(E^{'})Z(E,E^{'})\mathrm{d}E^{'}. \tag{2.21}$$

where $G(E) = g_{eq}(E) - g_r(E)$.

2.3.3 Comparison

Eq.(2.17) and Eq.(2.21) have the same form. If for $E \leqslant 0$,$G(E) = g_d(E)$, then the same shall hold for $E \geqslant 0$. However as we have calculated in the last paper, $g_d(E \leqslant 0) = g_{eq}(0)(\mathrm{e}^{-E/kT} - \gamma^{'}/\gamma)$. In order to satisfy $g_{eq}(E \leqslant 0) = g_d(E) + g_r(E)$ or $g_d(E \leqslant 0) = G(E)$, then $g_r(E)$ must be a constant $g_{eq}(0)\gamma^{'}/\gamma$.

2.4 Discussion

Is this a reasonable distribution?

$$\frac{\mathrm{d}g_{eq}(E)}{\mathrm{d}t} = -\int_{-\infty}^{\infty} g_{eq}(E)Z(E^{'},E)\mathrm{d}E^{'} + \int_{-\infty}^{\infty} g_{eq}(E^{'})Z(E,E^{'})\mathrm{d}E^{'}. \tag{2.22}$$

$$\frac{\mathrm{d}g_d(E)}{\mathrm{d}t} = -\int_{-\infty}^{\infty} g_r(E)Z(E^{'},E)\mathrm{d}E^{'} + \int_{-\infty}^{\infty} g_{eq}(E^{'})Z(E,E^{'})\mathrm{d}E^{'}. \tag{2.23}$$

Eq.(2.22)-Eq.(2.23),

$$\frac{\mathrm{d}G(E)}{\mathrm{d}t} = -\int_{-\infty}^{\infty} G(E)Z(E^{'},E)\mathrm{d}E^{'} + \int_{-\infty}^{\infty} G(E^{'})Z(E,E^{'})\mathrm{d}E^{'}. \tag{2.24}$$

With steady-state approximation, we can get

$$G(E) = g_d + \int_{0}^{\infty} g_d(E^{'})Z(E,E^{'})\mathrm{d}E^{'}. \tag{2.25}$$

So the dfference comes from that we have assumed earlier that at the low pressure limit in the dissociation reaction scheme, any reaction intermediate AB^* with $E \geqslant 0$ after one collision can dissociate into the separated reactants without a second collision as shown in the second term on the right hand side of the following master equation

$$\frac{\mathrm{d}g_d(E)}{\mathrm{d}t} = -\int_{-\infty}^{\infty} g_r(E)Z(E^{'},E)\mathrm{d}E^{'} + \int_{0}^{\infty} g_d(E^{'})Z(E,E^{'})\mathrm{d}E^{'}. \tag{2.26}$$

From our numerical result it is shown that the effect is around 10^{-2} or smaller. This is fairly small. Since the difference in k_0 is

$$\Delta k_0 = \int_{E^{'}=0}^{\infty}\int_{E=-\infty}^{0} (G(E) - g_r(E))Z(E^{'},E)\mathrm{d}E\,\mathrm{d}E^{'}, \tag{2.27}$$

it shall also be small compared with k_0.

2.5 Concluding remarks

Here we have studied the deviation from the equilibrium distribution. In general, the equilibrium distribution is the sum of the dissociation and recombination distributions. In the low pressure scheme, the deviation comes from the fact that no second collision happens before dissociation for the reactant with energy above

dissociation limit. However, the result shows that the deviation is small.

Chapter 3

Extension of the diffusion controlled electron transfer theory for intermittent fluorescence of quantum dots, inclusion of biexciton and the difference of ˜on˝and ˜off˝time distributions

3.1 Introduction

Single molecule spectroscopy is a powerful and sensitive technique that permits investigation of spatially heterogeneous samples one at a time possible and reveals phenomena masked by ensemble averaging. It has been widely used to study the fluorescence of single quantum dots [63–77], single fluorophores in porous silicon [78], single polymer segments [79], light harvesting complexes [80], fluorescent proteins [81,82], and single dye molecules on various surfaces [83–90]. An interesting phenomenon of blinking or fluorescence intermittency in which abrupt transitions between alternating episodes of absorption of light and fluorecence recycling is followed by sustained periods of darkness where no light is emitted has been observed in these experiemnts. Numerous experiments have been performed since the first observation [63] on the fluorescence blinking of quantum dots [67–77] Several models have been proposed to explain the phenomenon [91–98]. In the present paper we include a role for biexciton, prompted by recent results at higher light intensities by Klimov [99,100], Nesbitt [101], Bawendi [102,103] and Leone [104,105].

3.2 Theory

3.2.1 Diffusion-controlled electrom-transfer (DCET) model

The existence of an approximately $\sim -3/2$ power law for the blinking suggested that diffusion (a spectral diffusion) was involved in the blinking [93,106]. Subsequentially, to treat the intermittency phenomenon, a four-level DCET model was proposed [97,98,107]. A DCET mechanism is assumed to govern the charge transfer reactions between a bright (``on´´) state $|1\rangle$ of the quantum dot and a charge-separated state $|2\rangle$ which appears dark due to a fast Auger relaxation process from the excited state $|3\rangle$ (Figures 3.1 and 3.2) [108]. State $|2\rangle$ is a long-lived state, originally assumed to be a charge-separated state with a weak electronic coupling between the hole in the core of a QD and a surface-trapped electron [97,98]. More

recently to allow for the formation of a trapped state by an assumed Auger process, a resonance between $1S_e - 1P_e$ transition and $1S_h$-surface state transition it was assumed to have an electron in the S_e state of the QD and a hole in a surface state [107], in particular [109] a Se^- instead of Se^{2-} in a dangling surface atom of the CdSe QD. Here we adopt the latter as the definition of $|2\rangle$. Under continuous illumination, fast population recycling occurs between $|1\rangle$ and $|0\rangle$, the ground state, due to population pumping and fluorescence decay. Assuming a nonadiabatic electron transfer (ET) between $|1\rangle$ and $|2\rangle$, and an initial Boltzmann population at the $|0\rangle$ prior to the illuminaiton, the rate equation for the population density $\rho_j(Q,t)$ for the jth state ($j = 0, 1, 2, 3$) as shown in Figure 3.1 at reaction coordinate Q is given by [97]

$$\frac{\partial \rho_0(Q,t)}{\partial t} = \gamma_0 \rho_1(Q,t) - W_1 \rho_0(Q,t), \tag{3.1}$$

$$\frac{\partial \rho_1(Q,t)}{\partial t} = L_1 \rho_1(Q,t) - k_t \delta(Q - Q^{\neq})[\rho_1(Q,t) - \rho_2(Q,t)] - \gamma_0 \rho_1(Q,t) + W_1 \rho_0(Q,t), \tag{3.2}$$

$$\frac{\partial \rho_2(Q,t)}{\partial t} = \gamma_2 \rho_3(Q,t) - W_3 \rho_2(Q,t) - k_t \delta(Q - Q^{\neq})[\rho_2(Q,t) - \rho_1(Q,t)], \tag{3.3}$$

where k_t is the rate constant for the transition [107] between these electronic states [110], $Q^{\neq}$ is the value of the reaction coordinates Q where the two electronic states are in resonance and

$$\frac{\partial \rho_3(Q,t)}{\partial t} = L_3 \rho_3(Q,t) - \gamma_2 \rho_3(Q,t) + W_3 \rho_2(Q,t), \tag{3.4}$$

Here, L_j is the diffusion operator

$$L_j \equiv D_j \frac{\partial}{\partial Q}\left[\frac{\partial}{\partial Q} + \frac{1}{k_B T}\frac{\partial}{\partial Q} U_j(Q)\right], \tag{3.5}$$

where $\tau_{L,j}$ is the diffusion correlation time constant, D_j is the diffusion constant, W_1 is the pumping rate and γ_0 is the rate constant of the natural fluorescence decay.

When the QD is in state $|0\rangle$ or $|1\rangle$, the emitter is ``on´´. while when it is in state $|2\rangle$

or $|3\rangle$, the emitter is ``off''. So the ``on''population is $\rho_0+\rho_1$ and ``off''is $\rho_2+\rho_3$. In the following we denote the total population density of ``on''by ρ_l and that of ``off''by ρ_d. With $W_1 \ll \gamma_0$ and at any time $t \gg 1/W_1$, a quasiequilibrium is established between $|0\rangle$ and $|1\rangle$. There is a similar quasi-equilibrium between $|2\rangle$ and $|3\rangle$. Thus, eqs 3.2 and 3.3 can be approximated by

$$\frac{\partial \rho_{l/d}(Q,t)}{\partial t} = L_{l/d,eff}\rho_{l/d}(Q,t) - k_t\delta(Q-Q^{\neq})[\rho_k(Q,t) - \rho_{d/l}(Q,t)], \tag{3.6}$$

where $L_{l/d,eff} = \zeta_{l/d}L_j$,$\zeta_l \equiv W_1/(W_1+\gamma_0) \sim W_1/\gamma_0$,$\zeta_d \equiv 1$.

Solving these coupled rate equations, one obtains the time-evolution of the fluorescence decay. In the present paper, we focus on single quantum dots rather than also including ensembles.

3.2.2 Single quantum dot behavior in the time regime much shorter than the cut-off time

As indicated above the four-state model under steady-state approximation is treated as an effective two-state model. In this two-state interpretation, a single emitter is either in an ``on''or an ``off''state, and so can not be ``on''and ``off''at the same time. When the quantum dot has stayed in the ``on''or ``off''state for a time much shorter than the time of diffusing to the bottom of the ``on''or ``off''potential energy well from the point where the two free energy curves cross, the effect of the slope of the potential is not significant for the diffusion. In this case, the evolution equations for single dot are

$$\frac{\partial \rho_l(Q,t)}{\partial t} = D\frac{\partial^2 \rho_l(Q,t)}{\partial Q^2} - \delta(Q)k_1\rho_l(Q,t), \tag{3.7}$$

$$\frac{\partial \rho_d(Q,t)}{\partial t} = D\frac{\partial^2 \rho_d(Q,t)}{\partial Q^2} - \delta(Q)k_2\rho_d(Q,t), \tag{3.8}$$

There is a sink where the curves of ``on´´and ``off´´in Fugure 3.2 cross, since there the two electronic states are in resonance and so ``on´´to ``off´´or ``off´´to ``on´´electronic transitions can occur. We denote k_1 is by ``on´´to ``off´´ET rate constant and k_2 the ``off´´to ``on´´one at this intersection. In this purely two-state system, for the transition at this crossing point $k_1 = k_2$. Thus hereafter we use k_t instead of k_1 and k_2.

Using the Green function method to solve these equations, the solution is

$$\rho_{l/d}(Q,t) = \int \mathrm{d}Q^{'} \rho_{l/d}(Q,0) G_{l/d}(Q,Q^{'};t,0) - \int \mathrm{d}Q^{'} \int \mathrm{d}t^{'} \delta(Q^{'}) k_t \rho_{l/d}(Q^{'},t^{'}) G_{l/d}(Q,Q^{'};t,t^{'}), \tag{3.9}$$

where the Green function is [111]

$$G_{l/d}(Q,Q^{'};t,t^{'}) = \frac{1}{\sqrt{4\pi D(t-t^{'})}} \mathrm{e}^{-\frac{(Q-Q^{'})^2}{4D(t-t^{'})}} \equiv G_{l/d}(Q,Q^{'};t-t^{'}), \tag{3.10}$$

and the Laplace transform $G_{l/d}(Q,Q^{'};t,t^{'})$ is given by

$$\tilde{G_{l/d}}(Q,Q^{'};s) = \int_0^{\infty} \mathrm{d}(t-t^{'}) \mathrm{e}^{-st} G_{l/d}(Q,Q^{'};t-t^{'}) \approx \frac{1}{\sqrt{4\pi D}} \frac{1}{\sqrt{s+\Gamma_{l/d}}}. \tag{3.11}$$

The Laplace transform of eq 3.9 is

$$\tilde{\rho_{l/d}}(Q,s) = \tilde{G_{l/d}}(Q,0;s) - k_t \tilde{\rho_{l/d}}(0,s) \tilde{G_{l/d}}(Q,0;s), \tag{3.12}$$

Thus, for the ``on´´state, we have for $Q = 0$, the crossing point of the two free energy curves,

$$\tilde{\rho}_l(0,s) = \tilde{G}_l(0,0;s) - k_t \tilde{\rho}_l(0,s) \tilde{G}_l(0,0;s), \tag{3.13}$$

and so

$$\tilde{\rho}_l(0,s) = \frac{\tilde{G}_l(0,0;s)}{1 + k_t \tilde{G}_l(0,0;s)}, \tag{3.14}$$

From eqs 3.12 and 3.14, we obtain

$$\tilde{\rho}_l(Q,s) = \frac{\tilde{G}_l(Q,0;s)}{1 + k_t\tilde{G}_l(0,0;s)}. \tag{3.15}$$

The distribution of the ``on´´time $P_l(t)$ is the rate of the loss for the total population in the ``on´´state, $P_l(t) = -\frac{\mathrm{d}}{\mathrm{d}t}\int_{-\infty}^{\infty}\mathrm{d}Q\rho_l(Q,t)$ and the Laplace transform of $P_l(t)$ is

$$\tilde{P}_l(s) = -\int_0^{\infty}\mathrm{d}t\mathrm{e}^{-st}\frac{\mathrm{d}}{\mathrm{d}t}\int\mathrm{d}Q\rho_l(Q,t) = 1-s\int\mathrm{d}Q\frac{\tilde{G}_l(Q,0;s)}{1 + k_t\tilde{G}_l(0,0;s)} = 1-s\frac{\int_0^{\infty}\mathrm{d}t\mathrm{e}^{-st}\int\mathrm{d}QG_l(Q,0;t,0)}{1 + k_t\tilde{G}_l(0,0;s)} \tag{3.16}$$

Introducing eq 3.11 for $\tilde{G}_l(Q,Q';s)$, eq 3.11 into eq 3.16, we obtain

$$\tilde{P}_l(s) = \frac{1}{1 + \sqrt{\frac{s}{k_t^2/4D}}}. \tag{3.17}$$

The inverse Laplace transform yields

$$P_l(t) = \frac{1}{\sqrt{\pi t_c t}}[1 - \sqrt{\frac{\pi t}{t_c}}\mathrm{e}^{\frac{t}{t_c}}\mathrm{erfc}(\sqrt{\frac{t}{t_c}})], \tag{3.18}$$

where $t_c = \frac{4D}{k_t^2}$ is the critical time in which the population has largely been depleted near the sink (time to set up a steady-state) due to disappearance into the sink at the crossing.

When $t \ll t_c$,

$$P_l(t) \approx \frac{1}{\sqrt{\pi t_c t}}, \tag{3.19}$$

and when $t \gg t_c$,

$$P_l(t) \approx \frac{\sqrt{t_c}}{\sqrt{4\pi t^3}}. \tag{3.20}$$

There is a discontinuity in the approximate eqs 3.19 and 3.20 at t_c, but not for the exact eq 3.18. Results similar to eqs 3.18 - 3.20 are obtained for the ``off´´state.

In this section, only single photon excitation was considered, thereby only for low intensity laser excitation, since the probability of many photon excitation

is small. In experiments with higher laser light intensity [101, 103, 105, 112] the generation of multiexciton has been realized. No clear exponential cut-off has yet been observed within the current single trajectory experimental time regime for the ``off´´state. Nesbitt and coworkers propose that the exponential cut-off of the power law distribution for the ``on´´state time is due to multiexciton generation [101,105]. However, for the ``off´´state, because of the rapid Auger recombination from the excited state to the ground state, there is little chance for multiexciton generation. In the next section we modify the model so as to treat the increased light intensity effect of biexciton generation.

3.3 Many photon absorption, biexciton generation and the exponential tail of ``on´´time distribution

3.3.1 Model with multi photon absorption and biexciton generation

With biexciton generation, a four-level system is insufficient to describe the quantum dot fluorescence behavior. We now include the new species, a biexciton, as shown in Figure 3.3. We consider the biexciton species as a new level $|b\rangle$. Equations 3.1, 3.2 and 3.4 will be modified with $|b\rangle$,

$$\frac{\partial \rho_0(Q,t)}{\partial t} = \gamma_0 \rho_1(Q,t) - W_1 \rho_0(Q,t) - W_b \rho_0(Q,t), \tag{3.21}$$

$$\frac{\partial \rho_1(Q,t)}{\partial t} = L_1 \rho_1(Q,t) - k_t \delta(Q-Q^{\neq})[\rho_1(Q,t) - \rho_2(Q,t)] - \gamma_0 \rho_1(Q,t) + W_1 \rho_0(Q,t) + k_r \rho_b(Q,t), \tag{3.22}$$

$$\frac{\partial \rho_2(Q,t)}{\partial t} = \gamma_2 \rho_3(Q,t) - W_3 \rho_2(Q,t) - k_t \delta(Q-Q^{\neq})[\rho_2(Q,t) - \rho_1(Q,t)], \tag{3.23}$$

$$\frac{\partial \rho_3(Q,t)}{\partial t} = L_3\rho_3(Q,t) - \gamma_2\rho_3(Q,t) + W_3\rho_2(Q,t) + k_i\rho_b(Q,t), \tag{3.24}$$

$$\frac{\partial \rho_b(Q,t)}{\partial t} = L_b\rho_b(Q,t) - (k_r + k_i)\rho_3(Q,t) + W_b\rho_0(Q,t), \tag{3.25}$$

where W_b is the rate constant for biexciton formation, L_b is the diffusion operator for the biexciton state, k_r is the total recombination rate constant of the biexciton state for reformation of the single exciton state radiatively and nonradiatively and k_i is an Auger ionization rate constant to form the ``off'' state.

The probability of formation of biexciton is much smaller than that of single exciton at the light intensities we discuss in this paper, *i. e.*, $W_b \ll W_1$, so that we can assume a steady-state approximation for ρ_2,sufficiently small that we can neglect the diffusion operator, $L_{b,eff} = \frac{W_b}{W_b+W_1+\gamma_0}L_b \ll L_b$. And we obtain a population evolution equation similar to eq 3.6,

$$\frac{\partial \rho_{l/d}(Q,t)}{\partial t} = L_{l/d,eff}\rho_{l/d}(Q,t) - k_t\delta(Q-Q^{\neq})[\rho_{l/d}(Q,t) - \rho_{3-k}(Q,t)] - k_{l/d,b}\rho_{l/d}(Q,t), \tag{3.26}$$

where $L_{l,eff} = \frac{W_1}{W_b+W_1+\gamma_0}L_1 \sim \frac{W_1}{W_1+\gamma_0}L_1$, $L_{d,eff} = \frac{W_3}{W_3+\gamma_2}L_2$, $k_{l,b} = \frac{k_i}{k_r+k_i}W_b$ and $k_{d,b} = 0$.

Thereby, the evolution equation for the single quantum dot ``on'' state is modified to

$$\frac{\partial \rho_l(Q,t)}{\partial t} = D\frac{\partial^2 \rho_l(Q,t)}{\partial Q^2} - \delta(Q)k_t\rho_l(Q,t) - k_{l,b}\rho_l(Q,t). \tag{3.27}$$

while the ``off'' one remains the same, since we assume that for the ``off'' state, the relaxation to the ground state $|2\rangle$ after the light absorption is so fast that the probability of multiexciton generation is extremely small (smaller by a factor of 10^3)..

The solution of eq 3.27 is the solution of the previous equation that had no biexciton generation, multiplied by the term $\exp(-k_{l,b}t)$,

$$P_l(t) = \frac{1}{\sqrt{\pi t_c t}}[1 - \sqrt{\frac{\pi t}{t_c}}e^{\frac{t}{t_c}}\mathrm{erfc}(\sqrt{\frac{t}{t_c}})]\exp(-k_{l,b}t). \tag{3.28}$$

While the ``off''time distribution, during which the quantum dot is still wandering around the sink, remains a power law form, the ``on''time distribution is now a power law with an exponential tail. We shall in the following section derive a result that the tail has a quadratic dependence on the excitation light intensity as pointed out in experiments [101, 105] shown in Figures 3.4 and 3.5.

3.3.2 Quadratic dependence of the ``on''time distribution exponential tail on the excitation light intensity

Both pulsed laser excitation and continuous wave (cw) laser excitation have been used in QD fluorescence intermittence experiments [101]. We shall only derive the biexciton generation probability for the pulsed laser excitation [101]. The derivation for the cw laser will be very similar [101].

Compared with the fluorescence lifetime of QD, the laser pulse width τ_p is very short while the interval ΔT_i between pulses is long. Therefore, we can neglect the possibility of multi photon absorption from different pulses and only consider it from the same pulse [113], *i.e.*, the number of excitons per pulse. We denote this quantity by N_x and calculate $\langle N_x \rangle$.

A photon absorption depends on the absorption cross section σ, the laser beam area A and the number of photons entering in each pulse N [101, 103]. For a fixed frequency laser source, N/A is proportional to the laser excitation power I. The average exciton number of a QD for Gaussian beam excitation [101] is $\langle N_x \rangle = \frac{N\sigma \ln 2}{A}$. If we assume the absorption of photons consists of independent events, then it is Poisson distribution. The probability that n photons are absorbed per quantum dot per pulse or the probability that n excitons are generated per pulse is

$$P(n) = \mathrm{e}^{-\langle N_x \rangle} \frac{\langle N_x \rangle^n}{n!} \tag{3.29}$$

Thus the probability of generating a biexciton is

$$P(2) = \mathrm{e}^{-\langle N_x \rangle} \frac{\langle N_x \rangle^2}{2} \tag{3.30}$$

The excitation rate constant W_b is $P(2) f_p$ where f_p is the laser pulse frequency, *i.e.*, the number of pulses per second. We now can write

$$W_b = \mathrm{e}^{-\langle N_x \rangle} \frac{\langle N_x \rangle^2}{2} f_p \tag{3.31}$$

Under low intensity excitation, $\langle N_x \rangle \ll 1$, eq 3.31 can be approximated as $\frac{\langle N_x \rangle^2}{2} f_p$. With the number of photons per pulse $N = \frac{I}{\hbar \omega f_p}$, $W_b \propto I^2$, where I is the excitation intensity. If the k_r and k_i do not have I dependence, which is typically the case. Since $k_{l,b} = \frac{W_b}{k_r + k_i} k_i \equiv P_{ionization} W_b$ then $k_{l,b}$ will also be proportional to I^2. $P_{ionization}$ is the ionization efficiency [101]. Now we can see from eq 3.28 that the exponential tail has an I^2 dependence,

$$1/\tau_{fall-off} \equiv k_{l,b} = P_{ionization} W_b \approx P_{ionization} \frac{\langle N_x \rangle^2}{2} f_p \propto I^2. \tag{3.32}$$

Thereby, in the modified DCET model, the exponential cut-off of the ``on´´time distribution has an I^2 dependence.

3.4 Results and discussion

Fitting the ``on´´data in Figure 3.4 with the distribution $P_1(t) = At^{-m} \exp(-t/\tau_{cut-off})$ in which the exponential cut-off $1/\tau_{fall-off} \propto I^2$ is shown in Figure 3.6. However, the slope m is different from 3/2 nd the difference increases with the light intensity increase. Fitting with slopes of exactly 3/2 is shown in Figure 3.7 and one can clearly see the deviation of the short time data points from the fitting lines gets larger at higher light intensity. The mechanism of this light intensity dependence of the power law slope is not yet understood.

At low light intensity, we have $P_{ionization} \approx \frac{2}{\tau_{fall-off} \langle N_x \rangle^2 f_p}$. Following procedures in

ref 101, we can approximately calculate the ionization probability $P_{ionization}$. For a 5 MHz pulsed laser with excitation power 66 W/cm^2, $P_{ionization} \sim 10^{-5}$. As indicated in ref 101, this value of ionization efficiency is in reasonable agreement with the previous measurements [114–116]. According to Bawendi and coworkers [102] the quantum yield of biexciton η_b is

$$\eta_b = k_{radi}/(k_{radi} + k_{nonradi}) \sim 1 : 10, \tag{3.33}$$

where k_{radi} and $k_{nonradi}$ are the radiative and nonradiative recombination rate constants. The lifetime of biexciton is of the order of several hundred ps [103], thus the radiative recombination rate constant $k_{radi} \sim 10^9$/s and the nonradiative recombination rate constant $k_{nonradi} \sim 10^{10}$/s. The nonradiative recombination rate constant for biexciton is smaller than that of the dark exciton. However, if the nonradiative processes of the two species are both Auger kind, then $k_{nonradi}$ is supposed to be larger than the dark exciton one [103]. Thus as proposed in ref 103, the two processes are probably different. The total recombination rate constant $k_r + k_i$ is $\sim 10^{10}$/s. Since the ionization rate constant $k_i = (k_r + k_i)P_{ionization}$, $k_i \sim 10^6$/s. Therefore, the nonradiative ionization recombination is a slow process or a rare event compared with radiative or other nonradiative recombination.

3.5 Conclusion

The DCET model has been modified so as to explain the exponential cut-off of the power law time distribution of the ``on´´state of the single quantum dot fluorescence blinking process, the quadratic dependence of the exponential tail on the excitation intensity, and the asymmetry between ``on´´and ``off´´states, the former having an exponential tail in the observed time domain.

Figure 3.1 Schematic diagram for the DCET model.$|0\rangle$ and $|1\rangle$ are the ground and excited ``on´´states.The radiationless decay from the higher excited states to $|1\rangle$ is much faster than fluorescence decay $\gamma_0$ from $|1\rangle$ to $|0\rangle$, $W_1$ is the photoexcitation rate. The transition between $|1\rangle$ and the ground ``off´´state $|2\rangle$ represents the Auger-assisted resonace charge separation and recombination processes which involves several electrons and holes. Decay from the excited ``off´´state $|3\rangle$ to $|2\rangle$ caused by a (radiationless) Auger processes (γ_2) on ordinary sustrates, but can become radiative on gold surface. $|G\rangle$, $|L*\rangle$, $|D\rangle$ and $|D*\rangle$ in ref 97 correspond to $|0\rangle$, $|1\rangle$, $|2\rangle$ and $|3\rangle$ here.

Figure 3.2 Diffusion on the parabolic potential surfaces $|l\rangle$ and $|d\rangle$ across a sink at the energy-level crossing governs the intermittency phenomenon.(corresponding to Figure 2 (b) from ref 97)

Figure 3.3 Schematic diagram for the modified DCET model with biexciton generation. An biexciton state $|b\rangle$ is formed from the ground state $|0\rangle$ at rate W_b and can recombine to form the single exciton state $|1\rangle$ or get ionized to the ``off´´states.

Figure 3.4 On-time (left panel) and off-time (right panel) probability distributions measured under pulsed laser conditions at λ_{exc}=434 nm and laser intensities of 230 (red), 120 (blue), and 66 W/cm^2 (green). The dolid lines are fits to the data.(Figure 3 from ref 101)

Figure 3.5 Average falloff rate at λ_{exc}=434 nm determined from $\sim$ 40 QDs at each power level, error bars determined from standard deviation of the mean. The inset shows the same data plotted on a log-log scale, illustrating quadratic dependence of the average falloff rate on laser power. Solid lines are fits to the data.(Figure 4 from ref 101)

Figure 3.6 On-time probability distributions measured under pulsed laser conditions at λ_{exc}=434 nm and laser intensities of 230 (red), 120 (blue), and 66 W/cm^2 (green). The solid lines are fits to the data with exponential cut-off $1/\tau_{fall-off} \propto I^2$.

Figure 3.7 On-time probability distributions measured under pulsed laser conditions at λ_{exc}=434 nm and laser intensities of 230 (red), 120 (blue), and 66 W/cm^2 (green). The solid lines are fits to the data with exponential cut-off $1/\tau_{fall-off} \propto I^2$.

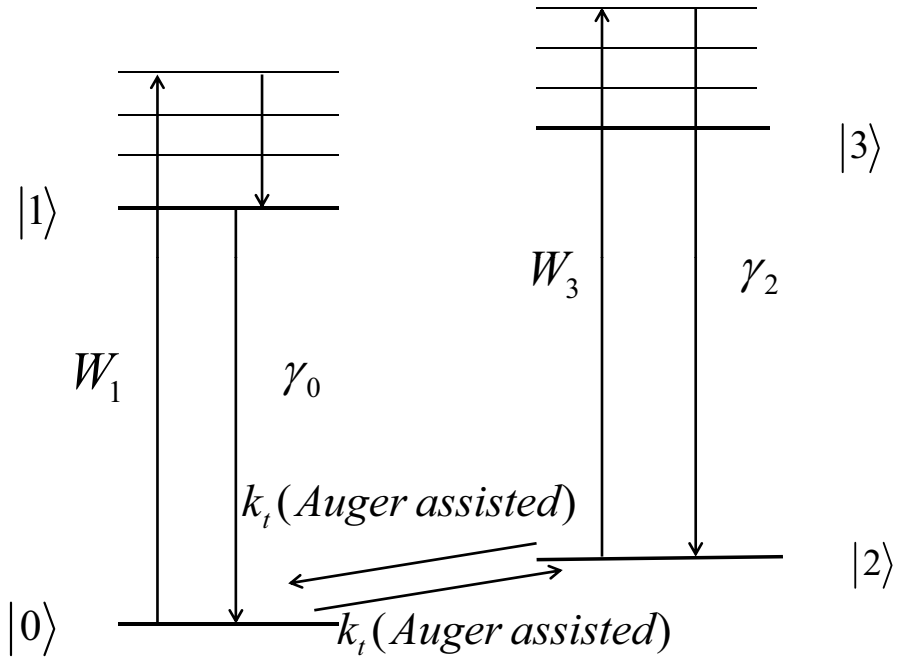

Figure 3.1:

The slopes of the power law part are 3/2.

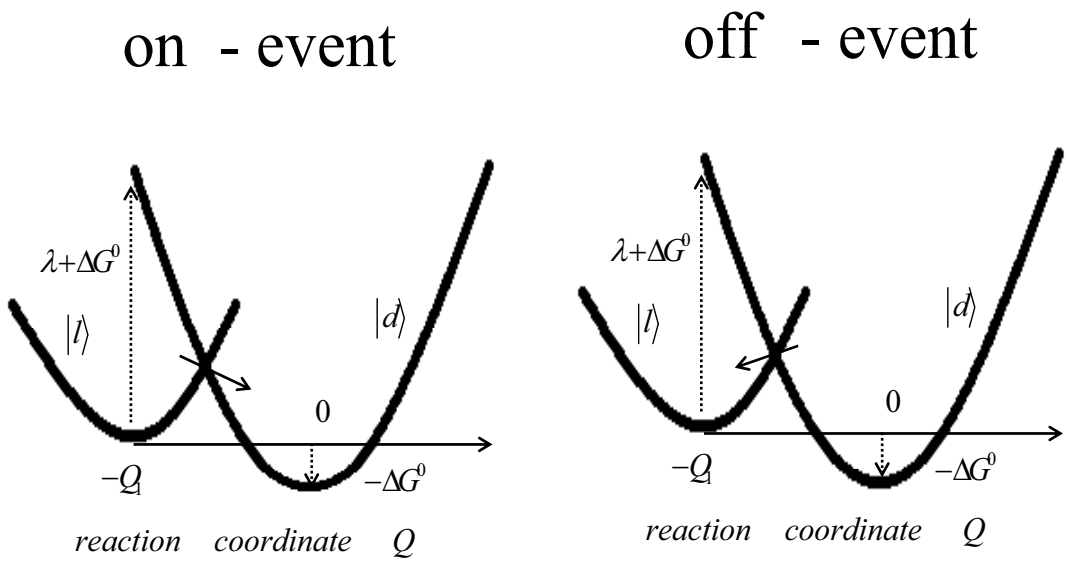
on - event
off - event
$\lambda+\Delta G^0$
$|l\rangle$
$|d\rangle$
0
$-Q_1$
$-\Delta G^0$
reaction coordinate Q
$\lambda+\Delta G^0$
$|l\rangle$
$|d\rangle$
0
$-Q_1$
$-\Delta G^0$
reaction coordinate Q

Figure 3.2:

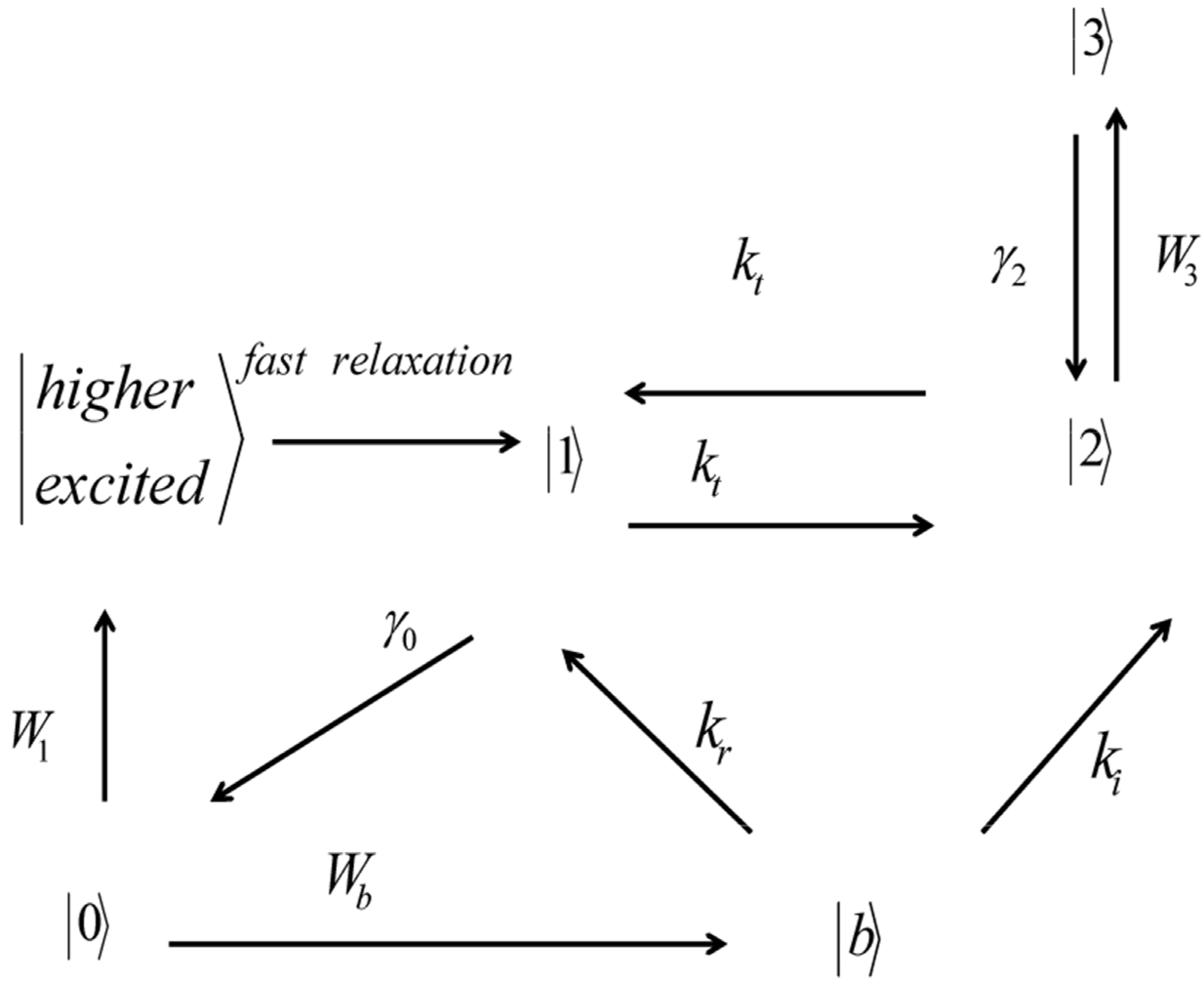
|3⟩
k_t
γ_2
W_3
|higher excited⟩
fast relaxation
|1⟩
k_t
|2⟩
γ_0
W_1
k_r
k_i
W_b
|0⟩
|b⟩

Figure 3.3:

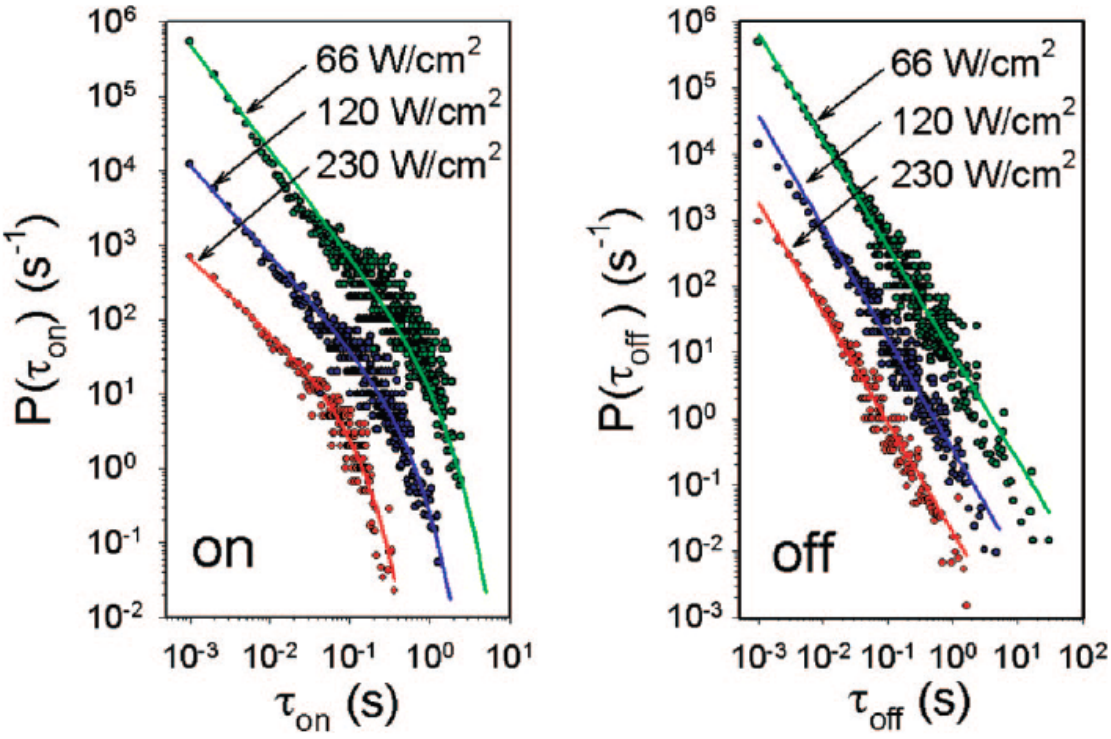

Figure 3.4:

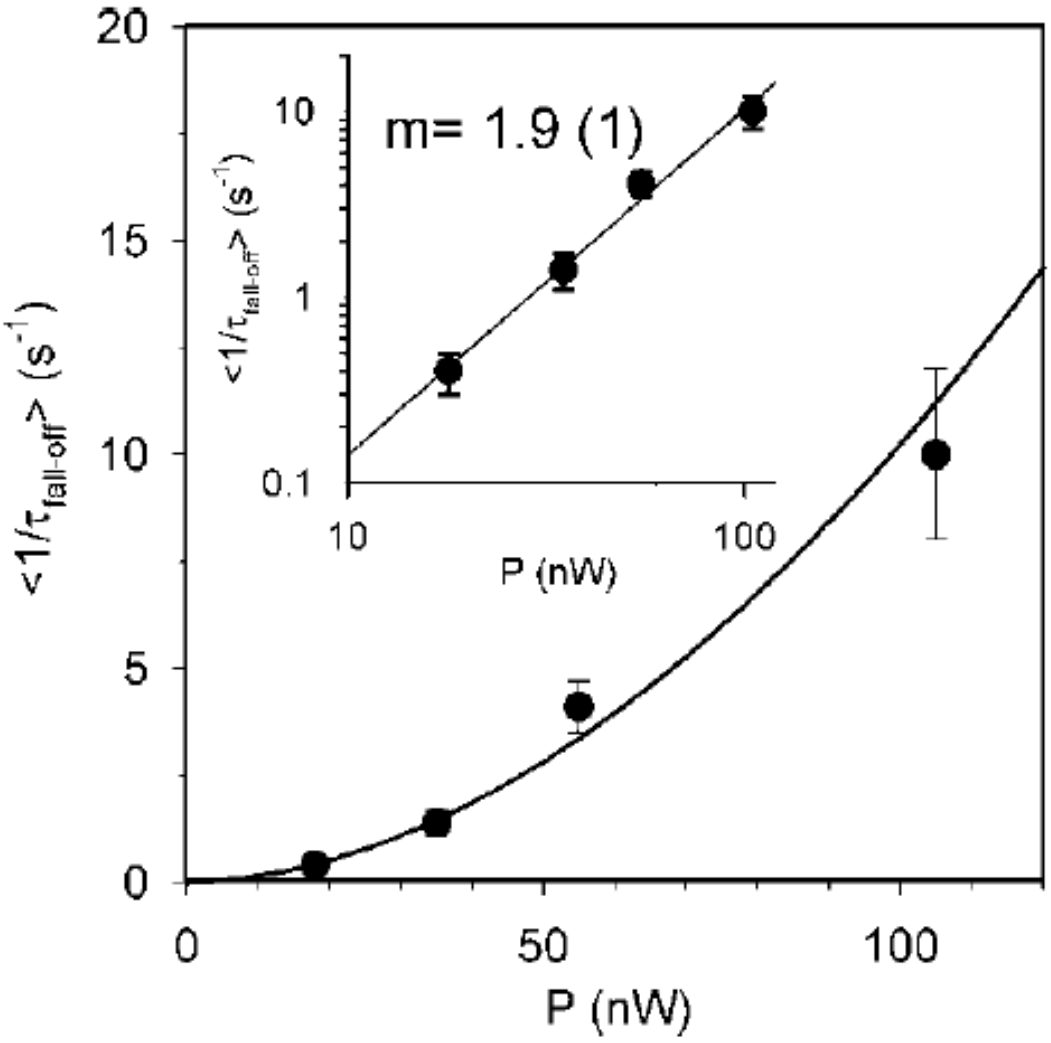
20
15
10
5
0
0
50
100
P (nW)
<1/τfall-off> (s-1)
m= 1.9 (1)
10
1
0.1
10
100
P (nW)
<1/τfall-off> (s-1)

Figure 3.5:

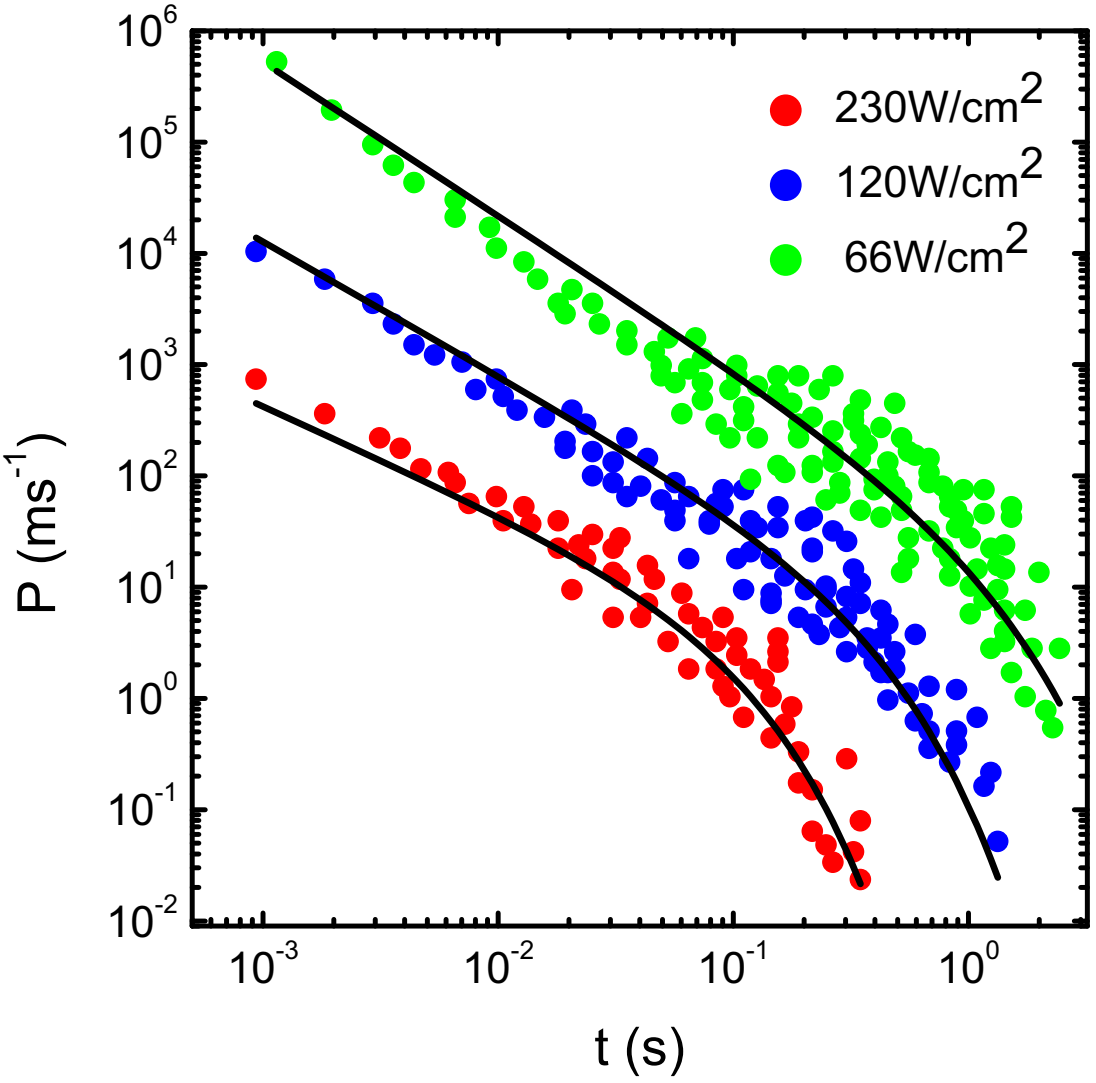
230W/cm2
120W/cm2
66W/cm2
P (ms-1)
t (s)
10^6
10^5
10^4
10^3
10^2
10^1
10^0
10^-1
10^-2
10^-3
10^-2
10^-1
10^0

Figure 3.6:

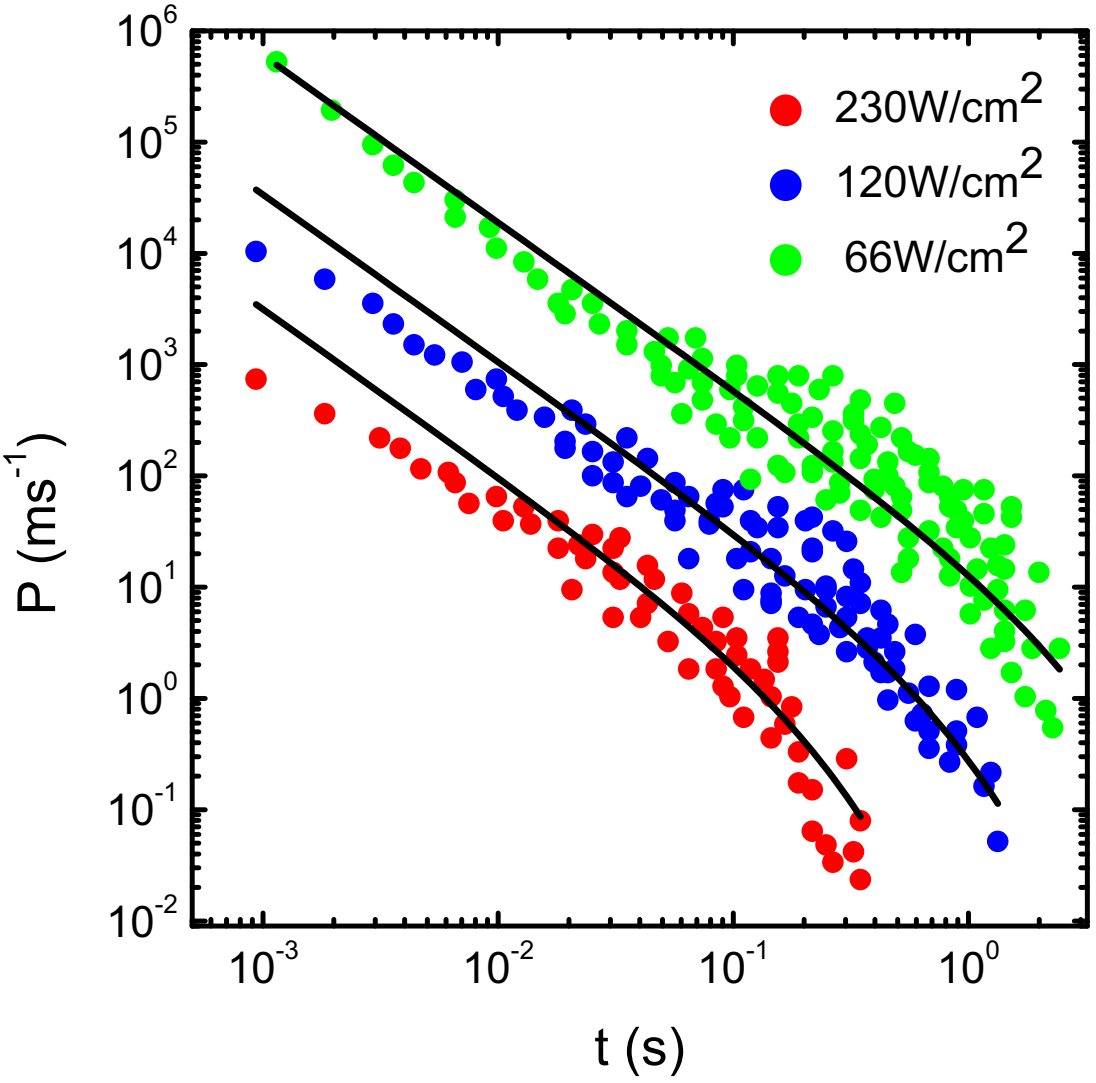
230W/cm2
120W/cm2
66W/cm2
P (ms-1)
t (s)
10^6
10^5
10^4
10^3
10^2
10^1
10^0
10^-1
10^-2
10^-3
10^-2
10^-1
10^0

Figure 3.7:

Chapter 4

Aging and nonergodicity phenonmena in quantum dots fluorescence process

4.1 Background

With the realization of single-molecule spectroscopy and single-photon sources [95,117–120], many single particle charateristics are also unveiled [66,68,69,71,72, 79,81,121–130] that supplement the ensemble properties. Among these properties the single semiconductor nanocrytals or quantum dots (QDs) fluorescence properties have attracted much attention because of their size-induced spetral tunability, high quantum yield, and remarkable photostability at room temperature. In single molecule level experiments, QDs, such as CdSe QDs, exhibit fluorescence intermittency or so called 'blinking' as a variety of other fluorescence systems which means that the fluorescence intensity switches from bright ('on') states to dark ('off') states under lumination [63,68,69,71,108,131]. Surprisingly, distributions of on and off times exhibit power law statistics. While the physical origin of the intermittency is still in debate [68,73,104,107,128,132], the statistical properties have been studied indetail [71,94,96,98,133,134].

The essence of this chapter is to show that although a 'cutoff' has not yet been observed for the 'off' state in single molecule experiments, ensemble measurements tell us that a 'cutoff' of the 'off' state does exist.

4.2 Time average correlation function and ensemble average correlation function

Statistical behavior of single QD or single molecule is commonly characterized by the intensity correlation functions [72, 94, 135]. Experiments on single QDs show how the correlation function method yields dynamical information over time scale from nanosecond to tens of seconds [135]. However, the process govens the blinking might not be ergodic and then we can't directly go from the time average correlation function of single trajectory (ST) to ensemble average. For ST, the time average correlation function of the fluorescence intensity $I(t)$ [96] in the

trajectory length T is defined as

$$C_{ST}(t,T) = \frac{\int_0^{T-t} I(t+t^{'})I(t^{'})\mathrm{d}t^{'}}{T-t}. \tag{4.1}$$

Nevertheless, if we generate many trajectories and obtain $I(t)I(t+t^{'})$ for each trajectory, weight and sum together, we get the ensemble average correlation function if the number of trajectories N is large enough,

$$C(t,t^{'}) = \lim_{N\to\infty} \frac{\sum_{i=1}^{N} I_i(t+t^{'})I_i(t)}{N}. \tag{4.2}$$

It is usually written as $C(t,t^{'}-t) = \lim_{N\to\infty} \frac{\sum_{i=1}^{N} I_i(t^{'})I_i(t)}{N}$ in the literature. We have a different notation. Hereafter we denote by $t^{'}$ the commonly used $t^{'}-t$ which is the time difference.

If the process is ergodic, then we can simplely write down $C(t,t^{'}) = C_{ST}(t,T)$. On the other hand, if the process is nonergodic the ensemble average will no longer be equal to the time average. And $C_{ST}(t,T)$ is not the same from one trajectory to another even as $T \to \infty$. In the next two sections we will discuss the aging behavior and ergodicity of the quantum dot fluorescence blinking process.

If the dots have sit in dark for a quite while, then they all go back to the bright state [74]. The initial fluorescence intensity will be defined as unity. The ensemble fluorescence intensity $< I(t) >$ hence is, $C(0,t)$.

4.3 Aging

Aging means that the ensemble intensity correlation function $C(t,t^{'})$ defined above not only depends on the time difference $t^{'}$ but also varies with t even at long t, *i.e.*, it is not a stationary process.

4.3.1 'On' and 'off' power law

If the 'on' and 'off' duration time distributions are both in power law form $P(t) = At^{-m}$, with the power exponent $1 < m < 2$ we will get infinite average 'on' and 'off' times, τ_{on} and τ_{off}. With the assumption that the 'on' and 'off' processes are symmetric, the power exponents for the two processes are the same. According to Barkai [96], the correlation function at long t and $t^{'}$ is

$$C(t,t^{'}) = B - C\frac{\sin\pi(m-1)}{\pi}\beta(\frac{1}{1+t/t^{'}};2-m,m-1) \equiv h(t/(t+t^{'})), \tag{4.3}$$

where $\beta(z;a,b) = \int_0^z x^{a-1}(1-x)^{b-1}\mathrm{d}x$ is the incomplte beta function.

Therefore the correlation function at long time limit is still varying with time t which proves that the system is not reaching stationarity and there is aging. And the ensemble fluorescence intensity $< I(t) >$ will go to 0 as $t \to \infty$. We will expect that no matter how long the experimental time is or how many trajectories we obtain, the sample size is not large enough to cover the whole mechanism.

4.3.2 Power law with exponential cutoff for 'on' and power law only for 'off'

The 'off' duration time distribution is still in the power law form $P(t) = At^{-m}$ but the 'on' one is $P(t) = At^{-m}\exp(-\Gamma t)$. Then τ_{on} is finite while τ_{off} is still infinite. The correlation function at long t and $t^{'}$ is govened by the 'off' process. As shown in [96],

$$C(t,t^{'}) =< I(t) >< I(t^{'}) > \tau_{on}^2 \sim (tt^{'})^{m-2}. \tag{4.4}$$

This is an aging system, too. And the ensemble fluorescence intensity $< I(t) >$ will also go to 0 as $t \to \infty$.

4.3.3 Power law with exponential cutoff for both 'on' and 'off'

The τ_{on} and τ_{off} are both finite and it should be similar with the exponential distribution 'on' and 'off' situation discussed in [94]. If the experimental time is much longer than τ_{on} and τ_{off}, then at long t, the process becomes stationary

$$C(t, t^{'}) = g(t^{'}). \tag{4.5}$$

At this steady state, the ensemble fluorescence intensity $< I(t) >$ will be $\frac{\tau_{on}}{\tau_{on}+\tau_{off}}$.

4.4 Nonergodicity, break down of Khinchin's theorem of aging system

In the derivation of Khinchin's theorem [136], one important assumption is that the process is stationary and the system reaches a steady state, *i.e.*,$C(t, t^{'}) = g(t^{'})$. If the correlation function is 'irreversible', $\lim_{t^{'}\to\infty} C(t, t^{'}) =< I >^2$, then the process is ergodic. As shown by Barkai [134], if the process is not stationary intead the system is aging, a stronger condition must be fulfilled to guarantee the ergodicity.

4.4.1 Ergodic theorem

Conceptually, ergodicity of a dynamical system is a certain irreducibility property. We denote by (p, q) the state of the system under investigation which is a general point in the phase space [137]. The dynamics is given by a one parameter flow k_t where t is the time. If an observable as a measurable function on state space is $I(p, q)$ then in time t it is $I(k_t(p, q))$. $(k_t(p, q)) \to (p, q)$ is a measure-preserving transformation. A general measure-preserving transformation admits a canonical decomposition into its ergodic components, each of which is ergodic. In the QD blinking case k_t stands for the blinking fluorescence process. And the time average

$$I(p, q, t) \equiv \frac{1}{t}\int_0^t I(k_{t'}(p, q))\mathrm{d}t^{'}, \tag{4.6}$$

while the ensemble average

$$< I(t) >\equiv \int I(k_t(p,q))\mu(\mathrm{d}(p,q)), \tag{4.7}$$

where μ is a stationary ensemble measurement of the system. Since it is stationary, the ensemble average is independent of time, thus $< I(t) >=< I >$ [134].

The ergodic theorem states that if the infinite time limit exists for μ-almost every state,

$$\lim_{t\to\infty} I(p,q,t) = I(p,q,\infty) \equiv I(p,q), \tag{4.8}$$

where the function $I(p,q)$ is constant on ergodic components and meanwhile there exists only one ergodic component, then

$$I(p,q) =< I >, \tag{4.9}$$

for μ-almost every state. In other words, the long time limit average is equivalent to the ensemble average of an observable.

4.4.2 Khinchin's theorem and two-time correlation function $C(t,t^{'})$

Khinchin also established the connection between the ergodic theorem for the obseivable I and its two-time correlation function $C(t,t^{'})$ of wide interest in statistical physics [138–140] which is: an observable is ergodic if the associated two-time correlation function is 'irreversible'

$$\lim_{t^{'}\to\infty} C(t,t^{'}) =< I >^2, \tag{4.10}$$

then the process is ergodic.

4.4.3 Break down of Khinchin's theorem

Barkai has proved that for nonstaionary systems, the irreversiblility is no longer enough to imply ergodicity [134].

While for process in which $< I(k_t(p,q)) >$ converges to a constant $< I(p,q) >=< I >$ holds, $< I(p,q)^2 >=< I >^2$ quantifies ergodicity. As defined in Eq. (4.6),

$$< I(p,q,t)^2 >= \frac{1}{t^2}\int_0^t\int_0^t < I(k_{t_1}(p,q))I(k_{t_2}(p,q)) > \mathrm{dt_1 dt_2} = \frac{2}{t^2}\int_0^t\int_0^{t_2} \mathrm{C(t_1, t_2 - t_1)dt_1 dt_2}. \tag{4.11}$$

For nonstationary process, even at long time limit $t^{'} \to \infty$, $C(t,t^{'})$ is still a function of both times, and no longer only dependent on $t^{'}$. Such as in the first case discussed above, $C(t,t^{'}) = h(t/(t+t^{'}))$,

$$< I(p,q,t)^2 >= \frac{2}{t^2}\int_0^t\int_0^t h(\frac{t_1}{t_2})\mathrm{dt_1 dt_2} = \int_0^1 \mathrm{h(x)dx}. \tag{4.12}$$

In order to get $< I(p,q)^2 >=< I >^2$, now $\int_0^1 h(x)\mathrm{dx} =< \mathrm{I} >^2$ needs to be fulfilled. However, irreversibility which is $\lim_{t^{'}\to\infty} h(t/(t+t^{'})) =< I >^2$ or $\lim_{x\to 0} h(x) =< I >^2$ is different from the condition. Hereafter, the irreversiblity is not sufficient to guarantee ergodicity in nonstationary processes and Khinchin's theorem does not hold. Instead, Eq. (4.11) needs to be fulfilled for ergodicity to happen.

4.5 QD fluorescence blinking process: steady state and exponential cutoff of the 'off' state distribution

Of the three cases discussed in the last section, the first two are aging processes and don't fulfill the stronger condition, hence are not ergodic. And in the ensemble experiments at long times the dots will all be in dark state with an unity porbability.

From the single dot experimental results usually a power law with exponential cutoff distribution is obtained for the 'on' time and a power law distribution for the 'off' time which is the second case discussed above. Therefore in these single

dot experiments, the blinking process is not ergodic and no steady state is reached. So the time average correlation function from single trajectory is not equivalent to the ensemble average.

Nevertheless, in ensemble experiments [74] a steady state is observed as shown in Fig. 4.1. And the fluorescence intensity of the steady state is around 10% - 20% of the initial value which means not all the dots end in the dark state. It can only be the third case. Thus instead of a infinite average 'off' time in this ensemble experimental time regime a cutoff does exist for the 'off' time.

If we expand the single dot experimental time window to a larger scale and do the experiments for a certain times we should be able to observe a cutoff of the 'off' state time power law distribution.

4.6 Break down of Wiener-Khinchin's theorem in the QD fluorescence blinking pocess

The Wiener-Khinchin's theorem states that the power spectrum is equal to the Fourier transform of the correlation function. However, this is also under the condition that the process is stationary and a steady state is reached for the system. For the current quantum dot system, the time average correlation function from single trajecotry is not the same as the ensemble average correlation function.

4.7 Discussion and conclusion

Correlation functions are commonly adopted to probe the temporal evolution of a system in experiments and can provide information on the influence of the current value of an observable on the future. Thus information on the dynamics can also be gained from the correlation functions. However, in aging and nonstationary processes, the Khinchin's theorem and Wiener-Khinchin's theorem break down. Extra care is needed to analyse the correlation function and power spectrum.

For the QD fluorescence blinking process which attracts the author's attention to the aging problem, there is ensemble experiments evidence for the existence of a steady state while in single dot experiments no clear cutoff of 'off' time power law distribution has yet been observed and in the last chapter we have ascribed the cutoff of 'on' to the multi exciton generation. It can be due to the relatively short observation time of single quantum dot experiments. If the experiments are performed in time long enough, a exponential truncation of the power law distribution should show up due to the saturation time.

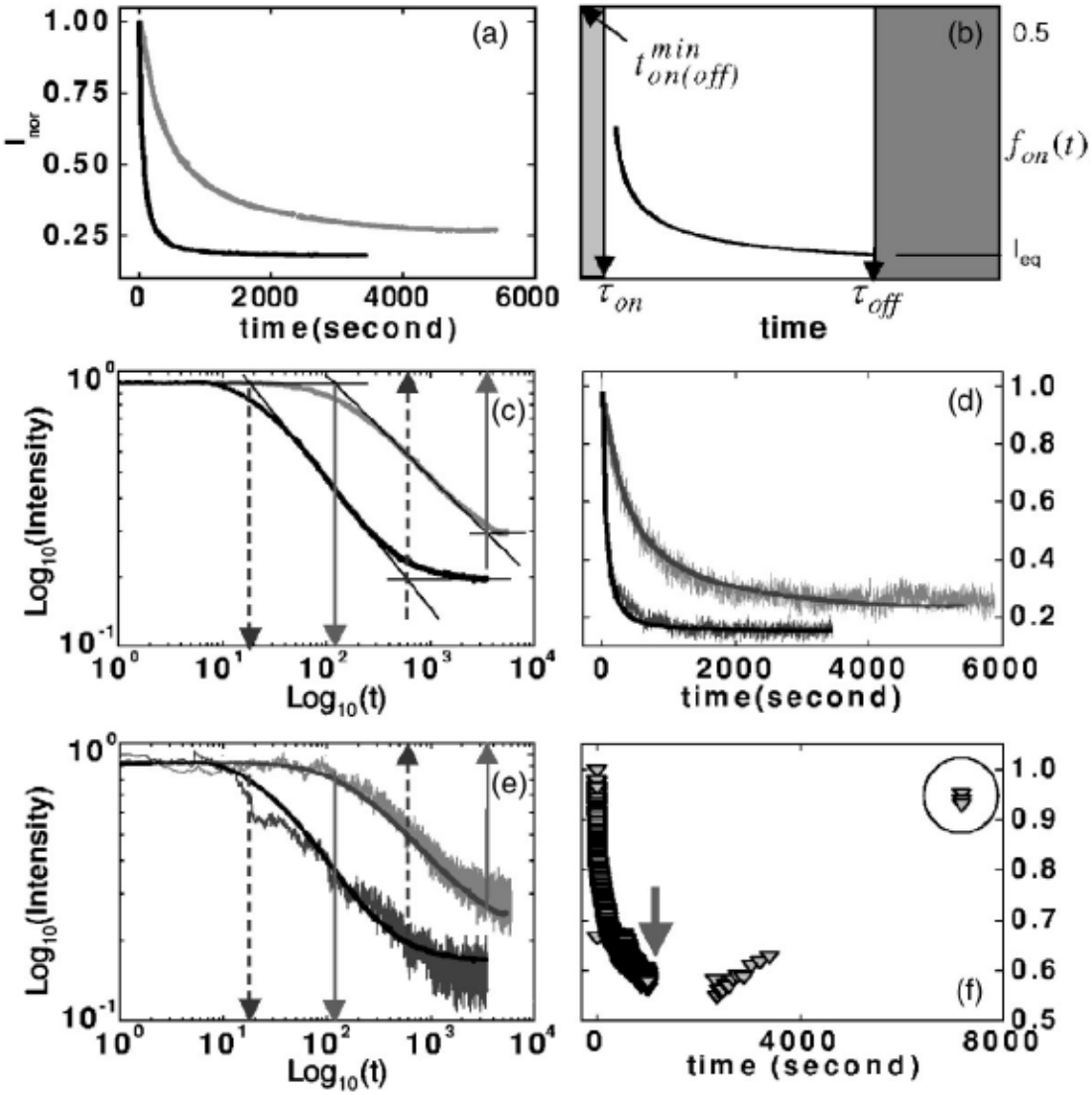

Figure 4.1: (a) Normal fluorescence intensity time traces from two collections of different (CdSe)ZnS(core) shell QD's with core radii of 2.5 nm (black and gray). (b) Plot of the analytical forma of $f_{on}(t)$ [Eq.(3)]. (c) Log-log plots of the experimental intensity time traces in (a). The beginning and end points of the power-law decays for the two plots are indicated by arrows pointing up for the beginning points and pointing down for the end points, respectively. These points are obtained as the intersections of the two slopes. These points experimentally determine τ_{on} and τ_{off}. (d) Intensity time traces obtained from adding 5000 different time traces generated using Monte Carlo simulations. The smooth solid lines are the experimental data in (a) for comparison. (e) Log-log plots of the simulated intensity time traces in (d) with plots in (c) overlayed. (f) Observed fluorescence intensity recovery after an initial decay, as described in the text, obtained from a collection of 2.4nm radius (CdSe)ZnS(core) shelll QD's. The arrow indicates the imte when continuous excitation was stopped.-FIG. 3. from [**?**]

Chapter 5

Precautions using the maximum likelihood method for power law distributions with slopes close to unity

5.1 Motivation

Single-molecule spectroscopy (SMS) has been an important tool in physics, chemistry and biology [95, 117–120]. It allows for photophysical measurements of individual luminophores, revealing behavior undetectable in ensemble measurements. With recent advances in technique [122], room temperature single-emitter experiments have provided observations of a pronounced blinking behavior which is defined as the random switching on and off of the fluorescence or luminescence intensity of a single emitter under continuous or pulsed excitation [79, 81, 121, 123–125]. A well known and intensively studied example is quantum dots blinking [66,68,69,71,72,126–130]. A unique feature of this blinking behavior is that the distribution of ``on´´ and ``off´´ duration times is a power law with broad range of decades duration intead of an exponential [66, 69, 79, 81, 121, 126, 141, 142].

Although the power law phenomenon is less intensively studied in the blinking of single dye molecules than of inorganic quantum dots, there are a few observations of power law behavior of organic dye molecules embedded in polymer or on a glass or inorganic crystal surface [86, 141, 142], in contrast with the numerous studies of quantum dots. However, due to the relatively low fluorescence efficiency and tendency to bleach limited data sets can be collected from experiments with the dyes. Recently, the maximum likelihood estimator (MLE) method has been adopted to analyze these power-law distributed data especially for the limited data sets [89, 143–146].

In a recent analysis of experimental results, the fitting obtained by MLE did not pass through or near many data points [89]. After a study of the method, we are able to understand the difficulty with the literature method and provide a solution.

5.2 Idea Behind MLE

We recall that MLE is a method of estimating the parameters of a statistical model. Given a statistical model and a set of data (observation), MLE provides

estimates of the model's parameters [147]. Suppose one makes N independent and identically distributed (iid) observations (measurements) $x_1, x_2, ..., x_N$ from a distribution with an unknown probability density function (pdf), $f_0(.)$. With certain experience it is then conjectured that $f_0(.)$ belongs to a certain family of distributions, $f_0(.|\theta), \theta \in \Theta$. So $f_0(.) = f_0(.|\theta_0)$ with θ_0 as the unknown 'true value' of the parameters in this parameter model.

The problem of obtaining the parameter closest to the 'true value' becomes equivalent to selecting the value that produces a distribution that gives the greatest probability (likelihood) for the observation.

5.3 MLE algorithm

For an iid sample the joint density function is

$$f(x_1, x_2, ..., x_n \mid \theta) = f(x_1 \mid \theta)\, f(x_2 \mid \theta) \ldots f(x_N \mid \theta) \tag{5.1}$$

The above joint density function can also be taken as the likelihood when we consider θ as the variable. $x_1, x_2, ..., x_N$ are the measurements in the following discussion.

In the method of maximum likelihood, one finds a value of θ, θ_0, that maximizes the likelihood. The likelihood is a multiplication and if we use a monotonic transformation of it, a logarithm, then we will have a summation, log-likelihood, which is easier to work with and maximize than the product form

$$\hat{l} = \sum_{i=1}^{N} \ln f(x_i \mid \theta) \tag{5.2}$$

5.4 MLE for power law distribution

5.4.1 Method

We indicate the model values as $\hat{X}$ in comparison with the experimental data X. In a perylene bisimide dye molecule fluorescence blinking case, which prompted our interest [89], the measurements are the ``on´´or ``off´´durations t_is, corresponding to the above x_is. The pdf of power law distribution is

$$\hat{p}(t) = A\, t^{-m} \tag{5.3}$$

The probability of an observation at t_i is $\hat{P}(t_i) \equiv \int_{t_i}^{t_i+\Delta t_i} \hat{p}(t)\mathrm{d}t$. In experiments, $P(t_i) = \frac{n_{t_i}}{\sum n_{t_i}}$ and $p(t_i) \equiv \frac{P(t_i)}{\Delta t_i}$ [89, 143–145]. n_i is the number of observations obtained in the time interval Δt_i around t_i. There are several ways of choosing Δt_i. We adopt the commonly used one $\Delta t_i = \frac{t_{i+1}-t_{i-1}}{2}$ for $1 < i < N$, and for Δt_1 and Δt_N we use the experimental data points at the cited times. In the model we use the approximation $\hat{p}(t_i) \simeq \frac{\hat{P}(t_i)}{\Delta t_i}$, $A(m) = \frac{1}{\sum t_i^{-m}\Delta t_i}$. We now have the model with parameter m,

$$\hat{p}(t) = \frac{1}{\sum t_i^{-m}\Delta t_i}\, t^{-m} \tag{5.4}$$

The likelihood function in terms of the model parameter m is $N!\Pi_{i=1}^{k} \hat{P}(t_i)^{n_i}/n_i!$. We obtain an estimation of m closest to m_0 by maximizing the log-likelihood function

$$\hat{l} = \ln N! + \sum [n_i \ln \hat{P}(t_i) - \ln n_i!] \tag{5.5}$$

More generally, if the functional form is $p(t|m)$ where we now denote by m the collective parameters, m_1, m_2, ..., then for $\hat{p}(t)$ we would have instead of eq 5.4,

$$\hat{p}(t) = \frac{p(t|m)}{\sum p(t_i|m)\Delta t_i}. \tag{5.6}$$

5.4.2 Comparison with an earlier MLE method

In order to normalize the PDF and get an expression of A as a function of m, we avoid the integration as in an earlier method [143]. Instead, we use the summation of the probability of all measurements. Unlike the requirement for the earlier method that $m \neq 1$, with the present method, even when the true value is $m = 1$, one can still fit the experimental data very well and get a m_0 close to m.

5.5 Results and discusstion

We next apply the method to the intermittent fluorescence data of the single perylene bisimide dye molecules on Al_2O_3 system [148]. Processing the fluorescence data in the algorithm described by eqs 5.3-5.5, we have obtained a power law distribution with slope around 1 for both off and on times, as in Figures 5.1 and 5.3. These results agree well with the diffusion-based model of Chen and Marcus [149].

In the ``on´´plot, the last two points deviate from the power law. One could fit these with an exponential tail as shown in 5.3. However, the two points occur where the error is large (small signal intensity) and should be given little or no weight. More data in that region are needed. If we remove these two points, as in 5.2, the fitting of a power law with the power exponent close to 1 is even better. Since there are only two data points, one can not decide definitively whether this occurrence is an exponential cutoff, bleaching of the dye molecule or other. There is, however, another photo excited dye-on-surface result that does show an exponential cut-off [90].

We next compare with an earlier method of implementing the MLE. In comparison with the normalization method used above to obtain the function $A(m)$, one can compare with the method of approximation used earlier in the literature [143]. The observation data points are within a range between the experimental resolution time t_{min} and the time window of the performed experiment t_{max}. So $\int_{t_{min}}^{t_{max}} \hat{p}(t)\mathrm{d}t = 1$,

and under the condition that $m_0 \neq 1$, $A(m) = \frac{m-1}{t_{min}^{1-m} - t_{max}^{1-m}}$ and we have

$$\hat{p}(t) = \frac{m-1}{t_{min}^{1-m} - t_{max}^{1-m}} t^{-m} \tag{5.7}$$

so that the integral of $\hat{p}(t)$ from t_{min} to t_{max} is unity. However, when m approaches unity, $\hat{p}(t)$ approaches $0/0$ and so is indeterminate.

Taking $t_{max} \gg t_{min}$ since the experimental time window spans several orders of magnitude, and presuming $m_0 > 1$, eq 5.7 becomes

$$\hat{p}(t) \cong \frac{m-1}{t_{min}^{1-m}} t^{-m} \tag{5.8}$$

This method was adopted earlier to analyze the fluorescence of tetraphenoxy-perylene diimide dye [144]. In that case, the diffusion process was a ``spectral diffusion'', rather than a particle diffusion, and one observed a power exponent $m \cong 1.5$ [97, 98, 107]. However, in the special case $m_0 \cong 1$ which applies when a particle diffusion is involved [89], the condition for the validity of eq 5.7 is no longer satisfied, and we can't retain the expression in eq 5.8. Indeed, eqs 5.7 and 5.8 did not give a close fit to the data (Figures 5.1 and 5.3). For the single molecule study of the electron injection from the dye onto a semiconductor surface, $m \cong 1$ is the theoretically expected value [149], and a treatment of this particular case is particularly necessary.

In analyzing data with forms other than power law, *e.g.*, power law with an exponential tail, the normalization demonstrated above can also be applied.

5.6 Concluding remarks

We have given a general MLE method to analyze experimental data with a distribution of a power law form that can be extended to a power law with an exponential tail and more generally, many other distribution forms.

Figure 5.1 ``Off´´probability density for 25 molecules observed on sapphire (0001),using original experimental data in ref 89 from Prof. Monti. The green line is from the original MLE fitting with $P = At^{-1.19}$ in ref 89 and the red line is obtained from the present modified MLE fitting with $P = At^{-0.91}$.

Figure 5.2 ``On´´probability density for 51 molecules observed on sapphire (0001), using original experimental data in ref 89 from Prof. Monti. The green line is from the original MLE fitting with $P = At^{-1.27}$ in ref 89, the red line is obtained from the present modified MLE fitting with $P = At^{-1.11}$ power law and the blue ine is with $P = At^{-0.84}\exp(-t/900)$, where t is in seconds.

Figure 5.3 The same data as in Fig. 5.2 but without the 2 data points with the longest ``on´´time, using original experimental data in ref 89 from Prof. Monti. The green line is from the original MLE fitting with $P = At^{-1.28}$ in ref 89 and the red line is obtained from the present modified MLE fitting with $P = At^{-0.97}$.

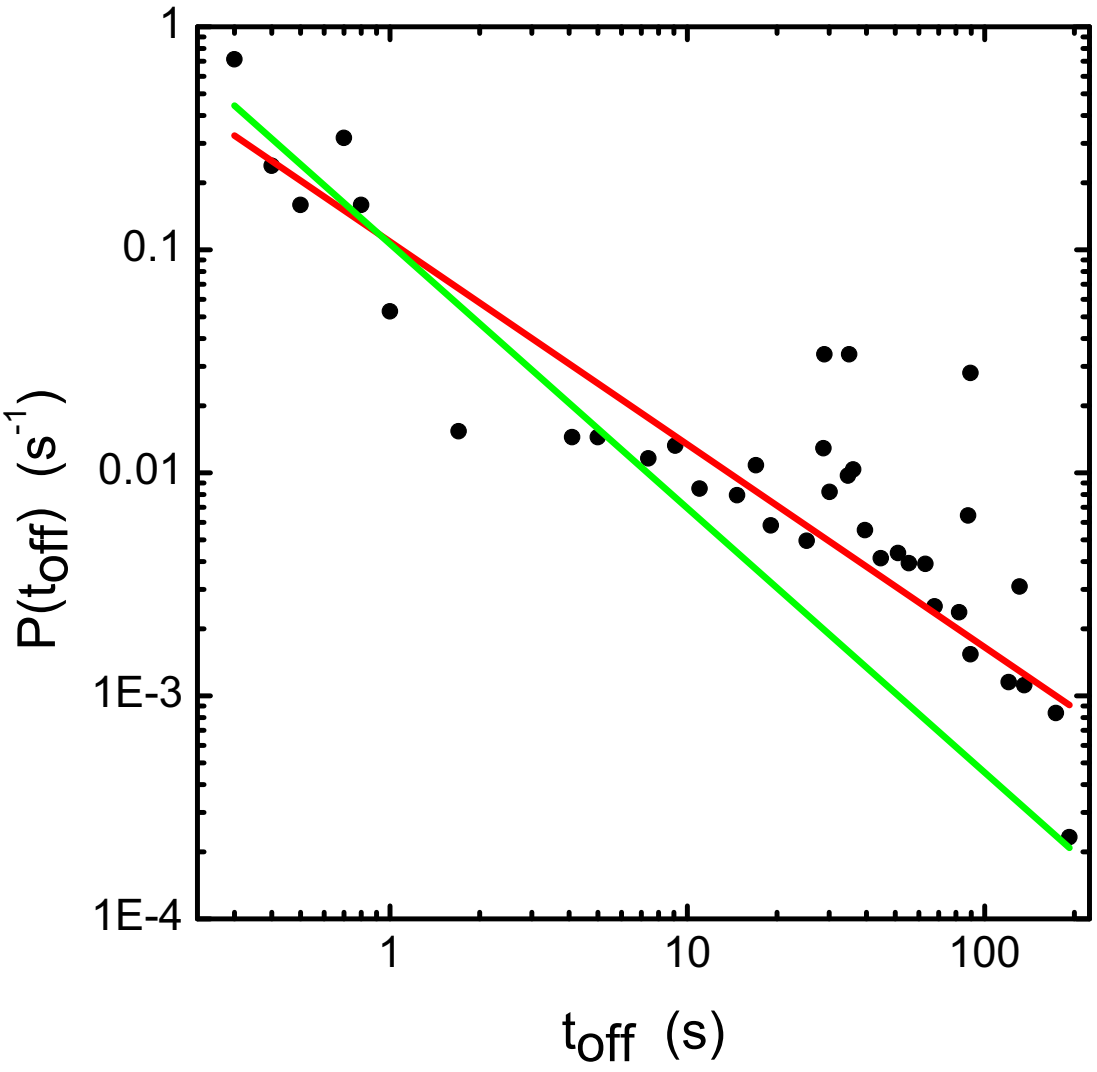

Figure 5.1:

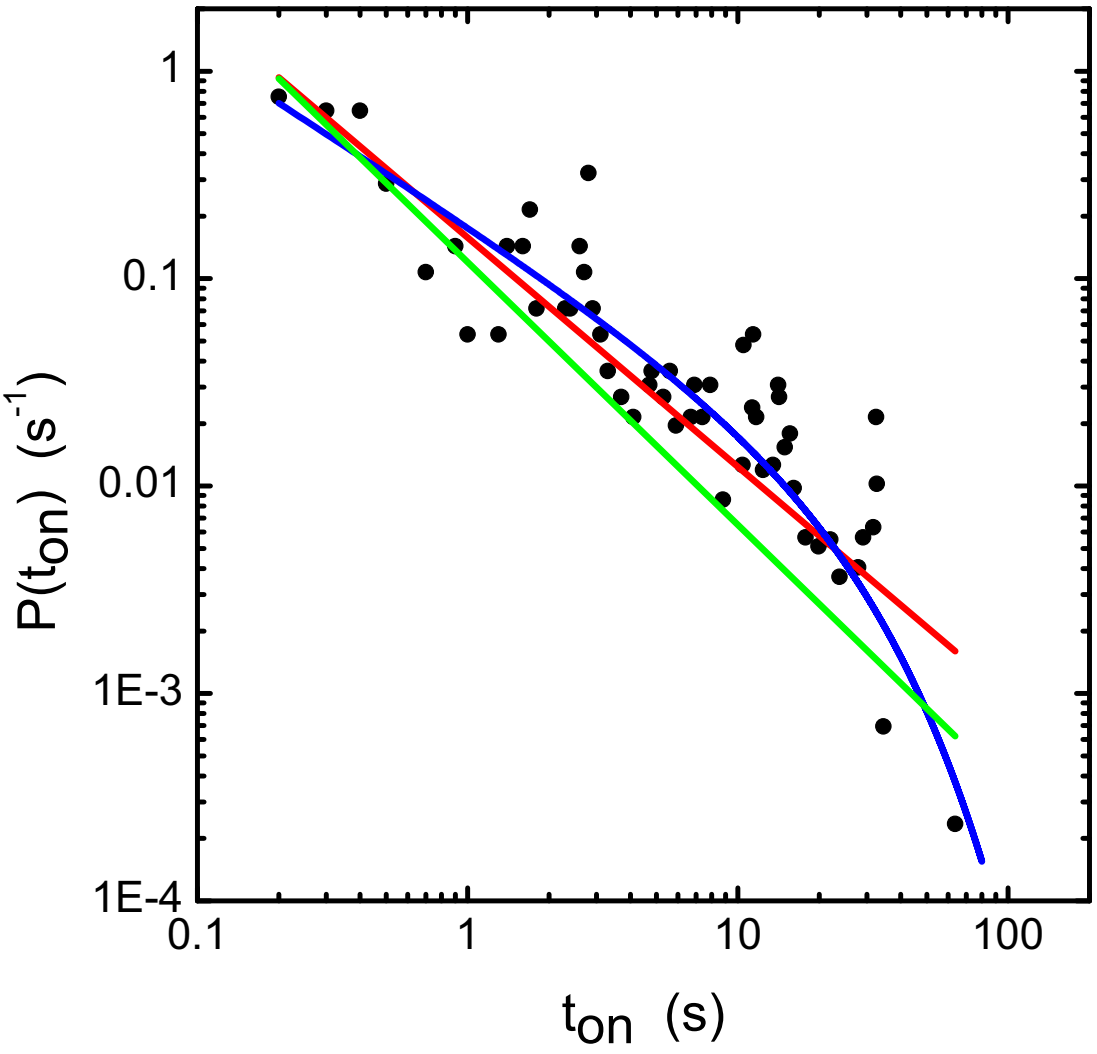

Figure 5.2:

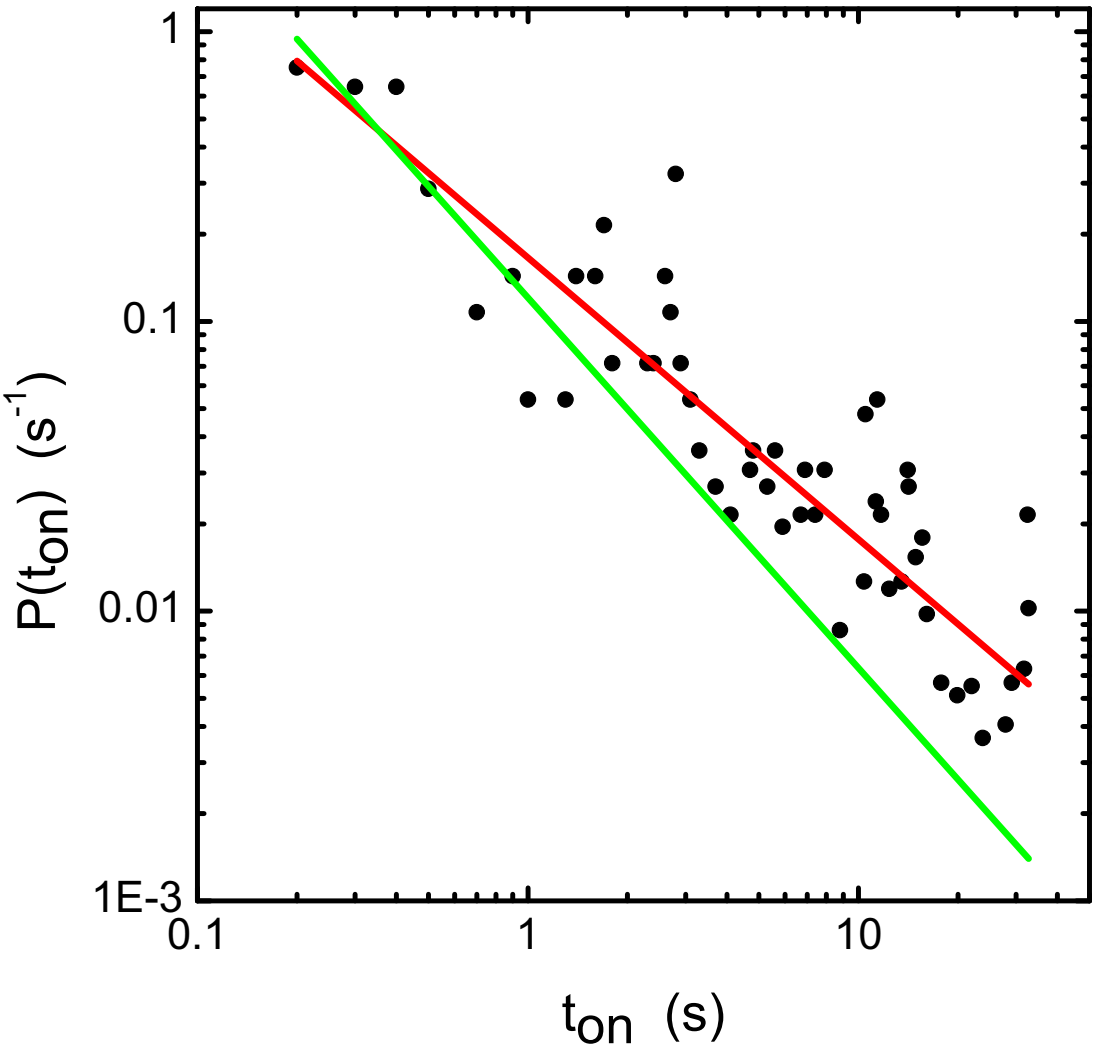

Figure 5.3:

Chapter 6

Summary

In the first chapter, The effect of the large impact parameter near-elastic peak of collisional energy transfer for unimolecular dissociation/bimolecular recombination reactions is studied. To this end the conventional single exponential model, a bi-exponential model that fits the literature classical trajectory data better, a model with a singularity at zero energy transfer, and the most realistic model, a model with a near-singularity, are fitted to classical trajectory data on collisional energy transfer in the literature. The results are then applied to see the effect on the recombination rate constant of $O + O_2 \rightarrow O_3$. The typical effect of the energy transfer on the recombination rate constant is maximal at low pressures and this region is the one studied here. The distribution function for the limiting dissociation rate constant k_0 at low pressures is shown to obey a Wiener-Hopf integral equation and is solved analytically for the first two models above and perturbatively for the other two. For the single exponential model this method yields the trial solution of Troe. The results are applied to the dissociation of O_3 in the presence of argon, for which classical mechanical trajectory data are available. The k_0s for various models are calculated and compared, the value for the near-singularity model being about 10 times larger than that for the first two models. This trend reflects the contribution to the cross-section from collisions with larger impact parameter. In the present study of the near-singularity model it is found that k_0 is not sensitive to reasonable values for the lower bound of the energy transfer. Energy transfer values $< \Delta E >$s are also calculated and compared, and can be similarly understood. However, unlike the k_0 values they are sensitive to the lower bound of the energy transfer, and so any comparison of a classical trajectory analysis for $< \Delta E >$s with the kinetic experimental data needs particular care.

In the second chapter, the hypothesis in the first chapter in the reaction $A + B \rightleftharpoons AB$ if a tagged A is followed in time in its progress to form AB, and if a tagged A in AB is followed in time in its progress to form $A + B$, beginning with an equilibrium concentrations of AB for the given A and B concentration, the sum of the tagged distribution functions at any energy E is equal to the equilibrium distribution at that E is tested. It is proved that the hypothesis is correct in general. At low

pressure scheme due to a certain assumption there is a minor deviation.

In the third chapter, the electron transfer process in the single quantum dot fluorescence blinking phenomenon is studied. Modification of the DCET model has been made to explain the exponential cutoff of the power law time distribution of the bright state and the quadratic dependence of the exponential tail on the excitation intensity.

In the fourth chapter, the non-stationary property of the quantum dots fluorescence process is discussed and a cutoff of the power law dark state time distribution in the long time run is proposed for single trajectory experiments.

In the fifth chapter, a general MLE method to analyze experimental data with a potential distribution of power law form which can be extended to a power law with an exponential tail and more generally, many other distribution forms is demonstrated.

Appendix A

Appendix A: Solution a Wiener-Hopf equation of the second kind for the single exponential model

We first note that $|\tilde{g}_-(z)| = |\int_{-\infty}^{\infty} e^{2\pi i z E} g_-(E) dE|$, and $\tilde{g}_-(z)$ is a function of z alone. Also, $|\tilde{g}_-(z)| = |\int_{-\infty}^{0} e^{2\pi i u E} g_-(E) e^{-2\pi v E} g_-(E) dE| \leqslant \int_{-\infty}^{\infty} e^{-2\pi v E} g_-(E) | dE$. If we can find a solution for $\tilde{g}_-(z)$ such that $|g_-(E)| < M_1 e^{2\pi v_- E}$, as $E \to -\infty$, where $v_- > 0$ and hence tends to zero as $E \to -\infty$, then we have

$$|\tilde{g}_-(z)| < M_1 e^{-2\pi v E} e^{2\pi v_- E} = M_1 \frac{1}{2\pi(v_- - v)} \tag{A.1}$$

Thereby, in the part of the lower half plane where $\mathrm{Im} z = v < v_-$, $|\tilde{g}_-(z)|$ has no singularity. So $\tilde{g}_-(z)$ is an analytic function in the half of the plane for which $\mathrm{Im} z < v_-$.

Next we consider $\tilde{g}_+(z)$:

$$|\tilde{g}_+(z)| = |\int_{-\infty}^{\infty} e^{2\pi i z E} g_+(E) dE| = |\int_{0}^{\infty} e^{2\pi i z E} g_+(E) dE| \tag{A.2}$$

since $|g_+(z) = 0|$ for $E < 0$. For $E > 0$ it follows from Eq. (1.25) that

$$|\tilde{g}_+(z)| = |\int_{0}^{\infty} e^{2\pi i z E} [\int_{-\infty}^{0} Z(E, E') g_-(E') dE'] dE| \; / \int_{-\infty}^{\infty} Z(E', E) dE'. \tag{A.3}$$

We note that $\tilde{g}_+(z)$ is a function of z alone, and also from Eqs. (2.13) and (A.3)

$$\begin{aligned} |\tilde{g}_+(z)| &= |\int_0^\infty e^{2\pi i u E} e^{-2\pi v E} [\int_{-\infty}^0 g_-(E') \frac{1}{\gamma+\gamma'} e^{-(E-E')/\gamma'} dE'] dE| \\ &\geqslant \int_0^\infty e^{-2\pi v E} |[\int_{-\infty}^0 g_-(E') \frac{1}{\gamma+\gamma'} e^{-(E-E')/\gamma'} dE']| dE. \end{aligned} \tag{A.4}$$

If we can find a solution $|g_-(E')| < M_1 e^{2\pi v_- E'}$ where $E' < 0$, then since $v_- > 0$ we have $v_- > -\frac{1}{2\pi\gamma'}$ and then

$$\begin{aligned} |\tilde{g}_+(z)| &\geqslant \int_0^\infty e^{-2\pi v E} |[\int_{-\infty}^0 g_-(E') \frac{1}{\gamma+\gamma'} e^{-(E-E')/\gamma'} dE']| dE \\ &= \frac{1}{\gamma+\gamma'} \frac{1}{2\pi v + 1/\gamma'} |\int_{-\infty}^0 g_-(E') e^{E'/\gamma'} dE'| \\ &< \frac{M_1}{\gamma+\gamma'} \frac{1}{2\pi v + 1/\gamma'} \frac{1}{2\pi v_- + 1/\gamma'}. \end{aligned} \tag{A.5}$$

Thereby, $|\tilde{g}_+(z)| \to 0$ as $\mathrm{Im} z = v \to \infty$, and we see that $\tilde{g}_+(z)$ has no singularity in the upper half plane for which $\mathrm{Im} z > -\frac{1}{2\pi\gamma'}$, and so is analytic in that upper half plane. The right hand side of Eq. (1.27) is therefore analytic in the upper half plane, $\mathrm{Im} z > -\frac{1}{2\pi\gamma'}$. We had seen earlier in this Appendix that $\tilde{g}_-(z)$ is analytic in the lower half plane, $\mathrm{Im} z < v_-$. From the derivation on the left hand side of Eq. (1.27), we need for analyticity of this side of the equation, $\mathrm{Im} z < -\frac{1}{2\pi kT}$. Thereby, we require that the left hand side of Eq. (1.27) is analytic in the lower half plane where $\mathrm{Im} z < -\frac{1}{2\pi kT}$. Since $v_- > 0 > -\frac{1}{2\pi\gamma'}$ we now see that both sides of Eq. (1.27) are analytic in the strip $-\frac{1}{2\pi\gamma'} < \mathrm{Im} z < -\frac{1}{2\pi kT}$. Since the analytic continuation is unique, there exists an entire function F in the complex plane which coincides with the right hand side of Eq. (1.27) in upper half plane $\mathrm{Im} z > -\frac{1}{2\pi\gamma'}$ and coincides with the left hand side of Eq. (1.27) in the lower half plane $\mathrm{Im} z < Min(-\frac{1}{2\pi kT}, v_-)$. Since $\tilde{g}_+(z)$ goes to 0 no slower than exponentially as $|z| \to \infty$, then the entire function F is bounded at infinity. One concludes that F is constant, which we denote by G_s, and so obtain

$$\tilde{g}_-(z) = G_s \frac{1/\gamma + 2\pi i z}{2\pi i z (2\pi i z - 1/kT)}, \tag{A.6}$$

$$\tilde{g}_{+}(z) = G_s \frac{1}{1/\gamma' - 2\pi i z}. \tag{A.7}$$

Appendix B

Appendix B: Solution of a Wiener-Hopf equation of the second kind for the bi-exponential model

Following similar procedure in Appendix A, we can now solve Eq. (1.35). As in Appendix A, $|\tilde{g}_-(z)| = |\int_{-\infty}^{\infty} e^{2\pi i z E} g_-(E) dE|$, and $\tilde{g}_-(z)$ is a function of z alone. Also, $|\tilde{g}_-(z)| = |\int_{-\infty}^{0} e^{2\pi i u E} g_-(E) e^{-2\pi v E} g_-(E) dE| \leqslant \int_{-\infty}^{\infty} e^{-2\pi v E} g_-(E) | dE$. If we can find a solution for $\tilde{g}_-(z)$ such that $|g_-(E)| < M_1 e^{2\pi v_- E}$, as $E \to -\infty$, where $v_- > 0$ and hence tends to zero as $E \to -\infty$, then we have

$$|\tilde{g}_-(z)| < M_1 e^{-2\pi v E} e^{2\pi v_- E} = M_1 \frac{1}{2\pi(v_- - v)} \tag{B.1}$$

Thereby, $|\tilde{g}_-(z)|$ has no singularity in the part of the lower half plane where $\mathrm{Im} z = v < v_-$. So $\tilde{g}_-(z)$ is analytic in the half of the z-plane for which $\mathrm{Im} z < v_-$.

Next we consider $\tilde{g}_+(z)$:

$$|\tilde{g}_+(z)| = |\int_{-\infty}^{\infty} e^{2\pi i z E} g_+(E) dE| = |\int_{0}^{\infty} e^{2\pi i z E} g_+(E) dE| \tag{B.2}$$

since $|g_+(z) = 0|$ for $E < 0$. For $E > 0$ it follows from Eq. (1.25) that

$$|\tilde{g}_+(z)| = |\int_{0}^{\infty} e^{2\pi i z E} [\int_{-\infty}^{0} Z(E, E') g_-(E') dE'] dE| \,/\, \int_{-\infty}^{\infty} Z(E', E) dE'. \tag{B.3}$$

We note that $\tilde{g}_+(z)$ is a function of z alone, and also from Eq. (B.3)

$$\begin{aligned} & | \quad \tilde{g}_+(z)| \\ = & \quad | \int_0^\infty \mathrm{e}^{2\pi i u E} \mathrm{e}^{-2\pi v E} [\int_{-\infty}^0 g_-(E^{'}) \frac{1}{\gamma + \gamma^{'} + cd + cd^{'}} (\mathrm{e}^{-(E-E^{'})/\gamma^{'}} + c\mathrm{e}^{-(E-E^{'})/d^{'}}) \mathrm{d}E^{'}] \mathrm{d}E \mid \\ \geqslant & \quad \int_0^\infty \mathrm{e}^{-2\pi v E} \mid [\int_{-\infty}^0 g_-(E^{'}) \frac{1}{\gamma + \gamma^{'} + cd + cd^{'}} (\mathrm{e}^{-(E-E^{'})/\gamma^{'}} + c\mathrm{e}^{-(E-E^{'})/d^{'}}) \mathrm{d}E^{'}] \mid \mathrm{d}E. \quad \text{(B.4)} \end{aligned}$$

If, as stated above, we can find a solution $|g_-(E^{'})| < M_1 \mathrm{e}^{2\pi v_- E^{'}}$ where $E^{'} < 0$, then

$$\begin{aligned} & | \quad \tilde{g}_+(z)| \\ \geqslant & \quad \int_0^\infty \mathrm{e}^{-2\pi v E} \mid [\int_{-\infty}^0 g_-(E^{'}) \frac{1}{\gamma + \gamma^{'} + cd + cd^{'}} (\mathrm{e}^{-(E-E^{'})/\gamma^{'}} + c\mathrm{e}^{-(E-E^{'})/d^{'}}) \mathrm{d}E^{'}] \mid \mathrm{d}E \\ = & \quad \frac{1}{\gamma + \gamma^{'} + cd + cd^{'}} \mid \frac{1}{2\pi v + 1/\gamma^{'}} \int_{-\infty}^0 g_-(E^{'}) \mathrm{e}^{E^{'}/\gamma^{'}} \mathrm{d}E^{'} \\ + & \quad \frac{c}{2\pi v + 1/d^{'}} \int_{-\infty}^0 g_-(E^{'}) \mathrm{e}^{E^{'}/d^{'}} \mathrm{d}E^{'} \mid \\ < & \quad \frac{M_1}{\gamma + \gamma^{'} + cd + cd^{'}} (\frac{1}{2\pi v + 1/\gamma^{'}} \frac{1}{2\pi v_- + 1/\gamma^{'}} + \frac{c}{2\pi v + 1/d^{'}} \frac{1}{2\pi v_- + 1/d^{'}}). \quad \text{(B.5)} \end{aligned}$$

Thereby, $|\tilde{g}_+(z)| \to 0$ as $\mathrm{Im}z = v \to \infty$, and $\tilde{g}_+(z)$ has no singularity in the upper half plane for which $\mathrm{Im}z > -\frac{1}{2\pi\gamma^{'}} > -\frac{1}{2\pi d^{'}}$ and since $v_- > 0 > -\frac{1}{2\pi\gamma^{'}} > -\frac{1}{2\pi d^{'}}$, it is analytic in that upper half plane. The right hand side of Eq. (1.9) is therefore analytic in the upper half plane for which this condition is fulfilled and where $\mathrm{Im}z > Max(-\frac{1}{2\pi\gamma^{'}}, -\frac{r_3}{2\pi})$, where $r_3 = 1/2kT + \sqrt{(1/2kT)^2 + [(\gamma+\gamma^{'})/dd^{'} + (cd+cd^{'})/\gamma\gamma^{'}]/(\gamma+\gamma^{'}+cd+cd^{'})}$. We had seen earlier in this Appendix that $\tilde{g}_-(z)$ is analytic in the lower half plane, $\mathrm{Im}z < v_-$. From the derivation on the left hand side of Eq. (1.9), we need for analyticity of this side of the equation, $\mathrm{Im}z < -\frac{1}{2\pi kT}$. Thereby, we require that the left hand side of Eq. (1.9) is analytic in the lower half plane where $\mathrm{Im}z < -\frac{1}{2\pi kT}$. Since $v_- > 0 > -\frac{1}{2\pi\gamma^{'}}$ we now see that both sides of Eq. (1.9) are analytic in the strip $Max(-\frac{1}{2\pi\gamma^{'}}, -\frac{r_3}{2\pi}) < \mathrm{Im}z < -\frac{1}{2\pi kT}$. Since the analytic continuation is unique, there exists an entire function F in the complex plane which coincides with the right hand side of Eq. (1.9) in upper half plane $\mathrm{Im}z > Max(-\frac{1}{2\pi\gamma^{'}}, -\frac{r_3}{2\pi})$ and coincides

with the left hand side of Eq. (1.9) in the lower half plane $\mathrm{Im} z < -\frac{1}{2\pi kT}$. Since $\tilde{g}_+(z)$ goes to 0 no slower than exponentially as $|z| \to \infty$, then the entire function F should be bounded at infinity. One concludes that F is constant, which we denote by G_{bi}, and so obtain

$$\tilde{g}_-(z) = G_{bi} \frac{(1/\gamma + 2\pi iz)(1/d + 2\pi iz)}{2\pi iz(2\pi iz - 1/kT)(2\pi iz - r_4)}. \tag{B.6}$$

Appendix C

Appendix C: On collisional energy transfer in recombination and dissociation reactions: A Wiener-Hopf problem and the effect of a near elastic peak

THE JOURNAL OF CHEMICAL PHYSICS **129**, 214106 (2008)

On collisional energy transfer in recombination and dissociation reactions: A Wiener–Hopf problem and the effect of a near elastic peak

Zhaoyan Zhu and R. A. Marcus[a)]
Noyes Laboratory of Chemical Physics, California Institute of Technology, Pasadena, California 91125, USA

(Received 12 June 2008; accepted 22 October 2008; published online 2 December 2008)

The effect of the large impact parameter near-elastic peak of collisional energy transfer for unimolecular dissociation/bimolecular recombination reactions is studied. To this end, the conventional single exponential model, a biexponential model that fits the literature classical trajectory data better, a model with a singularity at zero energy transfer, and the most realistic model, a model with a near-singularity, are fitted to the trajectory data in the literature. The typical effect of the energy transfer on the recombination rate constant is maximal at low pressures and this region is the one studied here. The distribution function for the limiting dissociation rate constant k_0 at low pressures is shown to obey a Wiener–Hopf integral equation and is solved analytically for the first two models and perturbatively for the other two. For the single exponential model, this method yields the trial solution of Troe. The results are applied to the dissociation of O_3 in the presence of argon, for which classical mechanical trajectory data are available. The k_0's for various models are calculated and compared, the value for the near-singularity model being about ten times larger than that for the first two models. This trend reflects the contribution to the cross section from collisions with larger impact parameter. In the present study of the near-singularity model, it is found that k_0 is not sensitive to reasonable values for the lower bound. Energy transfer values $\langle \Delta E \rangle$'s are also calculated and compared and can be similarly understood. However, unlike the k_0 values, they are sensitive to the lower bound, and so any comparison of a classical trajectory analysis for $\langle \Delta E \rangle$'s with the kinetic experimental data needs particular care. © *2008 American Institute of Physics*.
[DOI: 10.1063/1.3026605]

I. INTRODUCTION

In the treatment of gas phase dissociation, unimolecular isomerization, and bimolecular recombination reactions, it has been recognized for many years that "weak collisions" rather than "strong collisions" play a major role in the activation and deactivation of the vibrationally hot intermediate complexes in these reactions.[1–5] Our interest in the subject was prompted by studies of ozone whose formation and isotopic effects have been of much recent interest.[6–22] In general, the formation of a molecule AB is described by

$$A + B \rightleftarrows AB^*, \tag{1}$$

$$AB^* + M \rightarrow AB + M, \tag{2}$$

where M is a collision partner and AB^* is a vibrationally excited intermediate. In a weak collision assumption, unlike in a strong collision one, many collisions with M are required to activate and deactivate a reactant molecule. When the collision is "weak," the AB^* may still have enough energy after the collision in reaction (2) to redissociate into $A+B$, instead of always being "deactivated," and so a set of such equations with different energy is considered, leading to a master equation or to a steady-state equation. The latter is then solved for the probability distribution function for the vibrational energy in the energetic intermediate AB^*.

Information on the collisional energy transfer in reactions such as in Eq. (2) is usually obtained from the pressure dependence of the reaction rate of the overall reactions (1) and (2), using the solution of the collisional master or steady-state equation to fit these experimental reaction rate versus pressure data.[3,5] To this end, a functional form for the collision energy transfer probability, denoted here by $Z(E',E)$, is typically assumed, and its parameters are calculated from the fit. The functional forms used for this purpose are usually the exponential model introduced by Rabinovitch, used in Sec. II A, or a step ladder in which the reactant molecule gains or loses energy in collisions in discrete amounts called "steps."[1,2,23,24] Hold *et al.*[25] also introduced a stretched exponential model. A biexponential model was used by Brown and Miller[26] and modified by Hu and Hase.[27] Complementing these studies have been *ab initio* or semiempirical calculations of the collisional energy transfer, frequently using classical mechanical trajectories for the collisions.[26–36] Analytical treatments of vibrational energy transfer have been given for particular cases.[5,34–38] In particular, a detailed discussion of the original master equation and of its steady-state approximation is given by Penner and Forst,[38] who expressed the solution in terms of hypergeometric functions.

The $Z(E',E)$ is defined as the number of collisions per unit time with energy transfer for the vibrationally excited intermediate $E \rightarrow (E',E'+dE')$ per unit dE'. $Z(E',E)$ has units of s^{-1} energy^{-1} when it is chosen to be the product of

a)Electronic mail: ram@caltech.edu.

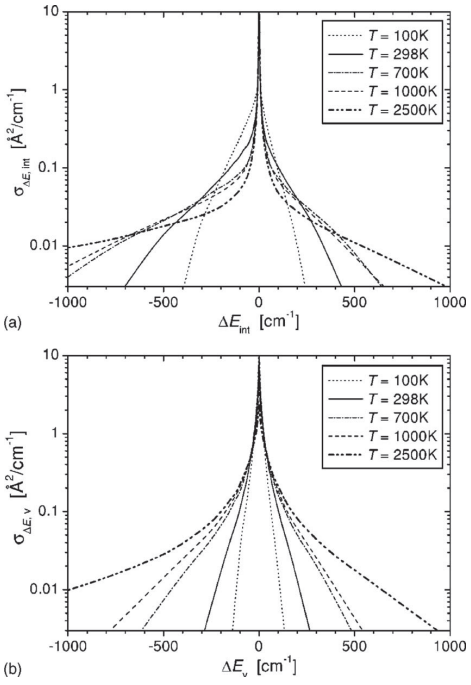

FIG. 1. Cross sections for internal (a) and vibrational (b) energy transfers as functions of ΔE_{int} and ΔE_v for different temperatures (Ref. 40).

the concentration of colliders and the bimolecular collision rate constant for the transition $E \rightarrow E'$ per dE'. Its theoretical calculation involves an integration over impact parameters b, using $2\pi bdb$ as a weighting factor. Collisions with large b contribute mainly to the energy transfer near $E'-E \approx 0$. When plotted versus $E'-E$, they yield an elastic-collision peak in the classical limit at $E=E'$ corresponding to $b=\infty$. The larger the average value of the energy transfer per collision in any reaction, the further the important energy transfer region is from the elastic $E'-E=0$ peak. Examples of the tendency toward a singular behavior at $E'=E$ are seen in Refs. 39–43. The data of Ivanov and Schinke[40] shown in Fig. 1 are used later as an example. From a quantum mechanical view, the inelastic collisions have a lower bound for the energy transfer $|E-E'|$, namely, a quantum of rotational or vibrational energy, depending upon the collision. So in quantum mechanical calculations, there is no such singularity, but instead there is a near-elastic peak. Therefore, a lower bound should be imposed. A maximum impact parameter $b_{\max}$ such that no trajectories lead to sizable energy transfer for $b > b_{\max}$ has usually been imposed in the literature to avoid this peak.[26–35] Then a single exponential, step-ladder or biexponential model was usually adopted to fit the trajectory data. For example, Brown and Miller[26] neglected the bin in which $E'-E \approx 0$ with a bin size of around 30 cm^{-1} in a biexponential fit to the trajectory data. Hu and Hase[27] suggested that $b_{\max}$ should be identified as the value of b at which the average energy transfer equals the inverse of the state density. In such a choice, the resulting collision cross section was considerably larger than the usually assumed value, but within 5% of the experimental value.[27]

The paper is organized as follows. The theory is described in Sec. II for the different models. It is applied to a particular system in Sec. III. The results are discussed in Sec. IV, with concluding remarks in Sec. V.

II. THEORY

A. General aspects

In using trajectories to calculate the transition rate $Z(E',E)$, a random sampling of trajectories is performed over the vibrational and rotational coordinates and their conjugate momenta of the vibrationally excited intermediate and over a Boltzmann-weighted distribution of relative velocities of the collision partners.[31–36] The calculations of energy transfer are typically made as a function of the internal energy E of the energetic intermediate, its total angular momentum J,[44] and occasionally K, the projection of J along a specified principal axis of rotation, typically that with the smallest moment of inertia. For notational simplicity, we suppress the symbol J in the following.

To obtain insight into the effect of the near-elastic peak at $|E'-E|=0$ in the comparison between experimental data and trajectories, it is convenient to consider the collisional steady-state/reaction equations, and obtain approximate analytical solutions. Examples of other treatments are also available.[45–59]

We focus on the limiting low pressure rate constant k_0. It is of particular interest partly because it describes the maximum effect of the collisions and partly because it is simpler to treat than the rate constant at higher pressures, where a solution of the complete master equation would have been necessary. While simple theoretical expressions for the distribution function of different (E,J) states of the reactants and for the energy transfer can also be obtained for the high-pressure limit of k, k_∞, they do not provide insight into the effect of energy transfer on k itself, since k_∞ is independent of $Z(E',E)$. The effect of the near-elastic peak should be largest at low pressures, since the average energy of the reacting vibrationally excited intermediate in a unimolecular reaction or a bimolecular recombination is well known to decrease when the pressure is decreased.[60] Accordingly, the vibrational energy of the typical molecule is closer to the energy dividing line between stable and unstable intermediates and so is closer to the near-elastic peak when the pressure is decreased.

To treat the kinetics for the recombination of two species $A+B \rightarrow AB$, one can either proceed from the reactants $(A+B)$ or from the product (AB). If a tagged A is followed in time in its progress to form AB, and if a tagged A in AB is followed in time in its progress to form $A+B$, beginning with an equilibrium concentrations of AB for the given A and B concentration, the sum of the tagged distribution functions at any energy E is equal to the equilibrium distribution at that E. Thus, to solve the problem, one can either begin with a tagged A or a tagged AB. To simplify the comparison with earlier work,[46–50] we begin with AB and use the result to calculate also the rate of recombination $A+B \rightarrow AB$.

We consider the reaction in the low pressure regime

$$M + AB(E) \underset{Z(E,E')}{\overset{Z(E',E)}{\rightleftarrows}} M + AB^*(E'), \tag{3}$$

$$AB^*(E') \rightarrow A + B \quad (\text{if } E' \geq 0), \tag{4}$$

where $E' \geq 0$ denotes the internal energies of any reaction intermediate AB^* that can dissociate into the separated reactants without a further collision. Energies E' in the reactant that are negative are insufficient for dissociation.

The scheme [Eqs. (3) and (4)] is appropriate only for the low pressure limit of the dissociation rate. At higher pressures, an $AB^*(E')$ on a second collision can also yield an AB^* with a different E', where both E's are greater than zero. At sufficiently low pressures, each $AB^*(E')$ formed in reaction (3) with $E' \geq 0$ ultimately dissociates into $A+B$ before any further collision. For this case, the problem simplifies and a large set of equations (the master equation) for $AB^*(E')$ is not needed for $E' > 0$.

We denote the probability energy distribution function for AB by $g(E)$ and write

$$k_0 = \int_{E'=0}^{\infty} \int_{E=-\infty}^{0} g(E) Z(E',E) dE' dE. \tag{5}$$

The equilibrium probability that AB has an energy in the range E, $E+dE$ is $g_{\text{eq}}(E)dE$, where

$$g_{\text{eq}}(E) = \rho(E) \exp(-E/kT)/Q \tag{6a}$$

and $\rho(E)$ denotes the density of quantum states of the molecule, Q is the partition function of AB in the center-of-mass system of coordinates. When the energy is measured relative to $E=0$, the dissociation limit Q is also calculated relative to that energy, and so contains a factor $\exp(D/kT)$, where D is the dissociation energy of AB measured from the bottom of its potential well to the dissociation level. When E becomes very negative in the steady-state problem, i.e., when $E \rightarrow -D$ and $g(E) \rightarrow g_{\text{eq}}(E)$. This condition on $g(E)$ serves as a boundary condition,

$$g(E) \rightarrow g_{\text{eq}}(E) \quad E \rightarrow -D. \tag{6b}$$

After a short initial period, $g(E)$ relaxes toward a steady state.[5] We use a steady-state approximation here. The steady-state equation for $g(E)$ is

$$0 = \int_{-\infty}^{0} Z(E,E') g(E') dE' - g(E) \int_{-\infty}^{\infty} Z(E',E) dE' \quad E \leq 0. \tag{7a}$$

The latter can be rewritten as

$$g(E) = \int_{-\infty}^{0} Z(E,E') g(E') dE' \Big/ \int_{-\infty}^{\infty} Z(E',E) dE', \quad E \leq 0. \tag{7b}$$

An analytical solution of this integral equation for a single exponential model for the energy transfer was first given by Troe,[5] who obtained it using a trial solution method. For the present article, we note instead that Eq. (7b) is a homogeneous Wiener–Hopf equation of the second kind and use the Wiener–Hopf method[61] to obtain a solution.

We first study the single exponential and biexponential models with this method. For the single exponential model, in terms of a deactivation constant γ and of an activation constant γ', we have

$$Z(E',E) = Z_0 \exp(-(E-E')/\gamma), \quad E' \leq E, \tag{8a}$$

$$Z(E',E) = Z_0 \exp(-(E'-E)/\gamma'), \quad E' \geq E, \tag{8b}$$

and for the biexponential model,

$$Z(E',E) = Z_0[\exp(-(E-E')/\gamma) + c \exp(-(E-E')/d)], \quad E' \leq E, \tag{9a}$$

$$Z(E',E) = Z_0[\exp(-(E'-E)/\gamma') + c \exp(-(E'-E)/d')], \quad E' \geq E, \tag{9b}$$

where Z_0 is a constant and γ, γ' and d, d' are related by microscopic reversibility (detailed balance).

The quantities $Z(E',E)$ and $Z(E,E')$ satisfy microscopic reversibility

$$\rho(E) Z(E',E) = \rho(E') Z(E,E') \exp(-(E'-E)/kT). \tag{10}$$

For practical purposes, we can typically treat the lower limit on E as $E \rightarrow -\infty$, a minor approximation when $D \gg kT$. Neglecting the effect of the change in $\rho(E)$ between E and E' in the vicinity of $E=0$, Eqs. (8a), (8b), (9a), (9b), and (10), yield

$$\frac{1}{\gamma'} = \frac{1}{\gamma} + \frac{1}{kT}, \tag{11a}$$

$$\frac{1}{d'} = \frac{1}{d} + \frac{1}{kT}. \tag{11b}$$

The constants c and d are obtained later from fitting classical trajectory calculations data for vibrational energy transfer.

We have also examined a model with singularity at $E'-E=0$ using another method,

$$Z(E',E) = Z[1 + C(E-E')^{-\alpha}] \exp(-(E-E')/\gamma), \quad E' \leq E, \tag{12a}$$

$$Z(E',E) = Z[1 + C(E'-E)^{-\alpha}] \exp(-(E'-E)/\gamma'), \quad E' \geq E, \tag{12b}$$

where γ and γ' are the same as those of the single exponential model. C and α and are obtained later from classical trajectory data.

B. Single exponential model

To compare with the earlier and insightful result in literature by Troe,[5] we use the single exponential expression for the collisional energy transfer rate, namely, Eqs. (8a) and (8b). The average "up-energy" transfer, defined as the average energy increase in the molecule for collisions that lead to an increase in energy, is

$$\langle \Delta E\rangle_{\mathrm{up}} = \int_E^\infty (E'-E)Z(E',E)dE' \Big/ \int_E^\infty Z(E',E)dE' = \gamma', \quad E' \geq E. \tag{13a}$$

Similarly the average "down"-energy transfer is

$$\langle \Delta E\rangle_{\mathrm{down}} = \int_{-\infty}^E (E'-E)Z(E',E)dE' \Big/ \int_{-\infty}^E Z(E',E)dE' = -\gamma, \quad E' \leq E. \tag{13b}$$

These quantities $\langle \Delta E\rangle_{\mathrm{up}}$ and $\langle \Delta E\rangle_{\mathrm{down}}$ are not observables in the usual reaction rate experiments and so cannot be directly compared with experiment. In computation, the quantity $\langle \Delta E^2\rangle$ is a more convenient parameter than $\langle \Delta E\rangle$.[62,63] Here in our discussion, the average over impact parameter b and the other initial variables is included in the definition of $Z(E',E)$ at the given E. The rate constant k on the other hand, as a function of pressure and its limiting value at low pressure k_0, are the observables in these experiments. Nevertheless, since the values of the moments are often calculated in the literature from classical trajectories or from approximate fits to those data, the values of these moments are often cited, and are calculated here, bearing in mind that they are not directly observable and are model dependent.

To solve Eq. (7b), we use a Wiener–Hopf procedure[61] and, as in the standard procedure, first extend the domain in Eqs. (7a) and (7b) from $E \leq 0$ to $E > 0$ by introducing the functions $g_-(E)$ and $g_+(E)$, $g(E) = g_-(E) + g_+(E)$, with the properties

$$g_-(E) = g(E), \quad E \leq 0, \qquad = 0, \quad E > 0, \tag{14a}$$

$$g_+(E) = 0, \quad E \leq 0, \qquad = g(E), \quad E > 0. \tag{14b}$$

Here, $g(E)$ is the unknown function. From Eqs. (7b) and (14), we then obtain for the entire E-range, $-\infty < E < \infty$,

$$g_-(E) + g_+(E) = \int_{-\infty}^\infty g_-(E')Z(E,E')dE' \Big/ \int_{-\infty}^\infty Z(E',E)dE', \quad -\infty < E < \infty. \tag{15a}$$

For $E \leq 0$, this equation becomes

$$g_-(E) = \int_{-\infty}^0 g_-(E')Z(E,E')dE' \Big/ \int_{-\infty}^\infty Z(E',E)dE', \quad -\infty < E \leq 0, \tag{15b}$$

which coincides with Eq. (7b) for $E \leq 0$. For $E > 0$, we have

$$g_+(E) = \int_{-\infty}^0 g_-(E')Z(E,E')dE' \Big/ \int_{-\infty}^\infty Z(E',E)dE', \quad 0 < E < \infty. \tag{15c}$$

The idea behind the Wiener–Hopf method is to solve this pair of equations for $g_+(E)$ and $g_-(E)$ and hence, from Eq. (14), for $g(E)$. Because $Z(E,E')$ has one form in Eq. (8) when $E' \geq E$ and has a different form when $E' \leq E$, there are two terms for $Z(E,E')$. On taking the Fourier transform $\tilde{f}(z) = \int_{-\infty}^\infty e^{2\pi i z E} f(E)dE$, $z = u + iv$, where u and v are real, and using the convolution theorem, we have from Eqs. (8) and (15a),

$$\tilde{g}_-(z) + \tilde{g}_+(z) = \frac{\tilde{g}_-(z)}{\gamma+\gamma'}\left(\frac{1}{1/\gamma + 2\pi i z} + \frac{1}{1/\gamma' - 2\pi i z}\right), \tag{16}$$

which can be rewritten as

$$\frac{2\pi i z(2\pi i z - 1/kT)\tilde{g}_-(z)}{1/\gamma + 2\pi i z} = \frac{(1/\gamma' - 2\pi i z)\tilde{g}_+(z)}{(\gamma+\gamma')}. \tag{17}$$

The solution for the $\tilde{g}_-(z)$ in Eq. (17) obtained in Appendix A is

$$\tilde{g}_-(z) = G_s \frac{(1/\gamma + 2\pi i z)}{2\pi i z(2\pi i z - 1/kT)}, \tag{18}$$

where G_s is a constant. The solution for $\tilde{g}_+(z)$ is not needed but is given for completeness in Appendix A. The inverse transformation of Eq. (18) for $\tilde{g}_-(z)$ yields

$$g_-(E) = \int_{-\infty+iv}^{\infty+iv} \tilde{g}_-(z)e^{-2\pi i z E}dz = G_s'\left(\frac{kT}{\gamma'}e^{-E/kt} - \frac{kT}{\gamma}\right), \tag{19}$$

where G_s' is a constant to be determined. We have from Eq. (14a) that $g_-(E) = g(E)$ for $E \leq 0$ and when $E \to -\infty$, we have $g(E) \to g_{\mathrm{eq}}(E)$. Writing $g_{\mathrm{eq}}(E)$ as $g_{\mathrm{eq}}(0)e^{(-E/kT)}$, a value is obtained for the constant G_s', $G_s' = g_{\mathrm{eq}}(0)\gamma'/kT$, and hence

$$g(E) = g_{\mathrm{eq}}(0)\left(e^{-E/kT} - \frac{\gamma'}{\gamma}\right), \tag{20}$$

which is the trial solution given by Troe.[5] Using it, the analytical solution for the low pressure "three-body" recombination rate constant k_0 can be obtained. From Eqs. (5) and (20),

$$k_0 = Z_0 g_{\mathrm{eq}}(0)\gamma\gamma'\left(1 - \frac{\gamma'^2}{\gamma^2}\right) = Z_0(\gamma+\gamma')\frac{\gamma'^2\rho(0)}{QkT}, \tag{21}$$

where Q contains the factor $\exp(D/kt)$. This result agrees with the trial solution of Troe.[5]

C. Biexponential model

In this model, the average up-energy transfer is given by

$$\langle \Delta E\rangle_{\mathrm{up}} = \int_{E'=E}^\infty (E'-E)Z(E',E)dE' \Big/ \int_{E'=E}^\infty Z(E',E)dE' = (\gamma'^2 + cd'^2)/(\gamma' + cd'). \tag{22a}$$

Similarly

$$\langle \Delta E\rangle_{\text{down}} = \int_{E'=-\infty}^{E} (E'-E)Z(E',E)dE' \Bigg/ \int_{E'=-\infty}^{E} Z(E',E)dE' = -(\gamma^2+cd^2)/(\gamma+cd). \tag{22b}$$

For the biexponential model, following a procedure similar to that in Sec. II B for the single exponential model, we obtain

$$\frac{2\pi iz(2\pi iz-1/kT)(2\pi iz-r_4)\tilde{g}_-(z)}{(1/\gamma+2\pi iz)(1/d+2\pi iz)} = -\frac{(1/\gamma'-2\pi iz)(1/d'-2\pi iz)\tilde{g}_+(z)}{2\pi iz-r_3}, \tag{23}$$

where

$$r_3 = 1/2kT \pm \sqrt{(1/2kT)^2+[(\gamma+\gamma')/dd'+(cd+cd')/\gamma\gamma']/(\gamma+\gamma'+cd+cd')}$$

and

$$r_4 = 1/2kT - \sqrt{(1/2kT)^2+[(\gamma+\gamma')/dd'+(cd+cd')/\gamma\gamma']/(\gamma+\gamma'+cd+cd')}$$

.

The solution for $\tilde{g}_-(z)$ in Eq. (23), obtained in Appendix B, is

$$\tilde{g}_-(z) = G_{bi}\frac{(1/\gamma+2\pi iz)(1/d+2\pi iz)}{2\pi iz(2\pi iz-1/kT)(2\pi iz-r_4)}. \tag{24}$$

Inversion yields

$$g(E) = g_{\text{eq}}(0)\left[e^{E/kT}+\frac{\gamma' d'}{\gamma d}\frac{1/kt-r_4}{r_4}-\frac{(1/\gamma+r_4)(1/d+r_4)\gamma' d'}{r_4 kt}e^{-r_4E}\right]. \tag{25}$$

This equation reduces to Eq. (19) when $d=\gamma$.

From these results, k_0 is given by

$$k_0 = Z_0\left[\gamma\gamma'+cdd'+\frac{(\gamma'^2+cd^2)\gamma' d' r_3}{\gamma d r_4}-\left(\frac{1}{\gamma}+r_4\right)\left(\frac{1}{d}+r_4\right)\frac{\gamma' d'}{r_4}\left(\frac{\gamma'}{1/\gamma+r_3}+\frac{cd'}{1/d+r_3}\right)\right]g_{\text{eq}}(0). \tag{26}$$

This equation reduces to Eq. (20) when $d=\gamma$.

D. Singularity model

The average up-energy transfer and down-energy transfer are given by

$$\langle \Delta E\rangle_{\text{up}} = \int_{E'=E}^{\infty} (E'-E)Z(E',E)dE' \Bigg/ \int_{E'=E}^{\infty} Z(E',E)dE' = \gamma'[1+C(\gamma')^{-\alpha}(1-\alpha)\Gamma(1-\alpha)]/[1+C(\gamma')^{-\alpha}\Gamma(1-\alpha)], \tag{27a}$$

$$\langle \Delta E\rangle_{\text{down}} = \int_{E'=-\infty}^{E} (E'-E)Z(E',E)dE' \Bigg/ \int_{E'=-\infty}^{E} Z(E',E)dE' = -\gamma[1+C(\gamma)^{-\alpha}(1-\alpha)\Gamma(1-\alpha)]/[1+C(\gamma)^{-\alpha}\Gamma(1-\alpha)]. \tag{27b}$$

To use a perturbation method for this case, although a suitable branch-point analysis might also be used, the $g(E)$ given by Eq. (20) and $Z(E',E)$ given by Eq. (12) are introduced into the right hand side of Eq. (7b). A new $g(E)$ is obtained, and this step is then iterated. After several iterations, we find that $g(E)$ for $E<-\gamma/100$ ceases to be affected further. For $-\gamma/100 < E \leq 0$, $g(E)$ becomes negligible because of continuity with $g(E)=0$ for $E>0$. Using this $g(E)$ to calculate k_0, we obtain a value close to the one obtained using $g(E)$ from Eq. (20), for $g(E)$ can be used here. The expression for the rate constant k_0 thus given by Eq. (5) is then

$$k_0 = Z_0\int_{E'=0}^{\infty}\int_{E=-\infty}^{0} g_{\text{eq}}(0)\left(e^{-E/kT}-\frac{\gamma'}{\gamma}\right)e^{-(E'-E)/\gamma'}(1+C(E'-E)^{-\alpha})dE'dE = Z_0 g_{\text{eq}}(0)\gamma'\gamma\left(1-\frac{\gamma'^2}{\gamma^2}\right)$$
$$+ CZ_0 g_{\text{eq}}(0)\int_{E'=0}^{\infty}\int_{E=-\infty}^{0}\left(e^{-E/kT}-\frac{\gamma'}{\gamma}\right)e^{-(E'-E)/\gamma'}(E'-E)^{-\alpha}dE'dE. \tag{28}$$

E. Near-singularity model

For this model, the same functions are adopted for $Z(E',E)$ as in the singularity model. Because of the quantum limit, we set a lower bound ε to the energy transfer in the integral when calculating the energy transfer and rate constant. Equation (27) then becomes

$$\langle \Delta E\rangle_{\mathrm{up}} = \int_{E'=E+\varepsilon}^{\infty} (E'-E)Z(E',E)dE' \Big/ \int_{E'=E+\varepsilon}^{\infty} Z(E',E)dE'$$
$$= \frac{\int_{E'=E+\varepsilon}^{\infty} (E'-E)[1+C(E'-E)^{-\alpha}]\exp(-(E'-E)/\gamma')dE'}{\int_{E'=E+\varepsilon}^{\infty} [1+C(E'-E)^{-\alpha}]\exp(-(E'-E)/\gamma')dE'}, \tag{29a}$$

$$\langle \Delta E\rangle_{\mathrm{down}} = \int_{E'=-\infty}^{E-\varepsilon} (E'-E)Z(E',E)dE' \Big/ \int_{E'=-\infty}^{E-\varepsilon} Z(E',E)dE'$$
$$= \frac{\int_{E'=E+\varepsilon}^{\infty} (E'-E)[1+C(E-E')^{-\alpha}]\exp(-(E-E')/\gamma)dE'}{\int_{E'=E+\varepsilon}^{\infty} [1+C(E-E')^{-\alpha}]\exp(-(E-E')/\gamma)dE'}, \tag{29b}$$

and we also have

$$k_0 = Z_0\left(\int_{E'=\varepsilon}^{\infty}\int_{E=-\infty}^{0} + \int_{E'=0}^{\varepsilon}\int_{E=-\infty}^{E'-\varepsilon}\right) g_{\mathrm{eq}}(0)\left(\mathrm{e}^{-E/kT} - \frac{\gamma'}{\gamma}\right)\mathrm{e}^{-(E'-E)/\gamma'}(1+C(E'-E)^{-\alpha})dE'dE$$
$$= Zg_{\mathrm{eq}}(0)\left[\gamma'\gamma\left(1-\frac{\gamma'^2}{\gamma^2}\right)\mathrm{e}^{-\varepsilon/\gamma'} - \gamma\gamma'\left(kT+\frac{\varepsilon\gamma'}{\gamma^2}\right)\mathrm{e}^{-\varepsilon/\gamma'} + \gamma kT\mathrm{e}^{-\varepsilon/\gamma}\right] + CZg_{\mathrm{eq}}(0)\left(\int_{E'=\varepsilon}^{\infty}\int_{E=-\infty}^{0} + \int_{E'=0}^{\varepsilon}\int_{E=-\infty}^{E'-\varepsilon}\right)$$
$$\times\left(\mathrm{e}^{-E/kT} - \frac{\gamma'}{\gamma}\right)\mathrm{e}^{-(E'-E)/\gamma'}(E'-E)^{-\alpha}dE'dE. \tag{30}$$

III. APPLICATION TO $Ar+O_3$

For the collisions of O_3 with Ar, we obtain, from the trajectory data,[40] the parameters for different temperatures and calculate $\langle \Delta E\rangle$ and k_0 for the single exponential model, the biexponential model, and the singularity model.

A. Comparison of single exponential and biexponential models

We determine γ, c, and d from classical trajectory data,[40] and γ' and d' are obtained from Eq. (11). The results for the $\langle \Delta E\rangle$ and k_0 for both models are given in Table I.

B. Comparison of single exponential and singularity models

We determine C and α from the classical trajectory data.[40] The average energy transfer and rate constants calculated from it are given in Table II.

C. Comparison of single exponential and near-singularity models

According to Ref. 40, collisional changes in K provide a major route for the vibrational energy transfer. On that basis, a lower bound for the energy transfer is the quantum cutoff for the rotational energy $(A-B)\langle 2K+1\rangle_J$, where A and B are the rotational constants and K is the projection of the angular momentum along the principal axis of rotation, as noted in Sec. III A. An average over J is used since we averaged over J in the calculation of energy transfer. In Ref. 40, $A\sim 3.5\ \mathrm{cm}^{-1}$ and $B\sim 0.4\ \mathrm{cm}^{-1}$. From these values, the estimated lower bounds are given in Table III, namely from 15 to 30 cm^{-1}, depending on the temperature. The resulting average energy transfer and rate constants are calculated and shown in Table III.

The cases $T=700$ K and $T=1000$ K are purely hypothetical since no experimental data are available for those conditions, only trajectory results[40] are available for these temperatures.

TABLE I. Example of correction of k_0, $\langle \Delta E \rangle_{up}$, and $\langle \Delta E \rangle_{down}$. Single exponential model (s) and biexponential model (bi).

Parameters	$\frac{k_{0bi}}{k_{0s}}$ [a]	$\frac{\langle \Delta E \rangle_{upbi}}{\langle \Delta E \rangle_{ups}}$ [b]	$\frac{\langle \Delta E \rangle_{downbi}}{\langle \Delta E \rangle_{downs}}$ [b]
γ=43 cm^{-1} [c], c=1.70 [c], d=3.70 cm^{-1} [c], T=298 K	1.02	0.86	0.88
γ=119 cm^{-1} [c], c=3.27 [c], d=7.16 cm^{-1} [c], T=700 K	1.01	0.82	0.84
γ=163 cm^{-1} [c], c=3.49 [c], d=8.57 cm^{-1} [c], T=1000 K	1.01	0.83	0.85

[a] k_{0s} refers to the rate constant of the single exponential model and k_{0bi} refers to the one of the biexponential model.
[b] A notation similar to that in footnote b is used for $\langle \Delta E \rangle_{up}$ and $\langle \Delta E \rangle_{down}$.
[c] Values of parameters were obtained using the trajectory results of O_3/Ar collisions from Ref. 40.

IV. DISCUSSION

For Ar+O_3, the $|\langle \Delta E \rangle|$ for the biexponential model is seen in Table I to be a little smaller than that from the single exponential model by about 10%–20%. The k_0 for this biexponential model is about the same as that for the single exponential model (Table I). The $|\langle \Delta E \rangle|$ for the singularity model is seen in Table II to be smaller than that from the single exponential model by 20%–40%. When we set a lower bound in ΔE for the singularity model, i.e., the near-singularity model, and calculate the average up- and down-energy transfer, the results shown in Table III agree well with those from Ref. 40, as they should if this truncated singularity model is a good description of the trajectory data. The k_0 for the singularity and near-singularity models is larger than that for the single exponential model by a large factor, 25, at room temperature, as seen in Tables II and III.

These results for k_0 can be interpreted in terms of the extra contribution from large b collisions for the biexponential, singularity, and near-singularity models, compared with the single exponential model. The single exponential model is fitted to the low b data. For the comparison of singularity and near-singularity models and the single exponential model, the difference for $\langle \Delta E \rangle_{up/down}$ is less than that for the k_0. This result can also be understood. k_0 is seen from Eq. (5) to have a larger contribution from small $|\Delta E|$ values to the integral than for the single exponential model. In the case of $|\langle \Delta E \rangle|$, the numerator in Eqs. (22), (27), and (29) is again enhanced by this enhanced $Z(E,E')$ but the denominator is enhanced even more, since the former is weighted by the small ΔE.

In Refs. 11–13, the average down-energy refers to the total internal energy transfer instead of only vibrational energy transfer treated here. So that value should be much larger than that if only vibrational energy transfer were considered. If we compare the total internal down-energy transfer $\langle \Delta E_{int}\downarrow \rangle$ in Ivanov and Schinke's trajectory work[40] with the values in Gao and Marcus' work[11–13] used to fit experimental data, there is only a small difference in $\langle \Delta E_{int}\downarrow \rangle$.

The authors of Ref. 40 gave a different reason for choosing a cutoff of 3 or 10 cm^{-1} for $|\Delta E_{int}|$, namely that the energy transfer averages gradually decrease as the value for $|\Delta E_{int}|$ cutoff decreases and decrease particularly rapidly for the cutoff below the ones they chose. It was suggested that b_{max} may be found by weighting the average nenrgy transfer versus impact parameter by the differential cross section.[63]

Another result seen in Table I is that both γ and d (γ' and d') for the trajectory data are proportional to kT, though are much smaller, and the ratios d/γ and d'/γ' remain almost the same. The increase in d and d' with temperature means that small energy transfer behavior becomes less important at higher temperatures, as expected. The typical system is further removed from the singularity or $E'-E=0$.

V. CONCLUDING REMARKS

Analytical solutions for the low pressure rate constant are given, using several different approximations to the trajectory data, the single exponential, a biexponential, a singularity, and a near-singularity models. The near-singularity model is the most realistic. The differences should be maximal in the low pressure regime. Expressions are obtained for the limiting low pressure rate constant k_0, $\langle \Delta E \rangle_{up}$, and $\langle \Delta E \rangle_{down}$. The values of k_0 from the biexponential are similar to those from the single exponential model. Those from the singularity and near-singularity models are an order of magnitude larger than those from the single exponential model. The origin of the difference is the large additional contribution of collisions with large cross sections in the singularity

TABLE II. Example of correction of k_0, $\langle \Delta E \rangle_{up}$, and $\langle \Delta E \rangle_{down}$. Single exponential model and the singularity model.

Parameters	$\frac{k_{0singu}}{k_{0s}}$ [a]	$\frac{\langle \Delta E \rangle_{upsingu}}{\langle \Delta E \rangle_{ups}}$ [b]	$\frac{\langle \Delta E \rangle_{downsingu}}{\langle \Delta E \rangle_{downs}}$ [b]
α=0.20 [c], γ=43 cm^{-1} [c], C=50 [c], T=298 K	25.1	0.81	0.81
α=0.35 [c], γ=119 cm^{-1} [c], C=50 [c], T=700 K	10.8	0.67	0.67
α=0.41 [c], γ=163 cm^{-1} [c], C=50 [c], T=1000 K	7.6	0.63	0.63

[a] k_{0singu} refers to the rate constant of the singularity model and k_{0s} refers to the single exponential model.
[b] A notation similar to that in footnote b is used for $\langle \Delta E \rangle_{up}$ and $\langle \Delta E \rangle_{down}$.
[c] Values of parameters were obtained using the trajectory results of O_3/Ar collisions from Ref. 40.

TABLE III. Example of cutoff effect for the near-singularity model.

Parameters	$\frac{k_{0n\text{-}singu}}{k_{0s}}$ [a]	$\frac{\langle\Delta E\rangle_{upn\text{-}singu}}{\langle\Delta E\rangle_{ups}}$ [b]	$\frac{\langle\Delta E\rangle_{downn\text{-}singu}}{\langle\Delta E\rangle_{downs}}$ [b]
α=0.20 [c], γ=43 cm^{-1} [c], C=50 [c], T=298 K	24.9	1.06	1.06
α=0.35 [c], γ=119 cm^{-1} [c], C=50 [c], T=700 K	10.8	0.86	0.98
α=0.41 [c], γ=163 cm^{-1} [c], C=50 [c], T=1000 K	7.6	1.04	1.04

[a] k_{0s} refers to the rate constant of the single exponential model and $k_{0n\text{-}singu}$ refers to the rate constant of the near-singularity model with a lower bound. This lower bound is 15 cm^{-1} for T=298 K, 25 cm^{-1} for T=700 K, and 30 cm^{-1} for T=1000 K.
[b] A notation similar to that in footnote b is used for $\langle\Delta E\rangle_{up}$ and $\langle\Delta E\rangle_{down}$.
[c] Values of parameters were obtained using the trajectory results of O_3/Ar collisions from Ref. 40.

and near-singularity models that is absent in the single exponential model. The values from single exponential model for the $\langle\Delta E\rangle$ are somewhat larger than those from the biexponential model by about 10%–20% and larger than those from the singularity model by 20%–40% but similar to those from the near-singularity model. The physical origin of these differences lies in the smaller contribution from the smaller cross sections with large energy transfer in the biexponential and singularity models, compared with that in the single exponential model. While the numerator in Eqs. (22), (27), and (29) is enhanced by this enhanced $Z(E,E')$, the denominator is enhanced even more, since the former is weighted by the small ΔE. For the near-singularity model, a big part of small energy transfer collision is removed. This cancels out the former effect.

ACKNOWLEDGMENTS

It is a pleasure to acknowledge the support of this research by the National Science Foundation and to thank Professor Jau Tang for a helpful discussion and Professor Reinhard Schinke and Dr. Mikhail V. Ivanov for providing their detailed classical trajectory data.

APPENDIX A: SOLUTION OF EQ. (7b) AS A WIENER–HOPF EQUATION OF THE SECOND KIND FOR THE SINGLE EXPONENTIAL MODEL

We first note that $|\tilde{g}_-(z)|=|\int_{-\infty}^{\infty}e^{2\pi izE}g_-(E)dE|$ and $\tilde{g}_-(z)$ is a function of z alone. Also, $|\tilde{g}_-(z)|=|\int_{-\infty}^{0}e^{2\pi iuE}e^{-2\pi\nu E}g_-(E)dE|\le\int_{-\infty}^{0}e^{-2\pi\nu E}|g_-(E)|dE$. If we can find a solution for $\tilde{g}_-(z)$ such that $|g_-(E)|<M_1e^{2\pi v_-E}$, as $E\to-\infty$, where $\nu_->0$ and hence tends to zero as $E\to-\infty$, then we have

$$|\tilde{g}_-(z)|<\int_{-\infty}^{0}e^{-2\pi\nu E}M_1e^{2\pi\nu_-E}dE=M_1\frac{1}{2\pi(\nu_--\nu)}. \quad \text{(A1)}$$

Thereby, in the part of the lower half plane where Im $z=v<v_-$, $|\tilde{g}_-(z)|$ has no singularity. So $\tilde{g}_-(z)$ is an analytic function in the half of the z-plane for which Im $z<v_-$.

Next we consider $\tilde{g}_+(z)$,

$$|\tilde{g}_+(z)|=|\int_{-\infty}^{\infty}e^{2\pi izE}g_+(E)dE|=|\int_{0}^{\infty}e^{2\pi izE}g_+(E)dE|, \quad \text{(A2)}$$

since $g_+(E)=0$ for $E<0$. For $E>0$ it follows from Eq. (14c) that

$$|\tilde{g}_+(z)|=|\int_0^\infty e^{2\pi izE}\times\left[\int_{-\infty}^{0}g_-(E')Z(E,E')dE'\right]dE|\Big/\int_{-\infty}^{\infty}Z(E',E)dE'. \quad \text{(A3)}$$

We note that $\tilde{g}_+(z)$ is a function of z alone, and also from Eqs. (8a) and (A3),

$$|\tilde{g}_+(z)|=\left|\int_0^\infty e^{2\pi iuE}e^{-2\pi\nu E}\left[\int_{-\infty}^{0}g_-(E')\frac{1}{\gamma+\gamma'}e^{-E-E'/\gamma'}dE'\right]\times dE\right|\le\int_0^\infty e^{-2\pi\nu E}\left|\int_{-\infty}^{0}g_-(E')\frac{1}{\gamma+\gamma'}\times e^{-E-E'/\gamma'}dE'\right|dE. \quad \text{(A4)}$$

If we can find a solution $|g_-(E')|<M_1e^{2\pi v_-E'}$, where $E'<0$, then since $\nu_->0$ we have $\nu_->-\frac{1}{2\pi\gamma'}$ and then

$$|\tilde{g}_+(z)|\le\int_0^\infty e^{-2\pi\nu E}\left|\int_{-\infty}^{0}g_-(E')\frac{1}{\gamma+\gamma'}e^{-E-E'/\gamma'}dE'\right|dE=\frac{1}{\gamma+\gamma'}\frac{1}{2\pi\nu+1/\gamma'}\left|\int_{-\infty}^{0}g_-(E')e^{E'/\gamma'}dE'\right|<\frac{M_1}{\gamma+\gamma'}\frac{1}{2\pi\nu+1/\gamma'}\frac{1}{2\pi\nu_-+1/\gamma'}. \quad \text{(A5)}$$

Thereby, $|\tilde{g}_+(z)|\to0$ as Im $z=\nu\to\infty$, and we see that $\tilde{g}_+(z)$ has no singularity in the upper half plane for which Im $z>-(1/2\pi\gamma')$, and so is analytic in that upper half plane. The right-hand side of Eq. (17) is therefore analytic in the upper half plane, Im $z>-(1/2\pi\gamma')$. We had seen earlier in Appendix A that $\tilde{g}_-(z)$ is analytic in the lower half plane Im $z<v_-$. From the derivation on the left-hand side of Eq. (17), we need for analyticity of this side of the equation, Im $z<-1/2\pi kT$. Thereby, we require that the left-hand side of Eq. (17) is analytic in the lower half plane where Im $z<-(1/2\pi kT)$. Since $v_->0>-(1/2\pi\gamma')$ we now see

that both sides of Eq. (17) are analytic in the strip $-(1/2\pi\gamma')<\mathrm{Im}\ z<-(1/2\pi kT)$. Since the analytic continuation is unique, there exists an entire function F in the complex plane which coincides with the right-hand side of Eq. (17) in upper half plane $\mathrm{Im}\ z>-(1/2\pi\gamma')$ and coincides with the left-hand side of Eq. (17) in the lower half plane $\mathrm{Im}\ z<\mathrm{Min}(-(1/2\pi kT),v_-)$. Since $\tilde{g}_+(z)$ goes to zero, no slower than exponentially as $|z|\to\infty$, then the entire function F is bounded at infinity. One concludes that F is constant, which we denote by G_s, and so obtain

$$\tilde{g}_-(z)=G_s\frac{(1/\gamma+2\pi iz)}{2\pi iz(2\pi iz-1/kT)}, \tag{A6}$$

$$\tilde{g}_+(z)=G_s\frac{\gamma+\gamma'}{1/\gamma'-2\pi iz}. \tag{A7}$$

APPENDIX B: SOLUTION OF EQ. (7b) AS A WIENER–HOPF EQUATION OF THE SECOND KIND FOR THE BIEXPONENTIAL MODEL

Following similar procedure in Appendix A, we can now solve Eq. (23). As in Appendix A, $|\tilde{g}_-(z)|=\left|\int_{-\infty}^{\infty}e^{2\pi izE}g_-(E)dE\right|$, and $\tilde{g}_-(z)$ is a function of z alone. Also, $|\tilde{g}_-(z)|=\left|\int_{-\infty}^{0}e^{2\pi iuE}e^{-2\pi\nu E}g_-(E)dE\right|\le\int_{-\infty}^{0}e^{-2\pi\nu E}|g_-(E)|dE$. If we can find a solution for $\tilde{g}_-(z)$ such that $|g_-(E)|<M_1e^{2\pi v_-E}$, as $E\to-\infty$, where $\nu_->0$ and hence tends to zero as $E\to-\infty$. Then we have

$$|\tilde{g}_-(z)|<\int_{-\infty}^{0}e^{-2\pi\nu E}M_1e^{2\pi\nu_-E}dE=M_1\frac{1}{2\pi(\nu_--\nu)}. \tag{B1}$$

Thereby, $|\tilde{g}_-(z)|$ has no singularity in the part of the lower half plane where $\mathrm{Im}\ z=v<v_-$. So $\tilde{g}_-(z)$ is analytic in the half of the z-plane for which $\mathrm{Im}\ z<v_-$.

Next we consider $\tilde{g}_+(z)$,

$$|\tilde{g}_+(z)|=\left|\int_{-\infty}^{\infty}e^{2\pi izE}g_+(E)dE\right|=\left|\int_{0}^{\infty}e^{2\pi izE}g_+(E)dE\right|. \tag{B2}$$

Since $g_+(E)=0$ for $E<0$, for $E>0$ it follows from Eq. (14c) that

$$|\tilde{g}_+(z)|=\left|\int_{0}^{\infty}e^{2\pi izE}\left[\int_{-\infty}^{0}g_-(E')Z(E,E')dE'\right]dE\Big/\int_{-\infty}^{\infty}Z(E',E)dE'\right|. \tag{B3}$$

We note that $\tilde{g}_+(z)$ is a function of z alone, and also from Eq. (9a)

$$\begin{aligned}|\tilde{g}_+(z)|&=\left|\int_{0}^{\infty}e^{2\pi iuE}e^{-2\pi\nu E}\left[\int_{-\infty}^{0}g_-(E')\frac{1}{\gamma+\gamma'+cd+cd'}(e^{-E-E'/\gamma'}+ce^{-E-E'/d'})dE'\right]dE\right|\\&\le\int_{0}^{\infty}e^{-2\pi\nu E}\left|\int_{-\infty}^{0}g_-(E')\frac{1}{\gamma+\gamma'+cd+cd'}(e^{-E-E'/\gamma'}+ce^{-E-E'/d'})dE'\right|dE.\end{aligned} \tag{B4}$$

If, as stated above, we can find a solution $|g_-(E')|<M_1e^{2\pi v_-E'}$, where $E'<0$, then

$$\begin{aligned}|\tilde{g}_+(z)|&\le\int_{0}^{\infty}e^{-2\pi\nu E}\left|\int_{-\infty}^{0}g_-(E')\frac{1}{\gamma+\gamma'+cd+cd'}(e^{-E-E'/\gamma'}+ce^{-E-E'/d'})dE'\right|dE\\&=\frac{1}{\gamma+\gamma'+cd+cd'}\left|\frac{1}{2\pi\nu+1/\gamma'}\int_{-\infty}^{0}g_-(E')e^{E'/\gamma'}dE'+\frac{1}{2\pi\nu+1/d'}\int_{-\infty}^{0}g_-(E')e^{E'/d'}dE'\right|\\&<\frac{M_1}{\gamma+\gamma'+cd+cd'}\left(\frac{1}{2\pi\nu+1/\gamma'}\frac{1}{2\pi\nu_-+1/\gamma'}+\frac{1}{2\pi\nu+1/d'}\frac{1}{2\pi\nu_-+1/d'}\right).\end{aligned} \tag{B5}$$

Thereby, $|\tilde{g}_+(z)|\to0$ as $\mathrm{Im}\ z=\nu\to\infty$, and $\tilde{g}_+(z)$ has no singularity in the upper half plane for which $\mathrm{Im}\ z>-(1/2\pi\gamma')>-(1/2\pi d')$ and since $\nu_->0>-(1/2\pi\gamma')>-(1/2\pi d')$, it is analytic in that upper half plane. The right-hand side of Eq. (23) is therefore analytic in the upper half plane for which this condition is fulfilled and where

$$\mathrm{Im}\ z>\max(-(1/2\pi\gamma'),(-r_3/2\pi)),$$

where

$$r_3=1/2kT+\sqrt{(1/2kT)^2+[(\gamma+\gamma')/dd'+(cd+cd')/\gamma\gamma']/(\gamma+\gamma'+cd+cd')}.$$

We had seen earlier in Appendix B that $\tilde{g}_-(z)$ is analytic in the lower half plane Im $z<v_-$. From the derivation on the left-hand side of Eq. (23), we need for analyticity of this side of the equation Im $z<-1/2\pi kT$. Thereby, we require that the left-hand side of Eq. (23) is analytic in the lower half plane where Im $z<-(1/2\pi kT)$. Since $v_->0>-(1/2\pi\gamma')$, we now see that both sides of Eq. (23) are analytic in the strip $\max(-(1/2\pi\gamma'),(-r_3/2\pi))<\mathrm{Im}\ z<-(1/2\pi kT)$. Since the analytic continuation is unique, there exists an entire function F in the complex plane which coincides with the right-hand side of Eq. (23) in upper half plane $\mathrm{Im}\ z>\max(-(1/2\pi\gamma'),(-r_3/2\pi))$ and coincides with the left-hand side of Eq. (23) in the lower half plane Im $z<-(1/2\pi kT)$. Since $\tilde{g}_+(z)$ goes to zero no slower than exponentially as $|z|\to\infty$, then the entire function F should be bounded at infinity. One concludes that F is constant, which we denote by G_{bi}, and so obtain

$$\tilde{g}_-(z)=G_{bi}\frac{(1/\gamma+2\pi iz)(1/d+2\pi iz)}{2\pi iz(2\pi iz-1/kT)(2\pi iz-r_4)}. \tag{B6}$$

[1] D. C. Tardy and B. S. Rabinovitch, J. Chem. Phys. **45**, 3720 (1966).
[2] R. C. Bhattacharjee and W. Forst, Sym. (Int.) Combust., [Proc.] **15**, 681 (1975).
[3] W. G. Valance and E. W. Schlag, J. Chem. Phys. **45**, 4280 (1966).
[4] J. E. Dove, W. S. Nip, and H. Teitelbaum, Sym. (Int.) Combust., [Proc.] **15**, 689 (1975).
[5] J. Troe, J. Chem. Phys. **66**, 4745 (1977).
[6] R. E. Weston, Jr., Chem. Rev. **99**, 2115 (1999).
[7] M. H. Thiemens and H. E. Heidenreich, Science **219**, 1073 (1983).
[8] J. Yang and S. Epstein, Geochim. Cosmochim. Acta **51**, 2011 (1987).
[9] K. Mauersberger, Geophys. Res. Lett. **14**, 80, DOI: 10.1029/GL014i001p00080 (1987).
[10] D. Krankowsky, P. Lammerzahl, and K. Mauersberger, Geophys. Res. Lett. **27**, 2593, DOI: 10.1029/2000GL011812 (2000).
[11] Y. Q. Gao and R. A. Marcus, Science **293**, 259 (2001).
[12] Y. Q. Gao and R. A. Marcus, J. Chem. Phys. **116**, 137 (2002).
[13] Y. Q. Gao and R. A. Marcus, J. Chem. Phys. **117**, 1536 (2002).
[14] B. C. Hathorn and R. A. Marcus, J. Chem. Phys. **111**, 4087 (1999).
[15] J. Morton, J. Barnes, B. Schueler, and K. Mauerberger, J. Geophys. Res. **95**, 901, DOI: 10.1029/JD095iD01p00901 (1990).
[16] M. H. Thiemens and T. Jackson, Geophys. Res. Lett. **17**, 717, DOI: 10.1029/GL017i006p00717 (1990).
[17] K. Mauersberger, B. Erbacher, D. Krankowsky, J. Gunther, and R. Nickel, Science **283**, 370 (1999).
[18] D. Charlo and D. C. Clary, J. Chem. Phys. **120**, 2700 (2004).
[19] R. Schinke, S. Y. Grebenshchikov, M. V. Ivanov, and P. Fleurat-Lessard, Annu. Rev. Phys. Chem. **57**, 625 (2006).
[20] D. Babikov, B. K. Kendrick, R. B. Walker, P. R. Fleurat-Lessard, and R. Schinke, J. Chem. Phys. **119**, 2577 (2003).
[21] B. C. Hathorn and R. A. Marcus, J. Chem. Phys. **113**, 9497 (2000).
[22] C. Janssen, J. Guenther, J. K. Mauersberger, and D. Krankowsky, Phys. Chem. Chem. Phys. **3**, 4718 (2001).
[23] G. H. Kohlmaier and B. S. Rabinovitch, J. Chem. Phys. **38**, 1692 (1963).
[24] J. W. Simons, B. S. Rabinovitch, and D. W. Setser, J. Chem. Phys. **41**, 800 (1964).
[25] U. Hold, T. Lenzer, K. Luther, K. Reihs, and A. Symonds, Ber. Bunsenges. Phys. Chem **101**, 552 (1997).
[26] N. J. Brown and J. A. Miller, J. Chem. Phys. **80**, 5568 (1984).
[27] X. Hu and W. L. Hase, J. Phys. Chem. **92**, 4040 (1988).
[28] H. Hippler and J. Troe, in *Advances in Gas Phase Photochemistry and Kinetics–Biomolecular Collisions*, edited by M. N. R. Ashfold and J. E. Baggott (The Chemical Society, London, 1989).
[29] D. L. Clarke, I. Oref, and R. G. Gilbert, J. Chem. Phys. **96**, 5983 (1992).
[30] K. F. Lim and R. G. Gilbert, J. Phys. Chem. **94**, 72 (1990).
[31] A. Gelb, J. Phys. Chem. **89**, 4189 (1985).
[32] H. Hippler, H. W. Schranz, and J. Troe, J. Phys. Chem. **90**, 6158 (1986).
[33] I. Koifman, E. I. Dashevskaya, E. E. Nikitin, and J. Troe, J. Phys. Chem. **99**, 15348 (1995).
[34] M. V. Ivanov, S. Y. Grebenshchikov, and R. Schinke, J. Chem. Phys. **120**, 10015 (2004).
[35] A. J. Stace and J. N. Murrell, J. Chem. Phys. **68**, 3028 (1978).
[36] A. J. Stace and J. N. Murrell, J. Chem. Soc., Faraday Trans. **74**, 2182 (1965).
[37] I. Oppenheim, K. E. Shuler, and G. Weiss, Adv. Mol. Relax. Processes **1**, 13 (1967).
[38] A. P. Penner and W. J. Forst, J. Chem. Phys. **67**, 5296 (1977).
[39] R. G. Gilbert and S. C. Smith, *Theory of Unimolecular and Recombination Reactions* (Blackwell Scientific, Oxford, 1990).
[40] M. V. Ivanov and R. Schinke, J. Chem. Phys. **122**, 234318 (2005).
[41] N. J. Brown and J. A. Miller, J. Chem. Phys. **80**, 5568 (1984).
[42] L. M. Yoder and J. R. Barker, J. Phys. Chem. A **104**, 10184 (2000).
[43] J. R. Barker, L. M. Yoder, and K. D. King, J. Phys. Chem. A **105**, 796 (2001).
[44] S. C. Smith and R. G. Gilbert, Int. J. Chem. Kinet. **20**, 307 (1988).
[45] J. A. Miller, S. J. Klippenstein, and C. Raffy, J. Phys. Chem. A **106**, 4904 (2002).
[46] J. Keck and G. J. Carrier, J. Chem. Phys. **43**, 2284 (1965).
[47] S. H. Robertson, M. J. Pilling, D. L. Baulch, and N. J. B. Green, J. Phys. Chem. **99**, 13452 (1995) (and references cited therein).
[48] S. H. Robertson, M. J. Pilling, K. E. Gates, and S. C. Smith, J. Comput. Chem. **18**, 1004 (1997).
[49] W. D. Lawrance, A. E. W. Knight, R. G. Gilbert, and K. D. King, Chem. Phys. Lett. **76**, 113 (1980) (and references cited therein).
[50] S. Nordholm, L. E. B. Börjesson, L. Ming, and H. Svedung, Ber. Bunsenges. Phys. Chem **101**, 574 (1997) (and references cited therein).
[51] M. J. Pilling and S. H. Robertson, Annu. Rev. Phys. Chem. **54**, 245 (2003).
[52] B. J. Gaynor, R. G. Gilbert, and K. D. King, Chem. Phys. Lett. **55**, 40 (1978) (and references cited therein).
[53] A. P. Penner and W. Forst, J. Chem. Phys. **67**, 5296 (1977).
[54] T. Kato, J. Chem. Phys. **108**, 6611 (1998).
[55] T. J. Frankcombe and S. C. Smith, J. Comput. Chem. **21**, 592 (2000).
[56] K. A. Holbrook, M. J. Pilling, and S. H. Robertson, *Unimolecular Reactions*, 2nd ed. (Wiley, New York, 1996).
[57] S. Nordholm and H. W. Schranz, in *Advances in Chemical Kinetics and Dynamics, Vol. 2A*, edited by J. R. Barker (JAI, Connecticut, 1995).
[58] S. H. Kang and K.-H. Jung, Chem. Phys. Lett. **131**, 496 (1986).
[59] H. O. Pritchard, J. Phys. Chem. A **108**, 5249 (2004).
[60] W. Forst, *Theory of Unimolecular Reactions* (Academic, New York, London, 1973).
[61] A. D. Polyanin and A. V. Manzhirov, *Handbook of Integral Equations* (CRC, Boca Raton, FL, 1998).
[62] A. R. Whyte, K. F. Lim, and R. G. Gilbert, Chem. Phys. Lett. **152**, 377 (1988).
[63] O. Meroueh and W. L. Hase, Int. J. Mass Spectrom. **201**, 233 (2000).

Bibliography

[1] MV Ivanov, SY Grebenshchikov, and R Schinke. Intra- and intermolecular energy transfer in highly excited ozone complexes. *J. Chem. Phys.*, 122:234318, JUN 1 2005.

[2] DC Tardy and BS Rabinovitch. COLLISIONAL ENERGY TRANSFER . THERMAL UNIMOLECULAR SYSTEMS IN LOW-PRESSURE REGION. *J. Chem. Phys.*, 45(10):3720, 1966.

[3] R.C. Bhattacharjee and W. Forst, editors. *Fifteenth Symposium (International) on Combustion*, volume 15, Pittsburg, 1975. The Combustion Institute.

[4] WG Valance and EW Schlag. NONEQUILIBRIUM EFFECTS IN UNIMOLECULAR REACTION THEORY. *J. Chem. Phys.*, 45(11):4280, 1966.

[5] J.E. Dove, W.S. Nip, and H. Teitelbaum, editors. *Fifteenth Symposium (International) on Combustion*, volume 15, Pittsburg, 1975. The Combustion Institute.

[6] J Troe. THEORY OF THERMAL UNIMOLECULAR REACTIONS AT LOW-PRESSURES .1. SOLUTIONS OF MASTER EQUATION. *J. Chem. Phys.*, 66(11):4745, 1977.

[7] RE Weston. Anomalous or mass-independent isotope effects. *Chem. Rev.*, 99(8):2115, AUG 1999.

[8] MH Thiemens and JE Heidenreich. THE MASS-INDEPENDENT FRACTIONATION OF OXYGEN - A NOVEL ISOTOPE EFFECT AND ITS POSSIBLE COSMOCHEMICAL IMPLICATIONS. *Science*, 219(4588):1073, 1983.

[9] JM Yang and S Epstein. THE EFFECT OF THE ISOTOPIC COMPOSITION OF OXYGEN ON THE NON-MASS-DEPENDENT ISOTOPIC FRACTIONATION IN THE FORMATION OF OZONE BY DISCHARGE OF O-2. *Geochim. Cosmochim. Acta*, 51(7):2011, JUL 1987.

[10] K Mauersberger. OZONE ISOTOPE MEASUREMENTS IN THE STRATOSPHERE. *Geophys. Res. Lett.*, 14(1):80, JAN 1987.

[11] D Krankowsky, P Lammerzahl, and K Mauersberger. Isotopic measurements of stratospheric ozone. *Geophys.. Res. Lett.*, 27(17):2593, SEP 1 2000.

[12] YQ Gao and RA Marcus. Strange and unconventional isotope effects in ozone formation. *Science*, 293(5528):259, JUL 13 2001.

[13] YQ Gao and RA Marcus. On the theory of the strange and unconventional isotopic effects in ozone formation. *J. Chem. Phys.*, 116(1):137, JAN 1 2002.

[14] YQ Gao, WC Chen, and RA Marcus. A theoretical study of ozone isotopic effects using a modified ab initio potential energy surface. *J. Chem. Phys.*, 117(4):1536, JUL 22 2002.

[15] BC Hathorn and RA Marcus. An intramolecular theory of the mass-independent isotope effect for ozone. I. *J. Chem. Phys.*, 111(9):4087, SEP 1 1999.

[16] J Morton, J Barnes, B Schueler, and K Mauersberger. LABORATORY STUDIES OF HEAVY OZONE. *J. Geophys. Res.*, 95(D1):901, JAN 20 1990.

[17] MH Thiemens and T Jackson. PRESSURE DEPENDENCY FOR HEAVY ISOTOPE ENHANCEMENT IN OZONE FORMATION. *Geophys. Res. Lett.*, 17(6):717, MAY 1990.

[18] K Mauersberger, B Erbacher, D Krankowsky, J Gunther, and R Nickel. Ozone isotope enrichment: Isotopomer-specific rate coefficients. *Science*, 283(5400):370, JAN 15 1999.

[19] D Charlo and DC Clary. Quantum-mechanical calculations on pressure and temperature dependence of three-body recombination reactions: Application to ozone formation rates. *J. Chem. Phys.*, 120(6):2700, FEB 8 2004.

[20] R Schinke, SY Grebenshchikov, MV Ivanov, and P Fleurat-Lessard. Dynamical studies of the ozone isotope effect: A status report. *Annu. Rev. Phys. Chem.*, 57:625, 2006.

[21] D Babikov, BK Kendrick, RB Walker, RT Pack, P Fleurat-Lesard, and R Schinke. Formation of ozone: Metastable states and anomalous isotope effect. *J. Chem. Phys.*, 119(5):2577, AUG 1 2003.

[22] BC Hathorn and RA Marcus. An intramolecular theory of the mass-independent isotope effect for ozone. II. Numerical implementation at low pressures using a loose transition state. *J. Chem. Phys.*, 113(21):9497, DEC 1 2000.

[23] C Janssen, J Guenther, K Mauersberger, and D Krankowsky. Kinetic origin of the ozone isotope effect: a critical analysis of enrichments and rate coefficients. *Phys. Chem. Chem. Phys.*, 3(21):4718, 2001.

[24] GH Kohlmaier and BS Rabinovitch. COLLISIONAL TRANSITION PROBABILITIES FOR VIBRATIONAL DEACTIVATION OF CHEMICALLY ACTIVATED SEC-BUTYL RADICALS - RARE GASES. *J. Chem. Phys.*, 38(7):1692, 1963.

[25] JW Simons, BS Rabinovitch, and DW Setser. COLLISIONAL DEACTIVATION OF HIGHLY VIBRATIONALLY EXCITED CYCLOPROPANE. *J. Chem. Phys.*, 41(3):800, 1964.

[26] U Hold, T Lenzer, K Luther, K Reihs, and A Symonds. Collisional energy transfer probabilities in the deactivation of highly vibrationally excited aromatics. *Ber. Bunsen-ges. Phys. Chem.*, 101(3):552, MAR 1997. Discussion

Meeting of the Deutsche-Bunsen-Gesellschaft on Unimolecular Reactions, TUTZING, GERMANY, OCT 21-24, 1996.

[27] NJ Brown and JA Miller. COLLISIONAL ENERGY-TRANSFER IN THE LOW-PRESSURE-LIMIT UNIMOLECULAR DISSOCIATION OF HO2. *J. Chem. Phys.*, 80(11):5568, 1984.

[28] XC Hu and WL Hase. EFFECT OF ANHARMONICITY ON INTERMOLECULAR ENERGY-TRANSFER FROM HIGHLY VIBRATIONALLY EXCITED MOLECULES. *J. Phys. Chem.*, 92(14):4040, JUL 14 1988.

[29] H. Hippler and J. Troe. *in Advances in Gas Phase Photochemistry and Kinetics-Biomolecular Collisions*. The Chemical Society, London, 1989.

[30] DL Clarke, I Oref, RG Gilbert, and KF Lim. COLLISIONAL ENERGY-TRANSFER IN HIGHLY EXCITED MOLECULES - CALCULATIONS OF THE DEPENDENCE ON TEMPERATURE AND INTERNAL, ROTATIONAL, AND TRANSLATIONAL ENERGY. *J. Chem. Phys.*, 96(8):5983, APR 15 1992.

[31] KF Lim and RG Gilbert. CALCULATION OF COLLISIONAL - ENERGY - TRANSFER RATES IN HIGHLY EXCITED MOLECULES. *J. Phys. Chem.*, 94(1):72, JAN 11 1990.

[32] A Gelb. CLASSICAL TRAJECTORY STUDY OF ENERGY - TRANSFER BETWEEN ARGON ATOMS AND VIBRATIONALLY ROTATIONALLY EXCITED OZONE MOLECULES. *J. Phys. Chem.*, 89(20):4189, 1985.

[33] H Hippler, HW Schranz, and J Troe. Trajectory calculations of intermolecular energy - transfer in SO2-Ar collisions method and representative results. *J. Phys. Chem.*, 90(23):6158, NOV 6 1986.

[34] I Koifman, EI Dashevskaya, EE Nikitin, and J Troe. ROTATIONAL GATEWAY FOR THE VIBRATIONAL - ENERGY TRANSFER FROM EXCITED

NONLINEAR TRIATOMIC - MOLECULES. *J. Phys. Chem.*, 99(42):15348, OCT 19 1995.

[35] MV Ivanov, SY Grebenshchikov, and R Schinke. Intra- and intermolecular energy transfer in highly excited ozone complexes. *J. Chem. Phys.*, 120(21):10015, Jun 1 2004.

[36] AJ Stace and JN Murrell. CLASSICAL TRAJECTORY STUDY OF COLLISIONAL ENERGY - TRANSFER IN THERMAL UNIMOLECULAR REACTIONS. *J. Chem. Phys.*, 68(7):3028, 1978.

[37] AJ Stace and JN Murrell. DYNAMICS OF THE OXYGEN - EXCHANGE REACTION. *J. Chem. Soc., Faraday Trans.*, 74(Part 12):2182, 1978.

[38] I Oppenheim, KE Shuler, and G Weiss. STOCHASTIC THEORY OF MULTISTATE RELAXATION PROCESSES. *Adv. Mol. Relax. Processes*, 1(1):13, 1967.

[39] AP Penner and W Forst. ANALYTIC SOLUTION OF RELAXATION IN A SYSTEM WITH EXPONENTIAL TRANSITION-PROBABILITIES. *J. Chem. Phys.*, 67(11):5296, 1977.

[40] R. G. Gilbert and S. C. Smith. *Theory of Unimolecular and Recombination Reactions*. Blackwell Scientific Publications, Oxford, 1990.

[41] LM Yoder and JR Barker. *J. Phys. Chem. A*, 104:10184, 2000.

[42] JR Barker, LM Yoder, and KD King. *J. Phys. Chem. A*, 105:796, 2001.

[43] SC Smith and RG Gilbert. *Int. J. Chem. Kinet.*, 20:307, 1988.

[44] JA Miller, SJ Klippenstein, and C Raffy. *J. Phys. Chem. A*, 106:4904, 2002.

[45] J Keck and G Carrier. Diffusion Theory of Nonequilibrium Dissociation and Recombination. *J. Chem. Phys.*, 43(7):2284, OCT 1 1965.

[46] SH Robertson, MJ Pilling, DL Baulch, and NJB Green. *J. Phys. Chem.*, 99:13452, 1995.

[47] SH Robertson, MJ Pilling, KE Gates, and SC Smith. Application of inverse iteration to 2-dimensional master equations. *J. Comput. Chem.*, 18(8):1004, JUN 1997.

[48] WD Lawrance, AEW Knight, RG Gilbert, and KD King. THERMAL UNIMOLECULAR REACTIONS IN THE FALL-OFF REGIME - A MASTER EQUATION ANALYSIS. *Chem. Phys. Lett.*, 76(1):113, 1980.

[49] S Nordholm, LEB Borjesson, L Ming, and H Svedung. Progress on the modeling of the collisional energy transfer mechanism in unimolecular reactions. *Ber. Bunsen-ges. Phys. Chem.*, 101(3):574, MAR 1997. Discussion Meeting of the Deutsche-Bunsen-Gesellschaft on Unimolecular Reactions, TUTZING, GERMANY, OCT 21-24, 1996.

[50] MJ Pilling and Robertson. . *Annu. Rev. Phys. Chem.*, 54(5):245, 2003.

[51] BJ Gaynor, RG Gilbert, and KD King. *Chem. Phys. Lett.*, 55:40, 1978.

[52] T Kato. *J. Chem. Phys.*, 108:6611, 1998.

[53] TJ Frankcombe and SC Smith. Isotopic measurements of stratospheric ozone. *J. Comput. Chem.*, 21:592, 2000.

[54] M. J. Pilling K. A. Holbrook. *Unimolecular Reactions, 2nd ed*. John Wiley & Sons: New York, 1996.

[55] S. Nordholm and H. W. Schranz. *Advances in Chemical Kinetics and Dynamics, Vol. 2A, edited by J. R. Barker*. JAI, Connecticut, 1995.

[56] SH Kang and K-H Jung. *Chem. Phys. Lett.*, 131:496, 1986.

[57] HO Pritchard. *J. Phys. Chem. A*, 108:5249, 2004.

[58] W. Forst. *Theory of Unimolecular Reactions*. Academic Press, New York and London, 1973.

[59] A. D. Polyanin and A. V. Manzhirov. *Handbook of Integral Equations*. CRC Press, Boca Raton, Florida, 1998.

[60] AR Whyte and RG Gilbert. *Chem. Phys. Lett.*, 152:377, 1988.

[61] O Meroueh and WL Hase. *Int. J. Mass. Spectrom.*, 201:233, 2000.

[62] Z. Zhu and R. A. Marcus. On collisional energy transfer in recombination and dissociation reactions: A Wiener-Hopf problem and the effect of a near elastic peak. *J. Chem. Phys.*, 129(21):214106, DEC 7 2008.

[63] M. Nirmal, B. O. Dabbousi, M. G. Bawendi, J. J. Macklin, J. K. Trautman, T. D. Harris, and L. E. Brus. *Nature*, 383:802, 1996.

[64] J. Tittel, W. Gohde, F. Koberling, A. Mews, A. Kornwski, H. Weller, A. Eychmuller, and T. Basche. *Ber. Bunsenges. Phys. Chem.*, 101:1626, 1997.

[65] U. Banin, M. Bruchez, A. P. Alivisatos, T. Ha, S. Weiss, and D. S. Chemla. *J. Chem. Phys.*, 110:1195, 1999.

[66] M. Kuno, D. P. Fromm, H. F. Hamann, A. Gallagher, and D. J. Nesbitt. *J. Chem. Phys.*, 112:3117, 2000.

[67] M. Kuno, D. P. Fromm, A. Gallagher, D. J. Nesbitt, O. I. Micic, and J. J. Nozik. *Nano Lett.*, 1:557, 2001.

[68] M. Kuno, D. P. Fromm, H. F. Hamann, A. Gallagher, and D. J. Nesbitt. *J. Chem. Phys.*, 115:1028, 2001.

[69] K. T. Shimizu, R. G. Neuhauser, C. A. Leatherdale, S. A. Empedocles, W. K. Woo, and M. G. Bawendi. *Phys. Rev. B*, 63:205316, 2001.

[70] K. T. Shimizu, R. G. Neuhauser, C. A. Leatherdale, S. A. Empedocles, W. K. Woo, and M. G. Bawendi. *Phys. Rev. Lett.*, 89:1117401, 2002.

[71] X. Brkmann, J. P. Hermier, G. Messin, P. Desbiolles, J. P. Bouchaud, and M. Dahan. *Phys. Rev. Lett.*, 90:080601, 2003.

[72] R. Ververk, A. M. van Oijen, and M. Orrit. *Phys. Rev. B*, 66:233202, 2002.

[73] M. Kuno, D. P. Fromm, S. T. Johnson, A. Gallagher, and D. J. Nesbitt. *Phys. Rev. B*, 67:125304, 2003.

[74] I. Chung and M. G. Bawendi. *Phys. Rev. B*, 70:165304, 2004.

[75] S. Cui, T. Tachikawa, S. Tojo, M. Fujitsuka, and T. Majima. *J. Phys. Chem.*, 112:19625, 2008.

[76] S. Cui, T. Tachikawa, S. Tojo, M. Fujitsuka, and T. Majima. *J. Phys. Chem.*, 114:1217, 2010.

[77] S. Cui, T. Tachikawa, S. Tojo, M. Fujitsuka, and T. Majima. *J. Phys. Chem.*, 115:1824, 2011.

[78] M. D. Mason, G. M. Credo, K. D. Weston, and S. K. Burrato. *Phys. Rev. Lett.*, 80:5405, 1998.

[79] D. A. Vandenbout, W. T. Yip, D. H. Hu, D. K. Fu, T. M. Swager, and P. F. Barbara. *Science*, 277:1074, 1997.

[80] M. A. Bopp, Y. Jia, L. Li, R. Cogdell, and R. M. Hochstrasser. *Proc. Natl. Acad. Sci. U. S. A.*, 94:10630, 1997.

[81] R. M. Dickson, A. B. Cubitt, R. Y. Tsien, and W. E. Moerner. *Nature*, 388:355, 1997.

[82] E. J. G. Peterman, S. Brasselet, and W. E. Moerner. *J. Phys. Chem. A*, 103:10553, 1999.

[83] H. P. Lu and X. S. Xie. *Nature*, 385:143, 1997.

[84] T. Ha, T. Enderle, D. S. Chemla, P. R. Selvin, and S. Weiss. *Chem. Phys. Lett.*, 271:1, 1998.

[85] K. D. Weston, P. J. Carson, H. Metiu, and S. K. Buratto. *J. Chem. Phys.*, 109:7474, 1998.

[86] E. K. L. Yeow, S. M. Melnikov, T. D. M. Bell, F. C. De Schryver, and J. Hofkens. *J. Phys. Chem. A*, 110:1726, 2006.

[87] T. Tachikawa, S. Cui, S. Tojo, M. Fujitsuka, and T. Majima. *Chem. Phys. Lett.*, 443:313, 2007.

[88] T. Tachikawa, T. Ishigki, J. Li, M. Fujitsuka, and T. Majima. *Angew. Chem.-Inter. Edi.*, 47:5348, 2008.

[89] L. K. Schirra, B. S. Tachett, M. L. Blumenfeld, and O. L. A. Monti. *J. Chem. Phys.*, 131:124702, 2008.

[90] Z. Bian, T. Tachikawa, S. Cui, S. Tojo, M. Fujitsuka, and T. Majima. *Chem. Sci.*, 3:370, 2012.

[91] J. Wang and P. Wolynes. *J. Chem. Phys.*, 110:4812, 1999.

[92] M. Boguna, A. M. Berezhkovskii, and G. H. Weiss. *Physica A*, 282:475, 2000.

[93] Y. Jung, E. Barkai, and R. J. Silbey. *Chem. Phys.*, 181:284, 2002.

[94] R. Verberk and M. Orrit. *J. Chem. Phys.*, 119:2214, 2003.

[95] E. Barkai, Y. J. Jung, and R. Silbey. *Annu. Rev. Phys. Chem.*, 55:457, 2004.

[96] G. Margolin and E. Barkai. *J. Chem. Phys.*, 121:1566, 2004.

[97] J. Tang and R. A. Marcus. *J. Chem. Phys.*, 123:054704, 2005.

[98] J. Tang and R. A. Marcus. *J. Chem. Phys.*, 123:204511, 2005.

[99] H. Htoon, M. Furis, S. A. Crooker, S. Jeong, and V. I. Klimov. *Phys. Rev. B*, 77:035328, 2008.

[100] V. I. Klimov, J. A. McGuire, R. D. Schaller, and V. I. Rupasov. *Phys. Rev. B*, 77:195324, 2008.

[101] J. J. Peterson and D. J. Nesbitt. *Nano Lett.*, 9:338, 2009.

[102] J. Zhao, G. Nair, B.R. Fisher, and M.G. Bawendi. *Phys. Rev. Lett.*, 104:157403, 2010.

[103] G. Nair, J. Zhao, and M.G. Bawendi. *Nano Lett.*, 11:1136, 2011.

[104] K. L. Knappenberger, D. B. Wong, Y. E. Romanyuk, and S. R. Leone. *Nano Lett.*, 7:3869, 2005.

[105] A. A. Cordones, T. J. Bixby, and S. R. Leone. *J. Phys. Chem. C*, 115:6341, 2011.

[106] S. A. Empedocles and M. G. Bawendi. *J. Phys. Chem. B*, 103:1826, 1999.

[107] P. A. Frantsuzov and R. A. Marcus. *Phys. Rev. B*, 72:155321, 2005.

[108] A. L. Efros and M. Rosen. *Phys. Rev. Lett.*, 78:1110, 1997.

[109] R. A. Marcus. *Phil. Trans. R. Soc. A*, 368:1109, 2010.

[110] In ref 97 the Landau-Zener expression was adopted for the rate constant k_r.

[111] R. K. Pathria. *Statitical Mechanics*. Pergamon, Oxford, 1972.

[112] C. H. Crouch, O. Sauter, X. Wu, R. Purcell, C. Querner, M. Drndic, and M. Pelton. *Nano Lett.*, 10:1692, 2010.

[113] In ref 103, the repetation rate is 2.5 MHz so that the time between pulses is 400 ns and is much longer than the single exciton fluorescence lifetime which is around 10-20 ns.

[114] T.D. Krauss, S. O'Brien, and L.E. Brus. *J. Phys. Chem. B*, 105:1725, 2001.

[115] D.H. Son, J. Wittenberg, and A.P. Alivisatos. *Phys. Rev. Lett.*, 92:127406, 2004.

[116] R.M. Kraus, P.G. Lagoudakis, J. Muller, A.L. Rogach, J.M. Lupton, J. Feldman, D.V. Talapin, and H. Weller. *J. Phys. Chem.*, 109:18214, 2005.

[117] W. E. Moerner and M. Orrit. *Science*, 283:1670, 1999.

[118] F. Kultzer and M. Orrit. *Annu. Rev. Phys. Chem.*, 55:585, 2004.

[119] P. Tinnefeld and M. Sauer. *Angew. Chem., Int. Ed.*, 44:2642, 2005.

[120] X. Michalet, A. N. Kapanidis, T. Laurence, F. Pinaud, S. Doose, M. Pflughoefft, and S. Weiss. *Annu. Rev. Biophys. Biomol. Struct.*, 32:161, 2003.

[121] T. Basche, S. Kummer, and C. Brauchle. *Nature*, 373:132, 1995.

[122] X. S. Xie. *Acc. Chem. Res.*, 29:598, 1996.

[123] F. Kohn, J. Hofkens, R. Gronheil, M. Van der Auweraer, and F. C. De Schryver. *J. Phys. Chem. A*, 106:4808, 2002.

[124] J. A. Veerman, M. F. Garcia-Parajo, L. Kuipers, and N. F. van Hulst. *Phys. Rev. Lett.*, 83:2155, 1999.

[125] F. Kulzer, S. Kummer, T. Basche, and C. Brauchle. *J. Inf. Rec.*, 22:567, 1996.

[126] R. G. Neuhauser, K. T. Shimizu, W. K. Woo, S. A. Empedocles, and M. G. Bawendi. *Phys. Rev. Lett.*, 85:3301, 2000.

[127] W. van Sark, P. Frederix, A. A. Bol, H. C. Gerritsen, and A. Meijerink. *Chem. Phys. Chem.*, 3:871, 2002.

[128] F. D. Stefani, W. Knoll, M. Kreiter, X. Zhong, and M. Y. Han. *Phys. Rev. B*, 72:125304, 2005.

[129] R. Verberk, J. W. M. Chon, M. Gu, and M. Orrit. *Physica E*, 26:19, 2005.

[130] A. Issac, C. von Borczyskowski, and F. Cichos. *Phys. Rev. B*, 71:161302, 2005.

[131] F. Cichos, C. von Borczyskowski, and M Orrit. *Curr. Opin. Colloid Interface Sci.*, 12:272, 2007.

[132] M. Pelton, G. Smith, N. F. Scherer, and R. A. Marcus. *PNAS*, 104:14249, 2007.

[133] G. Margolin and E. Barkai. *Phys. Rev. Lett.*, 94:080601, 2005.

[134] S. Burov, R. Metzler, and E. Barkai. *PNAS*, 107:13228, 2010.

[135] G. Messin, J. P. Hermier, E. Giacobino, P. Desbiolles, and M. Dahan. *Opt. Lett.*, 26:1891, 2001.

[136] Khinchin A. I. *Mathematical Foundations of Statistical Mechanics*. Dover, New York, 1949.

[137] P. Walters. *An Introduction to Ergodic Theory*. Springer, 1982.

[138] R. Kubo. *J. Phys. Soc. Jpn*, 12:570, 1995.

[139] J. Bao, P. Hänggi, and Y. Zhuo. *Phys. Rev. E*, 72:061107, 2005.

[140] L. C. Lapas and *et al*. *Phys. Rev. Lett.*, 101:230602, 2008.

[141] J. P. Hoogenboom, H. P. van Dijk, J. Hernando, N. F. van Hulst, and M. F. Garcia-Parajo. *Phys. Rev. Lett.*, 95:097401, 2005.

[142] J. Schuster, F. Cichos, and C. von Borczyskowski. *Appl. Phys. Lett.*, 87:051915, 2005.

[143] J. P. Hoogenboom, W. K. den Otter, and H. L. Offerhaus. *J. Chem. Phys.*, 125:204713, 2006.

[144] J. P. Hoogenboom, J. Hernando, M. F. Garca-Paraj, and N. F. van Hulst. *J. Phys. Chem.*, 112:3417, 2008.

[145] K. L. Wustholz, E. D. Bott, B. Kahr, and P. J. Reid. *J. Phys. Chem.*, 112:7877, 2008.

[146] L. P. Watkins and H. Yang. *J. Phys. Chem. B*, 109:617, 2005.

[147] J. Pfanzagl. *Parametric Statistical Theory*. de Gruyter, Berlin and New York, 1994.

[148] We thank Prof. Monti for providing us with their data points.

[149] W. Chen and R. A. Marcus. *to be submitted*.